Charge Transfer Studies of Semiconductor Interfaces

Thesis by

Amit Kumar

In Partial Fulfillment of the Requirements

for the Degree of

Doctor of Philosophy

California Institute of Technology

Pasadena, California

1992

(Defended September 16, 1991)

ACKNOWLEDGEMENTS

There have been many people who have supported me throughout my life and my graduate career. First and foremost are the members of my family.

I am indebted to my grandparents Ananti Devi and Bhubaneswari Prashad Verma for raising me as a small child. It was their love, support, and influence that shaped my values, ideals, and personality. In essence they are responsible for what I am.

My mother, Dr. Manju Kumar, had thrust upon her the task of raising three children by herself while maintaining a career as a medical doctor. Needless to say she succeeded admirably in both endeavors. I have the greatest love and admiration for my mother for what she is, what she made me, and for what she had to endure after my father's death in 1971. Although I never got to know my father, Saroj Nayn Kumar, very well, I have always loved him dearly. He gave me my name, and he is and will be in my heart always.

My little sister, Aneeta, and little brother, Sanjay, are the best sister and brother one could ask for. I am very proud of both of them, and we all know that each one of us will always be there for each other.

My aunt, Soma Verma, and uncle, Amar Nath Verma, have been like a second mother and father to me. Ther love and support is invaluable to me. Also, it was always worth the fifty mile drive to eat my aunt's cooking.

Eva, Anant, and Ashish, my three cousins, are the most wonderful little children I've known. They are my baby sister and brothers. One of my greatest pleasures will be watching them grow.

Over the years I have had the opportunity to work with a number of exceptional scientists. These people have not only been my colleagues but my friends.

Frank DeHaan of Occidental College taught me the joys of research and teaching. He put me on the academic path that has brought me to this point.

All the members of the Lewis Group (Ashish Bansal, Rik Blumenthal, Catherine Caley, Lou Casagrande, Laura Ferry, Malcolm Forbes, Delwyn Gilmore, Mike Heben, Tom Josephiak, Chris Kenyon, Paul Laibinis, Iver Laurman, Teri Longin, Sharon Lunt, George McManis, Gordon Miskelly, Charlotte Newcomb, Sonbinh Nguyen, Reginald Penner, Russ Pylkki, Mark Rosenblum, Mary Rosenbluth, Gail Ryba, Mike Sailor,Pat Santangelo, Gary Shreve, Daron Standley, Andy Sykes, Ming Tan, Bao Tsai, Bruce Tufts, Paul Wagknecht, Chris Wilisch, and Chong Zheng) have influenced me personally and scientifically. Special recognition goes to Bruce (WWSPT), Malcolm, Mike H., Mike S., Reggie, Gail, and Mary. What a great group of people we were.

Of all the people that I have mentioned, the one who influenced me the most scientifically was my research advisor, Nathan S. Lewis. Nate is one of the brightest scientists I've known. He taught me a great deal of science, and he taught me how to be a scientist. He taught me that I should be the greatest critic of my own work. This lesson, I feel, was the most valuable lesson of my graduate career. I know that I have become a better scientist because of Nate, and I am glad to have had the opportunity to work with him.

There are many people, personal and professional, that I have not mentioned. Their absence is not due to any lack of importance but due to a lack of space. Their influence on me can never be overestimated. I apologize for not being able to name them all.

Abstract

For all semiconductors (n-Si, p-Si, n-GaAs, n-InP, a-Si:H), the spectral response of liquids junctions, in the short wavelength region (200-600 nm), showed higher quantum yields than metal junctions. This general trend was independent of redox species, solvent, supporting electrolyte, and metal overlayer. This technique was also used to distinguish between Schottky barrier behavior from electrocatalytic behavior of metal overlayers.

Studies of n-Si photoelectrodes in aqueous and non-aqueous electrolytes have been conducted. For all n-Si/CH_3OH-dimethylferrocne$^{+/0}$($Me_2Fc^{+/0}$) cells, the forward bias dark currents,the open circuit voltage (V_{oc}), and temperature dependence of V_{oc} were independent redox species concentrations. All n-Si photoanodes (naked and coated with discontinuous metal overlayers) were found to be unstable in aqueous electrolytes.

Novel metal/insulator/semiconductor devices have been fabricated through the anodic growth of the insulator layer in a methanol based electrolyte. These devices do not suffer from Fermi level pining restrictions, and some exhibit electronic properties limited by minority carrier transport.

A theoretical framework has been formulated to describe the behavior of photoelectrolysis cells, and experiments at n-SrTiO3/5.0 **M** KOH(aq)/Pt junctions have been conducted. The data exhibits a photocurrent threshold in the short circuit electrolysis current at 0.02-0.03 mW/cm^2 of 325 nm illumination, which is consistent with the theoretical framework.

The behavior of Si/CH_3OH-$Me_2Fc^{+/0}$ junctions has been investigated under high injection conditions. With a structure having n+ diffused back contacts, V_{oc}s of 626+5 mV were obtained at short circuit photocurrent densities of 20 mA/cm^2. The diode quality factor and reverse saturation current were 1.8+0.1 and (2.6+1.5)x10^{-8} A/cm^2, respectively. These data are consistent with recombination dominated by the base and back contact regions, and not at the Si/CH_3OH interface.

Table of Contents

List of Figures

Chapter 5

Chapter 6

Chapter 7

List of Tables

Charge Transfer Studies of Semiconductor Interfaces

Chapter 1: Introduction

This thesis consists of several chapters all of which can stand alone. The following chapter (Chapter 2) is a short, qualitative introduction to the field of semiconductor/liquid junctions. It is not meant as an exhaustive discussion of the physical principles involved in the operation of semiconductor devices. Its primary purpose is to give the uninitiated reader a qualitative grasp of what this field encompasses. Subjects discussed in Chapter 2 will deal with issues such as the difference between solid-state devices and semiconductor/liquid junctions, the important problems and obstacles that have been encountered in this field, and the types of contributions that chemists can make. In addition a short historical perspective is presented that serves as a transition to the rest of the thesis.

Chapter 3 is the first of the experimental chapters. This chapter details a technique that was developed to examine directly the electron transfer properties of a variety of semiconductor interfaces. This technique was used on over 18 systems (solid-state and liquid junction), and various general differences in charge transfer properties for different junctions were observed.

Chapter 4 describes detailed experiments of n-Si and surface modified n-Si photoelectrodes in both non-aqueous and aqueous solvents. This work was aimed not only at studies of charge transfer, but also at examinations of stability and efficiency claims found in the recent literature. Much of the work, detailed in Chapter 4, was in disagreement with these recent claims. Based upon our experiments, alternative explanations and interpretations are presented for the controversial observations reported in the literature.

Chapter 5 describes work that was an extension of previous work with n-Si/liquid junctions. These experiments describe the use of a liquid junction as an aid in the fabrication of a solid-state device that cannot be prepared using state of the art solid-state

technology. This unique processing technique, using the liquid junction, was discovered somewhat inadvertently and underscores the usefulness of liquid junctions.

Chapter 6 is the only chapter that deals with a large bandgap semiconductor. Certain properties of large bandgap semiconductors allow the examination of particular issues that are not possible with small bandgap materials. The work described in this chapter was aimed at a fundamental question regarding the formalisms and physical aspects of charge transfer events at semiconductor/liquid interfaces.

Chapter 7, the final chapter, is a description of the operation of a novel type of liquid junction device. According to conventional wisdom, this type of device should not operate efficiently as a liquid junction, although similar solid-state devices are among the most efficient photovoltaic converter to date. Explanations and experiments to determine why these devices operate well in liquid junction form are discussed.

Charge Transfer Studies of Semiconductor Interfaces

Chapter 2: Background

I. INTRODUCTION

Recently, much effort has gone into the development of efficient solar energy conversion devices. Energy conversion efficiencies for semiconductor solid-state systems have reached levels that were thought to be unattainable twenty years ago. Although large scale terrestrial application of photovoltaics is currently not feasible economically, a high degree of sophistication has produced conversion systems that are practical for many small scale applications such as satellites and isolated terrestrial locations.

An alternative to the solid-state photovoltaic device is a photoelectrochemical cell (PEC). In such a structure, a semiconductor is still required, but the active junction occurs at a solid/liquid interface. This type of device is very attractive since it offers the possibility of producing chemical fuels that are easily stored or transported. In the early 1970's Honda and Fujishima used this approach to split water and produce hydrogen and oxygen.[1] This generated a great deal of interest in PECs, however, it was quickly realized that water splitting systems could not achieve the efficiencies required to be economically feasible. This was due to the fact that all water splitting systems required the use of large bandgap materials.

A slightly modified PEC uses a regenerative electrolyte to produce electricity rather than chemical fuels. This type of PEC has received the most attention in recent years. A major hindrance to the regenerative systems is the fact that most of the small bandgap materials are thermodynamically unstable in aqueous solutions.[2] They are extremely susceptible to corrosion and/or passivation in the dark and/or under illumination. With some notable exceptions, very few aqueous regenerative photoelectrochemical cells were reported to be stable. A solution to this problem was the use of non-aqueous electrolyte systems with kinetically fast, outer-sphere redox molecules for charge transport.[3] With

this modification, the thermodynamic pathways that caused instability were no longer kinetically accessible.

There are significant differences between regenerative photoelectrochemical cells and solid-state photovoltaic devices. The primary difference is the requirement of charge transfer from a semiconductor into solution for the PEC. Typically, the rate of charge transfer from a semiconductor into freely diffusing molecules in solution is kinetically slower than that from a semiconductor into a metal or into another semiconductor. This is due to the fact that solvent reorganization effects and low solution acceptor concentrations are usually involved. This kinetic sluggishness can lead to problems in obtaining efficient semiconductor/liquid junctions for photovoltaic energy conversion. Consideration of the rates of charge transfer with respect to recombination rates is important for superior device behavior. With recent discoveries of stable, well-characterized semiconductor/electrolyte interfaces, examinations of fundamental aspects of interfacial processes such as charge transfer can now be conducted.

From practical and fundamental viewpoints there are many reasons to study semiconductor/electrolyte interfaces. One of the most compelling is the ease with which semiconductor/liquid junction devices can be fabricated. Expensive clean room atmospheres, high temperature, and high vacuum processing systems are commonly required for the fabrication of solid-state semiconductor devices. In contrast liquid junction devices can be fabricated for study at a fraction of the cost in not only equipment but also labor. Furthermore, a liquid junction device is a renewable system which allows for the study of many junctions at the same electrode interface. The electrode can be easily removed from one electrolyte and inserted into another, without changing significantly the surface. Or the electrode can be removed from the electrolyte for direct analysis of the surface through the various available surface analytical spectroscopies. Also, the ability to change certain aspects of the interface, which is not possible with solid-state devices, is

facilitated by the use of liquid junctions. The non-destructive nature of the interface allows the examination of various modifications of the surface and the electrolyte. An example is the ability to bind molecules to the surface to affect the electronic properties of the device. Another is the ability to change concentrations and identities of the redox species in the solution to facilitate studies of charge transfer phenomenon. Of course, as mentioned above, another major motivation is the possibility for fabricating cheap, efficient solar conversion devices. All of these factors make the study of semiconductor/liquid junctions ideal for addressing many practical and fundamental issues relating to interface chemistry and physics.

Many advances in the field of semiconductor/liquid junctions have occurred in the last two decades of study. Hundreds of new materials have been identified to be semiconducting through photoelectrochemical study.[4] Many of these materials would not have been discovered if research had been restricted to conventional solid-state junctions. This is due to the ease with which photoeffects can be obtained in liquid junctions. Many semiconductor surfaces have been chemically and electronically modified through the binding or adsorption of metal ions,[5] molecules,[6] polymers,[7] and even enzymes.[8] Certain semiconductor/liquid systems have been shown to produce unique chemical reactions that are not possible at metal electrodes.[9] Quantization and "hot" electron transfer have been observed for semiconductor colloids and superlattice photoelectrodes.[10] Additionally, ideal behavior with regard to the energetics of barrier formation, which is not seen for semiconductor/metal junctions, has been observed for semiconductor/liquid interfaces.[11]

Technological and practical applications for semiconductor/liquid interfaces have also grown. Solar cell power conversion efficiencies have increased to the 10-15% level.[5,12-14] Particulate semiconductors have been used photochemically to oxidize toxic pollutants in aqueous and non-aqueous systems.[15] Liquid junctions have been used to process semiconductor interfaces, which have been fabricated into solid-state devices that

exhibit novel properties not attainable through conventional techniques.[16] Semiconductor devices with electroplated metal overlayers have been shown to exhibit properties that are significantly different from conventional thermally deposited metal overlayers.[17] Another application that is very promising is the use of liquid junctions for non-destructive, spatially resolved characterization of semiconductor materials and processing.

Many excellent reviews about the field have been published.[18-20] The purpose of this chapter is to discuss the aspects of both semiconductor device physics and electrochemical processes that are required to gain an understanding of the operation of PECs. It is outside the scope of this paper to deal with all issues quantitatively. Instead, the primary goal is to provide the uninitiated reader a good qualitative grasp of the principles involved. However, in certain situations where rigor is warranted, a quantitative discussion is presented.

II. CHARGE SEPARATION

The key process involved with the conversion of light into chemical or electrical energy is charge separation. Once a photon of light has been absorbed creating an electron and hole, a method to separate these species is required to prevent their recombination. One method of charge separation occurs in nature, in the photosynthetic reaction center.[21] Although photosynthesis is very complex and is not fully understood, the main features are clear. Upon absorption of a photon, the electron and hole are separated through a series of steps involving electron transfers. These electron transfers are driven by free energy (ΔG) gradients. The overall photosynthetic process results in the formation of carbohydrates through the fixation of carbon dioxide.

$$6H_2O + 6CO_2 \text{ -------> } C_6H_{12}O_6 + 6O_2 \qquad (1)$$

The efficiency of this process depends on various factors such as the ratio of successful charge separation to electron-hole recombination. The overall efficiency also depends on factors such as amount of light absorption, and quantum yields for electron transfer depends on excited state lifetimes. Although, quantum yields for this process are relatively high, the overall efficiency is relatively small (2-3 %).[21] Attempts to chemically mimic photosynthesis using man-made systems have resulted in some success recently,[22,23] and a great deal of fundamental knowledge about the photosynthetic process has been attained.

The charge separation process in semiconductor/liquid and solid-state semiconductor junction systems occurs through a related, but chemically different, series of processes. In the semiconductor, the spatial charge separation is not driven by a series of highly irreversible electron transfer steps. It is driven by an electric field that has been established in the semiconductor (*vide infra*). Since electrical contact can be easily made to semiconductor systems, these separated charges can be harvested in the form of electricity. Alternatively, they can be coupled to heterogeneous chemical reactions that can directly convert low energy materials into chemical fuels. However, the quantity of useful energy (electrical and/or chemical) is determined, as is the case for photosynthetic systems, by the ratio of successful charge separation versus electron-hole recombination. The recombination process in semiconductor based systems can occur through several mechanisms which are dependent on various properties of the specific system under consideration.

The intent of this chapter is to develop the theory for PEC operation from basic principles and to apply it to several systems of note. We will begin with the fundamentals and develop our understanding with successive sections. Many of the subjects mentioned

in this chapter will then be dealt with in greater detail in the following experimental chapters.

III. BAND THEORY

To understand charge-separation and current transport processes in a solid, one needs to understand the electronic properties of solids. The model that is most successful for the description of the behavior of solids is the free electron model. It is based upon the existence of molecular orbitals that are delocalized over all the nuclei that comprise the solid. This delocalization results in the formation of bands of states that are comprised of the substituent molecular orbitals.

A. Development of Bands

The origin of bands in a solid is a direct consequence of applying the Schroedinger equation to a periodic potential.[24] Although quantitative treatments of band theory are well-developed, for our purposes only a qualitative understanding is required.

Isolated atoms have discrete energy levels (orbitals) that can be occupied by electrons. When isolated atoms are brought together, such as in a molecule, orbitals of appropriate energies interact and form delocalized molecular orbitals. In a solid, these orbitals are delocalized over the whole material. This is a direct result of the periodic potential resulting from the periodic nature of the nuclear positions of the atoms comprising the material.[24] For example, since there are 2.7×10^{22} sodium atoms in a cubic centimeter, there are 2.7×10^{22} delocalized orbitals in a cubic centimeter resulting form the atomic 3s orbitals. As was the case for the atomic and molecular systems, the Pauli exclusion principle holds for the crystal. This leads us to conclude that there must exist a band of states comprised of 2.7×10^{22} sodium 3s orbitals per cubic centimeter that differ in energy by very small amounts.

Of course, what is true for the valence orbitals is also true for the core level orbitals and the unoccupied higher energy orbitals. However, we shall be concerned primarily with the highest occupied band (valence band) and the lowest unoccupied band (conduction band). These delocalized bands are directly analogous to the highest occupied molecular orbital and the lowest unoccupied molecular orbital, respectively. Therefore, to a first approximation we can consider crystals to be merely large molecules with delocalized orbitals.

The band theory allows the classification of solids into three general categories. Conductors are materials in which the highest occupied band is not completely filled, or the bandgap (the energy difference between the highest occupied and lowest unoccupied band) is very small. This is found to be the case for the sodium example above and the other metals. Insulators are materials in which the bandgap is large (>4 eV), and semiconductors have intermediate bandgaps. The differentiation between semiconducting and insulating behavior is somewhat arbitrary. Insulating materials such as diamond and glass have bandgaps greater that 5 eV. Technologically important semiconductors such as Si and GaAs have bandgaps of 1.1 and 1.4 eV respectively at room temperature, and other semiconductors useful for PEC applications such as CdS and TiO_2 have bandgaps ranging from 2.4 to 3 eV.

Perhaps the most important result that emerges from band theory is the existence of a bandgap. As is the case with the energy separation between molecular orbitals the energy separation between bands is a direct reflection of bond strength, since the bandgap energy corresponds to the amount of energy required to remove an electron from a bond and raise it to a sufficiently high energy that it is free to move throughout the crystal.

B. Doping

Up to this point we have been considering only pure crystals. For semiconductors under these conditions, the valence band will be completely full and the conduction band completely empty, except for the the small number of carriers that have been thermally excited from the valence band into the conduction band. To increase the conductivity and to control other electronic properties of the semiconductor, low concentrations of specific impurity atoms (on the order of one impurity atom per several million crystal atoms) can be introduced into the crystal lattice.[25] This process is known as doping.

Dopant atoms can either be donors (which donate an electron to the conduction band and become positively charged) or acceptors (which accept electrons from the valence band and become negatively charged). A material that has been doped with donors is n-type, since the majority carriers are electrons in the conduction band, through which the electrical conduction occurs. Conversely, a p-type semiconductor has been doped with acceptors and conduction occurs through the majority carriers which are holes in the valence band.

The nature of a dopant atom is dependent upon the characteristics of the dopant and of the crystal in which it is incorporated. For example in Si, which is a group IV element, group V elements such as P and As will be donors.[25] Since only four of the five valence electrons are required for tetrahedral bonding in the crystal, the fifth valence electron will be donated to the conduction band at room temperature. Conversely, group III elements such as B or Al are acceptors in Si, since they require an additional electron from the valence band to satisfy the tetrahedral bonding requirement. Under certain conditions a particular dopant atom can act either as a donor or as an acceptor depending upon its lattice position in the crystal. For example Si is a donor in GaAs if it occupies the position of a Ga atom, but it is an acceptor if it occupies an As lattice site.[25]

Other impurity atoms, such as transition metals, can have deeper levels or multiple levels. Additionally, interstitial atoms and crystal defects can also behave as dopants. All of these factors can significantly affect the electronic properties of the material even if they exist in the crystal in concentrations of parts per billion. Therefore, the manufacturing and processing of most semiconductor materials and devices are conducted under excruciatingly clean conditions to minimize the incorporation of unwanted impurities. For certain applications impurities with deep levels are incorporated into the semiconductor to control properties that cannot be easily controlled by dopant impurities.

IV. ELECTROCHEMICAL POTENTIALS

The operation of a PEC requires the formation of a semiconductor/liquid junction. This involves the simple act of introducing the semiconductor of interest to the solution of interest. The electrical junction formation at the solid/liquid interface is due to the equilibration of electrochemical potentials of the solid and the liquid. We will now discuss what the definition of electrochemical potentials are for liquids and solids.

A. Solution Electrochemical Potentials-Nernst Equation

The electrochemical potential for a solution is given by the Nernst equation.[26]

$$\mathbf{E}_f = \mathbf{E}^{o\prime} + (2.303RT/nF)\ln([A]/[A^-]) \qquad (2)$$

$\mathbf{E}_f$ is the redox potential of the solution. $\mathbf{E}^{o\prime}$, the formal potential, is specific to the solvent-molecule system. R is the ideal gas constant, T is the absolute temperature, n is the number of electrons involved in the redox process, F is the Faraday constant, and [A] and [A^-] are the activities or concentrations of the oxidized and reduced forms of the redox couple respectively.

The electrochemical potential or redox potential is often referred to as the solution Fermi level since it is derived using Fermi-Dirac statistics. The application of Fermi-Dirac statistics to a system is equivalent to filling the states (orbitals) of the system with the available electrons subject to the Pauli exclusion principle. The Fermi level is the energy at which the probability of finding an occupied state is 1/2. Throughout this paper we will use the terms Fermi level, redox potential, and electrochemical potential interchangeably.

The first term of equation (2), $E^{o'}$, is an intrinsic energy level that is dependent on the energy of the molecular orbital under consideration. Thus, its value depends on the identity of the molecule and interaction with the solvent.[26] The second term is a statistical factor that describes the electron occupancy of the orbitals of the molecules under consideration.[26] If the appropriate molecular orbital is occupied, the molecule is in its reduced form (A^-). If the orbital is unoccupied, the molecule is in its oxidized form (A). As we increase the number of electrons (i.e., increase the concentration of reduced species) the redox potential becomes more negative. Conversely, as we decrease the number of electrons (i.e., increase the concentration of oxidized species) the redox potential becomes more positive.

Electrochemical potentials cannot be measured without reference to another electrochemical potential consisting of its own redox couple. By definition the electrochemical potential of the standard hydrogen electrode (SHE) is considered to be zero.[26] The SHE consists of a Pt electrode in a pH =1 solution under 1 atm H_2. Since this electrode is somewhat difficult to use in routine experiments, other electrodes such as the saturated calomel electrode (SCE) are in common use. Nevertheless, all redox potentials can always be referenced to the SHE.

B. Semiconductor Electrochemical Potentials

The Fermi level of a solid is defined exactly the same way as that for a solution. The difference here is that instead of dealing with the occupancy of molecular orbitals that are unique to each individual molecule, one deals with states that are delocalized over the entire crystal.

The total number of states in a solid is equal to the number of states that were contributed by the individual constituents of the solid. The energetic distribution of these states can be calculated quantum mechanically. These states are again filled with the available electrons using the Fermi-Dirac distribution function. This results in the following equation for the Fermi level of a semiconductor.[25]

$$E_f = E_i + kT\ln(n/n_i) \qquad (3)$$

E_i is the intrinsic energy level for the semiconductor in the absence of doping, n is the excess concentration of electrons in the conduction band due to doping, and n_i is the intrinsic concentration of electrons in the absence of doping. Equation (3) can be written in several ways depending on the situation. The important thing to note is that the Fermi levels for solutions and solids are derived in the same manner and have the same meaning.

By definition for a solid, E_f is referenced to the energy of a free electron in vacuum (commonly referred to as the vacuum level).[26] Since the energy required to remove an electron from the Fermi level of the solid can be easily measured, it is reasonable to make this definition. However, this energy cannot be experimentally determined for a liquid. Therefore, it is difficult to quantitatively relate the position of a redox potential of a solution to the Fermi level of a solid. However, various theoretical constructs have indicated that the Fermi level of the SHE is approximately 4.5-4.7 eV positive of the vacuum level.[26] Although the exact number is not known, this approximation is sufficient for most of our needs.

V. JUNCTION FORMATION

Figures 1a-d depict n-type semiconductor/liquid junctions before and after charge transfer equilibration. When a semiconductor is brought into contact with another phase, an electrostatic double layer is established, because the electrochemical potentials must equilibrate. This results in the formation of an electrostatic barrier. Figure 1a and b depict the situation for a n-type semiconductor in contact with a liquid junction. Since the electrochemical potential of the semiconductor is more negative than that for the liquid, electrons from the semiconductor are transferred to the electrolyte. As these electrons are transferred to the electrolyte, positive charges are left in the semiconductor. This charge equilibration results in the development of a dipole. After a certain amount of charge equilibration, this dipole hinders the ability of further electrons to transfer into the solution. At this point the electrochemical potentials have equilibrated. Since these positive charges are the nuclei of the dopant atoms, their positions are stationary in the crystal, and the width over which the electrons have been depleted in the semiconductor is known as the depletion region.

The spatial distribution of positively charged nuclei in the depletion region results in an electric field, the magnitude of which is linearly dependent on distance. Integration of this electric field as a function of distance yields the potential energy *vs* distance diagram depicted in Figure 1b. One important parameter that controls the properties of the junction is the barrier height (Figure 1b). The barrier height energy, $q\phi_b$, is the energy required to take an electron from the Fermi level of the electrolyte and transfer it into the semiconductor conduction band. The junction depicted in Figure 1b is a rectifying contact since current will flow only in one direction. This ability to form a depletion region and a rectifying contact at a semiconductor junction is the basis for all the semiconductor devices that have

revolutionized the electronics industry in the last forty years. The current-voltage (I-V) properties of these contacts will be discussed later.

When the electrochemical potential of the electrolyte is negative of the electrochemical potential of the n-type semiconductor, electrons will transfer from the electrolyte into the semiconductor (Figures 1c-d). The effect of this is to bring the Fermi level of the semiconductor more negative so that it will equilibrate with the electrochemical potential of the electrolyte. When this happens the semiconductor Fermi level at the surface is in the conduction band. Such a situation results in no depletion region and non-rectifying characteristics, because the junction properties are similar to that of a metal/electrolyte system. Under these conditions the junction is said to be an accumulated system, since majority carrier have been accumulated at the interface instead of depleted. This type of junction is an ohmic junction since the I-V properties are controlled by Ohm's law.

Analogous considerations can be made for p-type semiconductors, except that holes are the majority carrier and their transfer is what results in the equilibration of electrochemical potentials. For such situations, if the electrolyte Fermi level is negative of the semiconductor electrochemical potential, the contact will be rectifying. If the electrolyte Fermi level is positive of the semiconductor electrochemical potential, the contact will be ohmic. For these junctions the barrier height energy, $q\phi_b$, is the energy required to take a hole from the electrolyte Fermi level and transfer it into the valence band of the semiconductor.

For an ideal system, the equilibrium energetics of the junction will be determined by the difference in the electrochemical potential of the semiconductor and the electrochemical potential of the contacting phase. However, for many solid-state systems (semiconductor/metal contacts) this is not the case.[25,27] When the junction energetics are

independent of the difference in electrochemical potentials of the contacting phases, the system is said to suffer from Fermi level pinning (FLP), since the semiconductor Fermi level is "pinned" at a position that is not dependent on the contacting phase Fermi level. Although, most semiconductor/metal systems suffer from FLP restrictions, many analogous semiconductor/liquid junctions do not.

VI. REGENERATIVE PECS-CURRENT-VOLTAGE (I-V) PROPERTIES

Now that we have illustrated junction formation, the I-V properties of these contacts need to be examined. We will examine the rectifying I-V behavior of an ideal system in the dark and then under illumination. This analysis is for regenerative-electrolyte, electricity producing, systems. Non-regenerative photoelectrolytic (chemical fuel) systems will be discussed subsequently. Initially the discussion will be qualitative. This will be followed by a quantitative discussion of the parameters that control the I-V characteristics of regenerative-electrolyte PECs. Although the following discussion will be for n-type systems, analogous effects are observed for p-type semiconductor/electrolyte contacts.

We will use the following conventions for currents and voltages. The applied voltage is positive if a positive potential is applied to the semiconductor, or a negative voltage is applied to a counter electrode in solution. On the energy *vs* distance diagrams (for example Figure 1) positive is down and negative is up. The current is positive if excess electrons are going into the semiconductor or holes are going into the electrolyte.

Figure 2a displays a rectifying junction involving an n-type semiconductor and an electrolyte at equilibrium in the dark. This condition is known as the short-circuit condition since the Fermi levels are equilibrated. Under these conditions no net current is flowing. However, there are small, equal and opposite exchange currents flowing. These are displayed by the arrows in Figure 2a. Although these arrows display exchange between the electrolyte and the conduction band, this need not be the dominant path in all systems.

The exchange can also occur through the valence band, however, for our purposes we will depict the exchange currents as in Figure 2a. The magnitude of the exchange currents is an important quantity and will be discussed below. The positive exchange currents consist of electrons from the electrolyte that are thermally activated over the barrier, $q\phi_b$. The opposite current is due to activated electron flow from the semiconductor to the electrolyte, over the barrier .

When a potential is applied to the semiconductor with respect to a reference electrode, the system is displaced from the short circuit condition. For an ideal system we will assume that all applied potential is dropped across the semiconductor. When a positive potential is applied to the semiconductor, the bands are displaced down, Figure 2b. Inspection of the diagram shows that the positive current (from the electrolyte into the conduction band) does not change in magnitude, since the barrier remains the same. However, the negative current (from the conduction band into the electrolyte) decreases because the barrier to electron flow into the electrolyte has changed from $(qV_{bi}+ qV_n)$ to $(qV_{bi}+ qV_n + qV_{app})$, where V_{bi} is positive. This condition is known as reverse bias, since the applied voltage has induced greater band-bending in the junction than that which existed at equilibrium. Therefore, the net current under reverse bias is positive. Its magnitude is equal to the equilibrium exchange current since the applied voltage has reduced the negative current to a negligible value.

Conversely, when a negative voltage is applied to the semiconductor, the bands are displaced up, Figure 2c. This condition is known as forward bias. Again the positive current value has remained constant. However, the negative current from the semiconductor into the electrolyte has increased since the activation barrier for this electron flow has been reduced to $(qV_{bi}+ qV_n + qV_{app})$ where V_n is the difference between the conduction band and the Fermi level in the bulk of the semiconductor, and V_{app} is negative.

The increase in electron flow is exponential with reduction in the activation barrier, since activated transfer over a barrier is known to be governed by an Arrhenius type term.

Figure 2d displays the expected I-V response for the junction discussed with appropriate indications of the band bending conditions of Figures 2a-c. By inspection we can write an equation that displays this behavior.

$$J = -J_o(\exp(-qV/AkT) - 1) \qquad (4)$$

In this equation we have used current densities (J in Amps/cm^2) rather than currents, since the current densities are the important quantities for real systems. J_o is the exchange current density. It is often called the reverse saturation current density, since this is the saturation current under reverse bias. J is the total current density, q is the charge on an electron, V is the applied voltage, k is the Boltzmann constant, and T is the absolute temperature. A is a parameter known as the diode quality factor. Its physical meaning is dependent upon transport mechanisms that control J_o.

We can qualitatively show that equation (4) satisfactorily depicts the I-V curve of Figure 2d. At positive applied voltages, the Boltzmann term becomes negligible and the total current density J, is equal to J_o. At zero applied voltage, we observe that J = 0. At negative applied voltage, the (-1) becomes negligible and the total current density, J, is negative and varies exponentially with voltage. More rigorous derivations of this equation known as the ideal diode equation can be found in text books on semiconductor device physics.

Under illumination a photocurrent, J_{ph}, will be observed to be superposed on the dark current. The ideal diode equation can be modified to take into account the photocurrent density.

$$J = -J_o(\exp(-qV/AkT) - 1) + J_{ph} \qquad (5)$$

This equation is a mathematical statement of the superposition principle. This model says that the photocurrent can be directly superposed onto the dark current. Often the superposition principle is not in effect for semiconductor/liquid junctions. This is due to the fact that under illumination, the mechanism that controls J_0 may be different in the dark and under illumination. Consequently, the magnitude of J_0 and the diode quality factor, A, often change from their values in the dark. However, equation (5) is still useful in analyzing the behavior of most PECs.

The magnitude of the photocurrent depends on various factors that will be discussed in detail later. Figure 3a shows the processes that occur during illumination. Electron-hole pairs are created by the absorption of photons. They are separated by the electric field; the holes are driven toward the interface, and the electrons are driven toward the back of the semiconductor and around the circuit. The holes oxidize a molecule (A^-), and the electrons traverse the circuit and reduce the molecule (A) at the platinum electrode. Therefore, no net change in the electrolyte occurs, but the electron hole pairs are separated and forced to produce electricity. Figure 3b displays the I-V curve for an ideal semiconductor/liquid junction under illumination, with the respective contributions due to the dark current and the superposed photocurrent. The important parameters in Figure 3b, each of which will be discussed in more detail, are the short-circuit photocurrent density (J_{sc}), the open-circuit voltage (V_{oc}), and the fill factor (ff).

A. Short-Circuit Photocurrent

The photocurrent is merely the difference between the number of electron-hole pairs created by the absorption of light and the number of these pairs that recombine through various mechanisms and consequently are not separated. Therefore the observed photocurrent for a particular junction will depend on the quantum yield, which is defined as the ratio of successful charge separation to the total number of electron hole pairs that were

created. The number of carriers that recombine (*ie* are not successfully separated) depends on many factors such as wavelength of the excitation light, the semiconductor material quality, the junction energetics, the type of contact, the abruptness of junction, the electronic quality of the interfacial surface, *etc*.

Since the absorption coefficient is dependent on the excitation wavelength the position of carrier creation in the semiconductor can be controlled by control of the exitation wavelength.[28] In general, the shorter the wavelength, the larger the absorption coefficient. Consequently, modulation of the excitation wavelength yields control of the position of carrier generation. This property becomes useful for studying current transport across a junction. (See Chapter 3.)

For a typical semiconductor/liquid junction the distance over which the bands are bent, the thickness of the depletion layer, is on the order of one tenth of a micron. When carriers are created in this region, the charge separation process is very efficient due to the existence of the electric field (usually on the order of 10^5 V/cm). For most systems, the quantum yield for carriers generated in the depletion layer is unity.[29] However, longer wavelength photons result in carrier generation deep in the semiconductor, where electric field induced charge separation cannot occur. When carriers are created outside the depletion layer, they will diffuse until they recombine or until they diffuse into the depletion layer and are swept away. (See Chapter 3.) If the material quality is poor and carriers recombine quickly then a relatively small fraction will reach the depletion layer for subsequent separation. If the material quality is excellent (i.e., carriers can diffuse for a relatively long time before recombining) a larger fraction will reach the depletion layer and the quantum yield will be high. Consequently, an excellent method to examine material quality is to study the quantum yield as a function of wavelength. This type of measurement is known as a spectral response.

In addition if excitation occurs extremely close to the interface, even though the carriers are generated in the depletion layer a certain number of majority carriers can diffuse against the field due to a chemical potential gradient and recombine through charge transfer (Chapter 3). For this process to be significantly large enough for experimental measurement, excitation wavelengths in the UV (200-400 nm) must be used to create the carriers sufficiently close to the interface. Since most solar cells (liquid junction and solid-state) are designed for terrestrial operation, the UV response has traditionally been neglected. However, recent work has shown that studies of quantum yield as a function of wavelength in the UV region of the spectrum can provide information regarding interfacial charge transfer rates at various contacts. (See Chapter 3.)

To determine the total photocurrent available from a particular junction, one merely has to integrate the spectral response of the junction over the wavelength region of the light source taking into consideration the wavelength dependent intensity of the source. For most applications the light source used is the terrestrial intensity of the sun at various times during the day. To maximize efficiency, photocurrent must be maximized, and various methods, such as increasing crystal quality and decreasing reflectivity losses, have been used to maximize the quantum yields of photovoltaic devices.

B. Open-Circuit Voltage

The open-circuit voltage for photovoltaic devices is dependent on many factors that govern the quantity of recombination occurring in a particular system. By definition, the open-circuit voltage is the voltage at which no net current is flowing. This voltage can be converted into the maximum free-energy available from a junction for specified conditions of temperature and illumination intensity.

If we let the total current equal zero in equation (5), we obtain the following.

$$V_{oc} = [(AkT)/q]\ln(J_{sc}/J_o) \qquad (6)$$

Thus we observe that the open-circuit voltage is proportional to the ratio of the short circuit photocurrent to the reverse saturation (recombination) current. This equation holds regardless of whether the superposition principle is obeyed by a particular junction. Obviously, any factors that increase J_{sc} and/or reduce J_o will effect an increase in the V_{oc}. Consequently, the material quality that was important in determining the spectral response properties of a junction (*vide supra*) is also important in determining the V_{oc}.

In addition the energetics at the interface are important in determining the magnitude of J_o. Figure 4 displays the various mechanisms that contribute to the reverse saturation current. Process a) is known as thermionic emission. This involves the activation of carriers over the built in barrier into the contacting phase. Process b), although similar to thermionic emission, involves the actual tunneling of carriers through the barrier into the contacting phase. If a particular junction has detrimental electronic states at the semiconductor surface, process c), surface-state recombination, can make a significant contribution to the reverse saturation current. Depletion region recombination, d), involves the injection of a minority carrier (a hole for this junction) that subsequently recombines with a majority carrier (an electron) in the depletion layer. Process e) is known as bulk-diffusion/recombination. It involves the diffusion of a minority carrier in the field-free region of the semiconductor until recombination with a majority carrier occurs.

For any given junction all five mechanisms will contribute to the total reverse saturation current, however, only one usually will dominate, and the others will be negligible enough that they need not be considered. All the recombination processes have functional dependencies on properties of the junction. We will now quantitatively examine two of these processes, thermionic emission and bulk/diffusion recombination.

1) Thermionic Emission

Before electrons can be emitted over the barrier, they must reach the interface. While transversing the depletion region, their motion is governed by the usual mechanisms of drift and diffusion. Once they have reached the interface, their emission across the interface is dependent upon the transfer kinetics of the particular junction. Since traversing the depletion region requires an activation, the transport of the majority carriers to the interface is dependent exponentially on the magnitude of the barrier. Therefore, we can write the following equation.

$$J_{o(th)} = K\exp(-q\phi_b/kT) \qquad (7)$$

K is a temperature dependent constant that takes into account both the number of electrons incident per unit area at the interface and the probability of transfer. Its value is dependent upon the magnitude of the drift and diffusion processes. The drift velocity of carriers is μE, where μ is the carrier mobility and E is the electric field strength. When the primary mechanism for carrier transport to the interface is through diffusion, $K = qN_c\mu E$, where N_c is the density of states in the conduction band. For semiconductor/metal contacts, when drift is the primary mechanism for carriers to reach the interface, $K=A^*T^2$. T is the absolute temperature, and A^* is known as the Richardson constant. For liquid junctions, the value of K involves many parameters that depend upon the constituents of the electrolyte and their concentration (see Section **VIII** on Charge Transfer). The important point to note is that for both liquid and solid contacts, the energetics of the interface (i.e., the barrier height) control the magnitude of the thermionic emission contribution to the reverse saturation current. Calculations show that an increase in ϕ_b of 59 mV at room temperature will result in a decrease of $J_{o(th)}$ by one order of magnitude, assuming that K remains unchanged.

If we substitute equation (7) into equation (6) and rearrange, we obtain the following equation for the V_{oc} of a semiconductor junction that is controlled by the thermionic emission mechanism.

$$V_{oc} = kT/q \ln(J_{ph}/K) + \phi_b \qquad (8)$$

We note from examination of equation (8) that for maximum efficiency, the barrier height must be as large as possible in order to obtain the maximum V_{oc}.

2) Bulk-Diffusion/Recombination

For any photovoltaic device in order to improve the V_{oc}, the goal is to decrease the magnitude of all recombination pathways. The rates of all the interfacial recombination mechanisms and depletion region recombination can be reduced by varying system parameters or the quality of the junction. For example, depletion region recombination can be reduced by decreasing the width of the depletion region through increasing the dopant density. Tunneling across the barrier and surface state recombination can be reduced by using moderately doped semiconductors and creating a better quality junction, respectively. Of course, thermionic emission can be reduced by creating a junction with a larger barrier height. This leaves bulk-diffusion/recombination. The magnitude of this recombination pathway is not dependent upon properties of the interface or the junction. This recombination process occurs in the bulk of the semiconductor in the field-free region. Therefore, its value is dependent upon the bulk crystal parameters. Consequently, the magnitude of bulk-diffusion/recombination current kinetically limits the maximum V_{oc} obtainable from a particular junction. (See Chapters 4,5,7.)

If we examine the diffusion and recombination of carriers in a field-free region we obtain the following equation for bulk-diffusion/recombination.[30]

$$J_{o(bulk)} = (qD_p n_i^2)/(L_p N_d) \quad (9)$$

D_p is the diffusion coefficient of minority carriers in the material. It is related to the mobility of the holes, μ_p, through the Einstein relations, $D_p = (kT/q)\mu_p$. L_p is the average diffusion length of minority carriers. This length is a characteristic distance over which most of the carriers can travel before they recombine. N_d is the dopant density, and all the other terms have their usual meanings. If we substitute equation (9) into the V_{oc} expression we obtain the following equation for the bulk-diffusion/recombination limited open-circuit voltage.

$$V_{oc} = (kT/q)\ln[(J_{ph}L_p N_d)/(qD_p n_i^2)] \quad (10)$$

Inspection of this equation indicates what parameters are required to maximize V_{oc} for a bulk-diffusion/recombination limited photovoltaic device. The values of the parameters in the denominator of the ln term are either constants or relatively invariant. Therefore, at a constant photocurrent density, the maximization of the product $N_d L_p$ is required to maximize V_{oc}. Typically this can be achieved by simply increasing the dopant density. However, at very large concentrations of dopants, L_p often degrades or non-rectifying behavior is observed. (See Chapters 4,7.)

An interesting approach is to use a semiconductor with a very low dopant density. In this case L_p is very large, since N_d is minimal. In the dark junctions based upon this material exhibit very resistive bahavior. However, under illumination, conductivity is induced through the existence of photogenerated carriers. This is called the high injection condition,[31] since the number of carriers generated is greater than the initial dopant density. This type of device has allowed the attainment of V_{oc} values greater than those from conventional devices under similar conditions. Solid-state photovoltaic cells of this design

have demonstrated record efficiencies for conversion of light to electricity.[31] Chapter 7 deals with liquid junctions operated under high injection conditions.

C. Fill Factor

In addition to maximizing the currents and voltages of photovoltaic systems, the fill factor, which is a measure of the squareness of the I-V curve under illumination, must be maximized. The definition of the fill factor, FF, is given by equation (11).

$$FF = [(V_{max}J_{max})/(V_{oc}J_{sc})]100\% \qquad (11)$$

V_{max} and J_{max} are the values of the voltage and current density where the (V)(J) product is a maximum. Figure 3b displays geometrically a fill factor.

Maximization of the fill factor, or the VJ product, is extremely important for practical photovoltaic devices. At open circuit the largest possible voltage is obtained, however, no net current is flowing. At short circuit the maximum current will flow, however, no potential difference is obtained. Therefore, although maximization and studies of V_{oc} and J_{sc} are important to gain knowledge of the physics of the junction, a practical device will be operated at a voltage and current density where the VJ product is greatest. This is known as the power point, $P_{max} = V_{max}J_{max}$. Inspection of equation (11) indicates that the ff is a measure of how great the VJ product is relative to the V_{oc} and J_{sc}.

Properties that can affect the fill factor include large uncompensated series resistances in the device, poor heterogeneous charge transfer kinetics, and for photoelectrochemical cells, concentration overpotentials due to inefficient mass transport of electroactive molecules to the junction interface. Uncompensated series resistances will result in significant potential drops in regions other than the depletion layer of the semiconductor. Poor charge transfer kinetics and large concentration polarizations will

result in the requirement of a large applied potential, or driving force, for the passage of current.

All of these effects can be represented as resistances in an equivalent circuit for the cell, and they will decrease the squareness of the illuminated I-V curve and hence reduce the fill factor. A simple way to think about the effects of these resistances is to realize that when current flows through a resistor, it heats up and dissipates power. Consequently, the larger the effect of these resistors, the larger the losses of energy that can be harvested in the form of currents and voltages.

VII. PHOTOELECTROLYSIS CELLS

A photoelectrolytic system is one in which a net chemical change occurs in the electrolyte. This change is in the form of the production of fuels from feedstocks. In this type of PEC, light is converted directly into chemical fuels, which can be harvested and utilized at a later time. The principles of operation of this type of cell are the same as those for regenerative electrolyte cells. The only difference is that there are effectively two redox couples in the electrolyte that act to accept and donate electrons.

The classic photoelectrolytic reaction is the splitting of water,[1] hence this specific electrolytic process will be used to illustrate the operation of a general photoelectrolytic cell. The minimum free energy required to split water is 1.23 eV. Photons of this energy or greater are abundant at the Earths surface. However, water does not absorb in this region and direct photoelectrolysis of water is not possible. A threshold energy of 6.5 eV is required for direct photodecomposition. Photons of this energy are not able to traverse the terrestrial atmosphere.[32]

The sequential photodecomposition of water is possible using appropriate homogeneous catalysts.[33] Additionally, under the correct energetic conditions

photoelectrolysis of water can be achieved with a semiconductor (see Chapter 6). Upon excitation of a carrier, the hole from the valence band can oxidize water to produce oxygen, and the electron can traverse the circuit and reduce water at the counter electrode to produce hydrogen. Figure 5 diagrams the processes involved in water photelectrolysis with a semiconductor. In this light, a semiconductor can be viewed merely as a catalyst for the water splitting reaction.

Two simple conditions must be met simultaneously for the photoelectrolysis cell to operate. The valence band of the semiconductor must be positive of the H_2O/O_2 redox potential, and the conduction band must be negative of the H_2O/H_2 redox potential.[34] These characteristics are required since the holes must be oxidizing enough to oxidize water and the electrons must have a high enough reduction potential to reduce water.

In principle an open circuit voltage slightly greater than 1.23 V is required for the photoelectrolysis. However, in practical systems the total redox potential difference must be great enough to overcome resistive losses and the overpotential losses of the oxygen evolution and hydrogen evolution reactions at the appropriate electrodes. Consequently, the bandgap of the material that can be utilized for this type of cell is restricted to the following condition.

$$E_g > (\Delta G_{rxn})/(nF) + q\eta_a + q\eta_c + iR \qquad (12)$$

η_a and η_c are the anodic and cathodic overpotentials respectively, i is the current flowing in the cell, and R is the uncompensated series resistance. Because of these requirements, only semiconductors with very large bandgaps (> 3eV) have been found to effectively photoelectrolyze water. Utilization of large bandgap semiconductors, however, is not practical for terrestrial applications since only a very small amount of the solar spectrum (the UV region) will generate the carriers

The I-V curves of photoelectrolytic cells will be similar to regenerative electrolyte PECs. In the dark, the Fermi level of the semiconductor may equilibrate with one of the redox couples or with a mixed potential, depending on the exchange current magnitudes. Under forward bias, electrons will be transferred to one or both redox systems, depending upon kinetics. Under illumination, electrons and holes will conduct the appropriate reduction and oxidation reactions respectively. If the junction allows the development of a V_{oc} greater than the sum of the voltages required to conduct the photoelectrolysis reaction, the anodic and cathodic overpotentials, and iR losses, the system is able to conduct the photoelectrolysis unaided by an external source. If the V_{oc} is not this large, an external source will be required to assist the photoelectrolysis reaction. (See Chapter 6.)

VIII. CHARGE TRANSFER

In PECs, since carrier transfer across the semiconductor/electrolyte interface results either in oxidation or reduction of molecules, the dynamics of electron transfer must be considered to quantitatively depict the charge transfer process. The model we will use to describe charge transfer will be a version of Marcus' electron transfer theory that has been modified to apply to heterogeneous electron transfer across a semiconductor/electrolyte interface.[35] It is outside the scope of this work to derive quantitatively the expression for electron transfer at semiconductor/electrolyte interfaces. Instead we will develop the expression semi-quantitatively and discuss the physical ramifications. Detailed reviews of the derivation are available in the literature.

For the sake of simplicity let us consider only electron transfer from the conduction band of an n-type semiconductor to the oxidized form of the redox couple. The rate of electron transfer written as a current density, J, is as follows:

$$J = q(k_{et})(n_s)C_{ox}(E) \qquad (13)$$

$C_{ox}(E)$ is the concentration of oxidized species whose distribution is a function of energy. n_S is the concentration of electrons at the surface, which is dependent on the band bending, k_{et} is the electron transfer rate constant, which is dependent on various geometric and molecular parameters. We must now describe explicitly the energy distribution of the oxidized molecules in solution, the concentration of surface electrons, and the rate constant.

In the electrolyte there will be a distribution of empty states (oxidized molecules) and filled states (reduced molecules) with which electron exchange can occur with the bands of the solid. Once an electron is accepted by the oxidized form or donated by the reduced form of the molecule, the solvent molecules must reorganize to stabilize the new ionic charge. This reorganization energy, λ, can be calculated using dielectric continuum theory. Figure 6 depicts the relevant energy level diagram. The electron transfer will occur when the energy level of the molecule is isoenergetic with the energy level of the electron in the semiconductor. In addition this transfer will occur at a rate faster than the motion of solvent molecules, therefore, the solvent shell around the molecule will reorganize after the electron transfer has occurred. Since for our example, we are interested in the overlap of the oxidized states with the conduction band of the semiconductor we can write the following expression for $C_{ox}(E)$.

$$C_{ox}(E) = C_{ox}\exp[-(\mathbf{E}^{0'}-\lambda-\mathbf{E}_{cb})^2/(4\lambda kT)][kT(\pi\lambda)]^{1/2} \qquad (16)$$

C_{ox} is the total concentration of oxidized molecules and the term in parentheses describes the overlap of the oxidized species with the conduction band edge. $\mathbf{E}^{0'}$ is the formal potential of the redox system. The expression for n_s involves the Boltzmann term.

$$n_s = N_c\exp[(\mathbf{E}_{cb}-\mathbf{E}(A/A^-))/kT] \qquad (17)$$

$(\mathbf{E}_{cb}-\mathbf{E}(A/A^-))$ is merely the barrier height.

The explicit expression for k_{et} involves the thermal velocity of electrons in the semiconductor, v_{th}, a reaction distance, δ, and a cross section for electron capture, σ.

$$k_{et} = \sigma\delta v_{th} \tag{17}$$

Consequently, the compete expression for J is

$$J = q\sigma\delta v_{th}[kT/\pi\lambda]^{1/2}N_cC_{ox}\exp[(\mathbf{E}_{cb}-\mathbf{E}(A/A^-))/kT]\exp[-(\mathbf{E}^{0''}-\lambda-\mathbf{E}_{cb})^2/(4\lambda kT)] \tag{18}$$

Expression (18) has been used to depict charge transfer at semiconductor/liquid interfaces for many years, despite the fact that many aspects of this expression have never been verified. No system has been shown to rigorously obey this expression. A reason for this is the fact that the primary impetus for study of semiconductor/liquid junctions has been practical applications, not fundamental studies. Additionally, few, if any, systems have been discovered that do not exhibit specific interactions, such as electrolyte adsorption, semiconductor corrosion, *etc.* However, it is instructive to examine charge transfer studies in light of the prevailing model.

In summary the work in this thesis addresses some of the important issues in the field of semiconductor photochemistry. The subjects discussed qualitatively in this chapter are dealt with more quantitatively in the following chapters. Especially interesting are the aspects of charge transfer at semiconductor/liquid junctions that are similar to or different from those at semiconductor/solid junctions. Whenever appropriate, direct comparisons between semicondutor/liquid and semiconductor/solid devices are made. These comparisons between relatively well characterized systems (semiconductor/solid) and poorly characterized systems (semiconductor/liqud) are extremely instructive.

REFERENCES

1. Honda, K.; Fujishima, A. *Nature*, **1972**, *238*, 37.

2. Finklea, H.O. ed. *Semiconductor Electrodes; Studies in Physical and Theoretical Chemistry*, Vol: 55, Elsevier: New York, 1988.

3a. Shneemeyer, L.F.; Wrighton, M.S. *J. Am. Chem. Soc.* **1977**, *101*, 6496. b) Gronet, C.M.; Lewis, N.S. *Appl. Phys. Lett.* **1983**, *43*, 115. c) Lewis, N.S. *Acc. Chem. Res.* **1990**, *23*, 176.

4. Nozik, A.J. *Nouv. J. Chem.* **1987**, *11*, 205.

5a. Parkinson, B. A.; Heller, A.; Miller, B. *J. Electrochem. Soc.* **1979**, *126*, 954. b) Tufts, B.J.; Abrahams, I.L.; Santangelo, P.G.; Ryba, G.N.; Casagrande, L.G.; Lewis, N.S. *Nature*, **1987**, *326*, 861.

6. Legg, K.D.; Ellis, A.B.; Bolts, J.M.; Wrighton, M.S. *Proc. Natl. Acad. Sci. USA*, **1977**, *74*, 4116.

7. Bolts, J.M.; Bocarsley, A.B.; Palazzotto, M.C.; Walton, C.G.; Lewis, N.S.; Wrighton, M.S. *J. Am. Chem. Soc.* **1977**, *101*, 1378.

8. Madou, M.J.; Morrison, S.R. *Chemical Sensing with Solid State Devices*, Academic: New York, 1989.

9. Al-Ekabi, H.; Serpone, N.; Pelizzetti, E.; Minero, C.; Fox, M.A.; Draper, R.B. *Langmuir*, **1989**, *5*, 250.

10. Nozik, A.J., Thacker, B.R.; Olson, J.M.; *Nature*, **1985**, *316*, 51.

11. Lewis, N.S. *Ann. Rev. Mater. Sci.* **1984**, *14*, 95.

12. Heller, A.; Miller, B; Thiel, F.A. *Appl. Phys. Lett.* **1981**, *38*, 282.

13. Licht, S.; Peramunage, D. *Nature*, **1990**, *345*, 330.

14. Gibbons, J.F.; Cogan, G.W.; Gronet, C.M.; Lewis, N.S. *Appl. Phys. Lett.* **1984**, *45*, 1095.

15. Serpone, N.; Borgarello, E.; Pelizzetti, E. in *Photocatalyisis and Environment; NATO ASI Series C: Mathematical and Phsical Sciences*, Vol 237; Schiavello, M. ed. Kluwer Academic; Dordrecht, 1988.

16. Kumar, A.; Rosenblum. M.D.; Gilmore, D.L. Tufts, B.J.; Rosenbluth, M.L.; Lewis, N.S. *Appl. Phys. Lett.* **1990**, *56*, 1919.

17. Heller, A.; Vadimsky, R.G.; *Phys. Rev. Lett.* **1981**, *46*, 1153.

18. Koval, C.A.; Howard, J.N. *Chem. Rev.*, in press.

19. Peter, L.M. *Chem. Rev.* **1990**, *90*, 753.

20. Lewis, N.S. *Ann. Rev. Phys. Chem.* **1991**, *42*, in press.

21. Gregory, R.P.F. *Photosynthesis*, Chapman and Hall: New York, 1989.

22. Calvin, M. in *Photochemical Conversion and Storage of Solar Energy*, J.S. Connoly ed. Academic: New York, 1981.

23. Katz, J.J. in *Photochemical Conversion and Storage of Solar Energy*, J.S. Connoly ed. Academic: New York, 1981.

24. Kittel, C. *Introduction to Solid State Physics*, 6th ed. John Wiley and Sons, New York, 1986.

25. Sze. S.M. *The Physics of Semiconductor Devices*, John Wiley and Sons: New York, 1981.

26. Bard, A.J.; Faulkner, L. *Electrochemical Methods: Fundamentals and Applications*, John Wiley and Sons: New York, 1980.

27. Sharma, B.L. *Metal-Semiconductor Schottky Barrier Junctions and their Applications*, Plenum Press: New York, 1984.

28. Kumar, A.; Lewis, N.S. *J. Phys. Chem.* **1990**, *94*, 6002.

29. Gartner, W.W. *Phys. Rev.* **1959**, *116*, 84.

30. Fonash, S.J. *Solar Cell Device Physics*, Academic Press: New York, 1981.

31. King, R.R.; Sinton, R.A.; Swanson, R.M. *Appl. Phys. Lett.* **1989**, *54*, 1460.

32. Chandra, S. *Photoelectrochemical Cells*, Academic: New York, 1985.

33. Lehn, J.M. in *Photochemical Conversion and Storage of Solar Energy*, J.S. Connoly ed. Academic: New York, 1981.

34. Nozik, A.J. *Ann. Rev. Phys. Chem.* **1978**, *29*, 198.

35. Gerischer, H. *Adv. Electrochem. Electrochem. Engnr.* **1961**, *1*, 139.

Figure 1: Depictions of band equilibration for n-type semiconductor/liquid junctions. a) and b) are the pre-equilibrated and equilibrated states, respectively, for a n-type semiconductor and a solution containing a redox couple with a redox potential that is positive of the semiconductor Fermi level. This results in the formation of a rectifying contact. c) and d) are the pre-equilibrated and equilibrated states, respectively, for a n-type semiconductor and a solution containing a redox couple with a redox potential that is negative of the semiconductor Fermi level. This results in an ohmic contact.

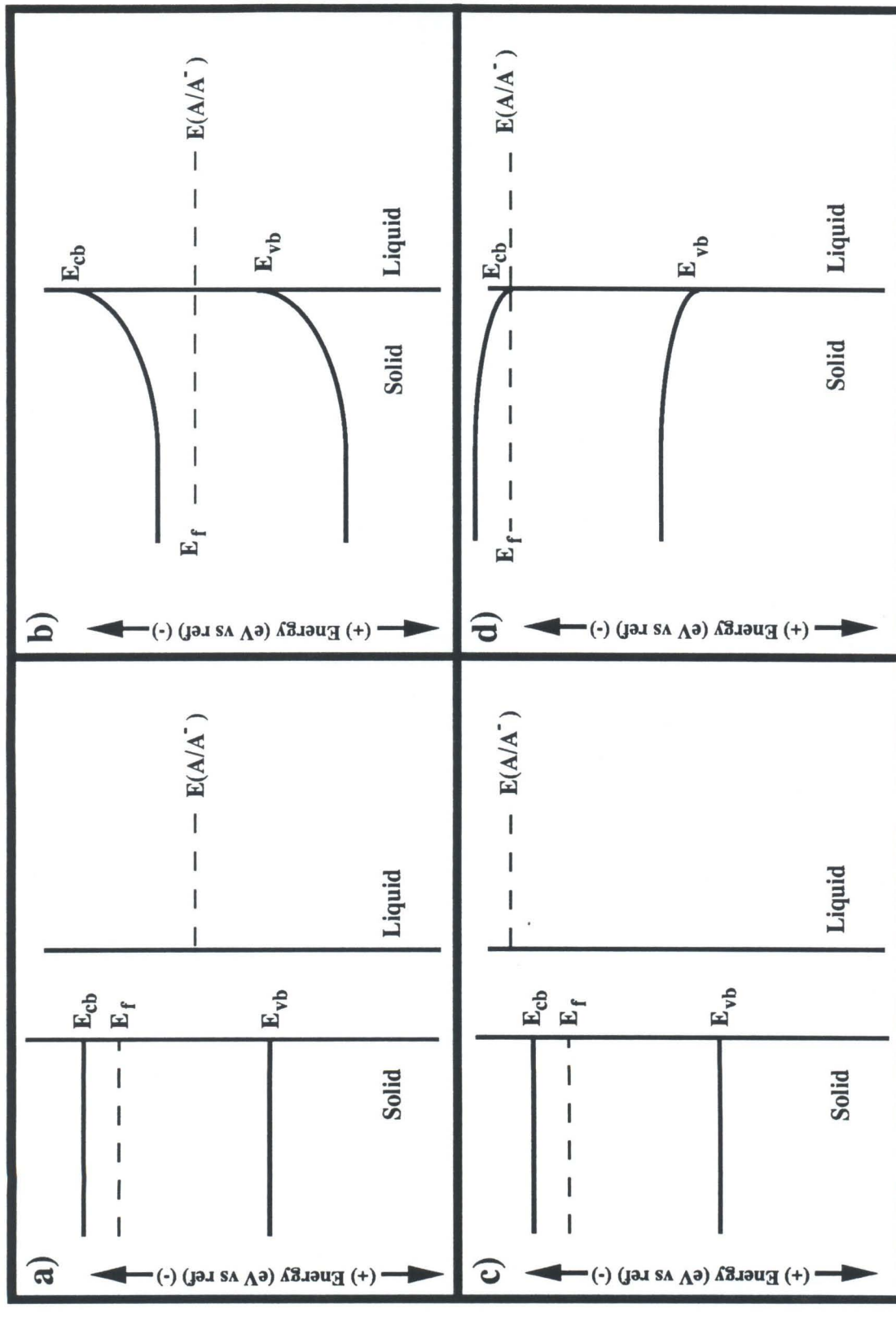
a)
(+) Energy (eV vs ref) (-)
E_{cb}
E_f
E_{vb}
Solid
Liquid
E(A/A⁻)
b)
(+) Energy (eV vs ref) (-)
E_{cb}
E_f
E_{vb}
Solid
Liquid
E(A/A⁻)
c)
(+) Energy (eV vs ref) (-)
E_{cb}
E_f
E_{vb}
Solid
Liquid
E(A/A⁻)
d)
(+) Energy (eV vs ref) (-)
E_{cb}
E_f
E_{vb}
Solid
Liquid
E(A/A⁻)

Figure 2: Depiction of band energetics and current-voltage properties for a rectifying junction. a) Short-circuit condition. b) Reverse bias. c) Forward bias. d) Current-voltage property showing appropriate band energetics.

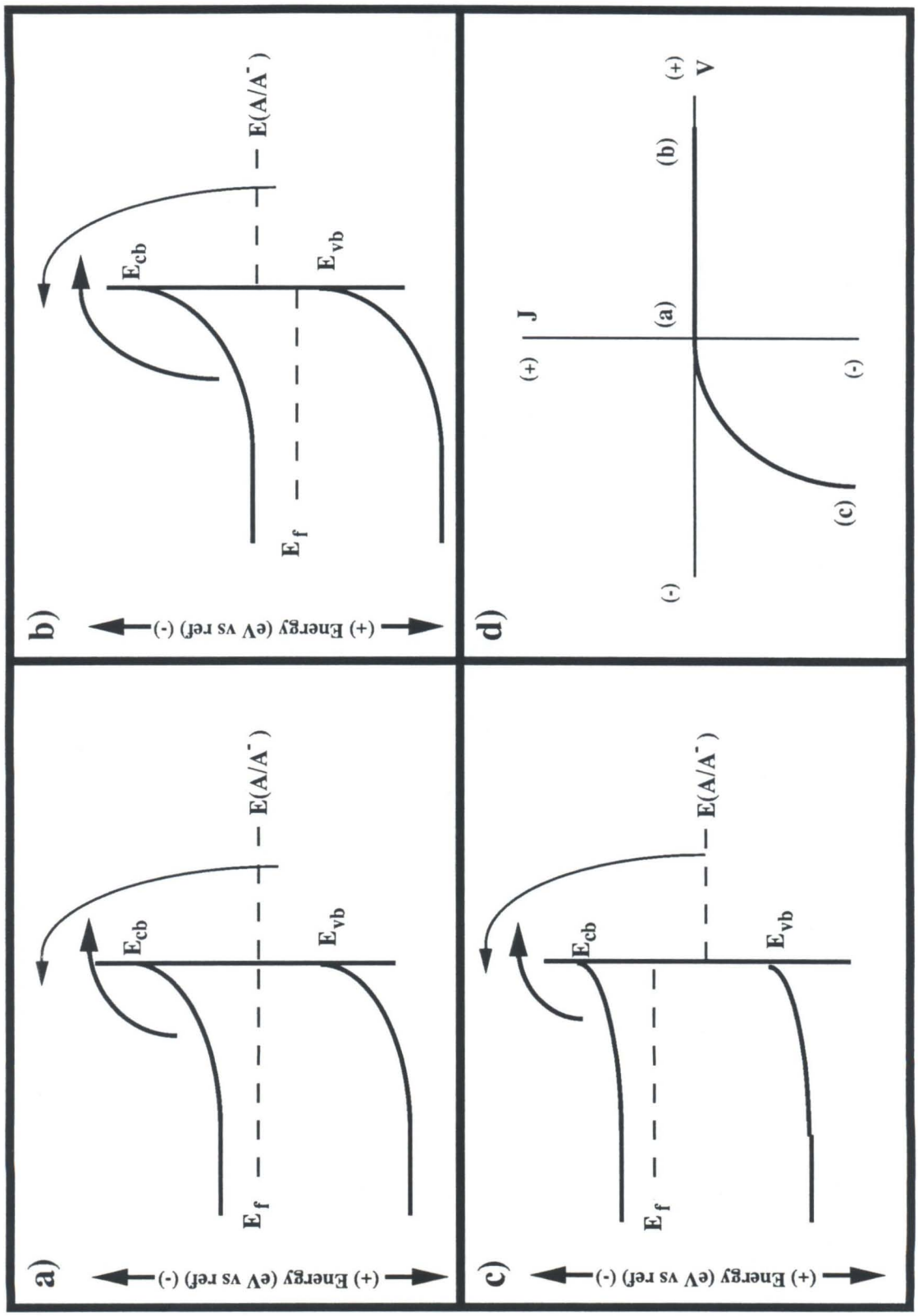
a)
b)
c)
d)
(+) Energy (eV vs ref) (-)
E(A/A⁻)
E_cb
E_vb
E_f
J
V
(+)
(-)
(a)
(b)
(c)

Figure 3: Photoelectrochemical cell and appropriate current-voltage curve under illumination. a) Schematic description of a photoelectrochemical cell operating under short-circuit conditions under illumination. In this n-type example upon carrier photogeneration, the holes are swept toward the interface where the oxidize A^- to A. Simultaneously the electrons are swept toward the back of the semiconductor where they traverse the circuit and reduce A to A^- at the counter electrode. Consequently, no net change in the electrolyte will occur. b) Current-voltage curve under illumination. The short circuit photocurrent, J_{sc}, open-circuit voltage, V_{oc}, maximum power, P_{max}, and fill factor are defined.

a)

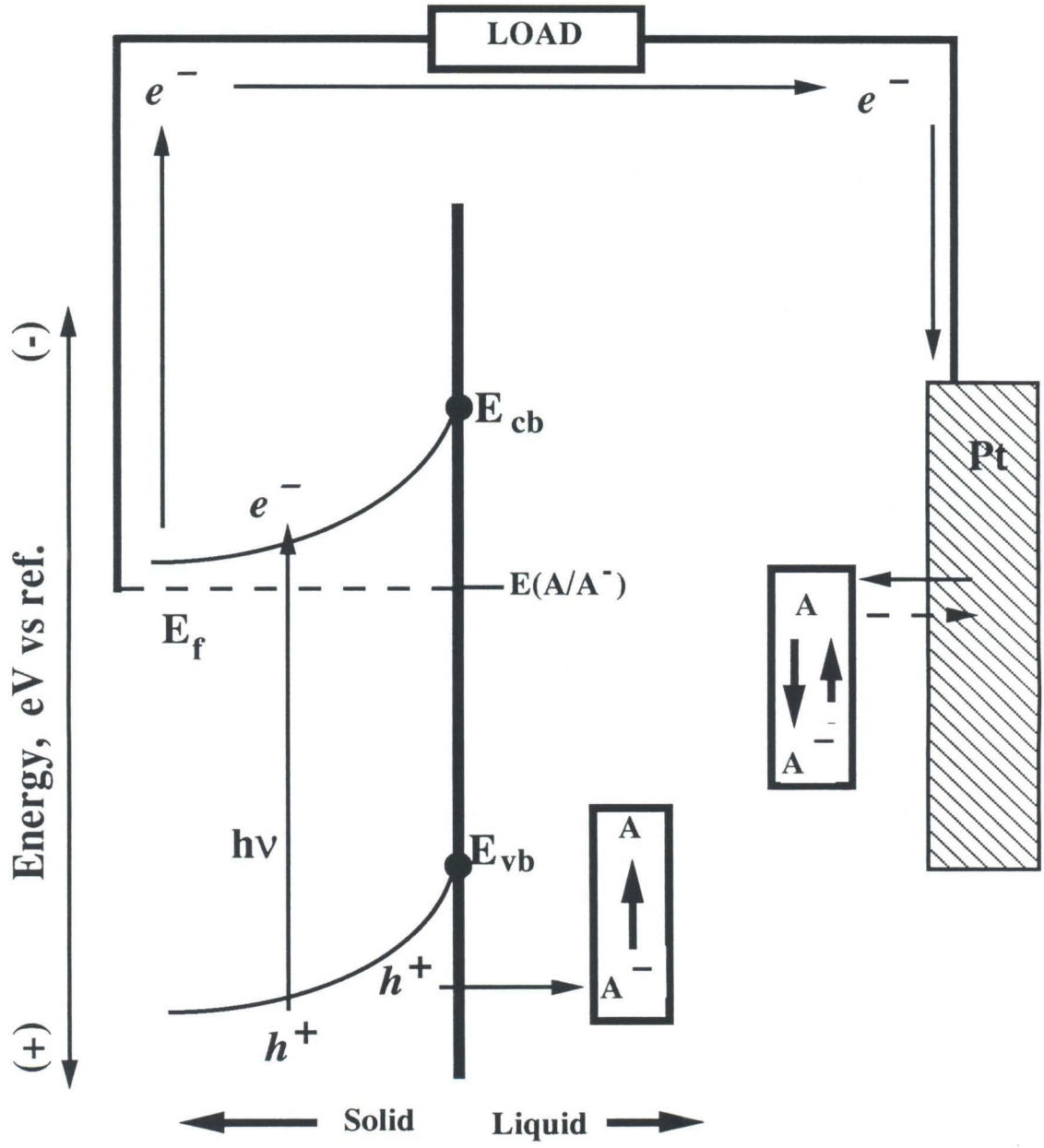
LOAD
e⁻
e⁻
(-)
Energy, eV vs ref.
(+)
E cb
e⁻
E(A/A⁻)
E f
hν
E vb
h⁺
h⁺
A
A⁻
A
A⁻
Pt
Solid
Liquid

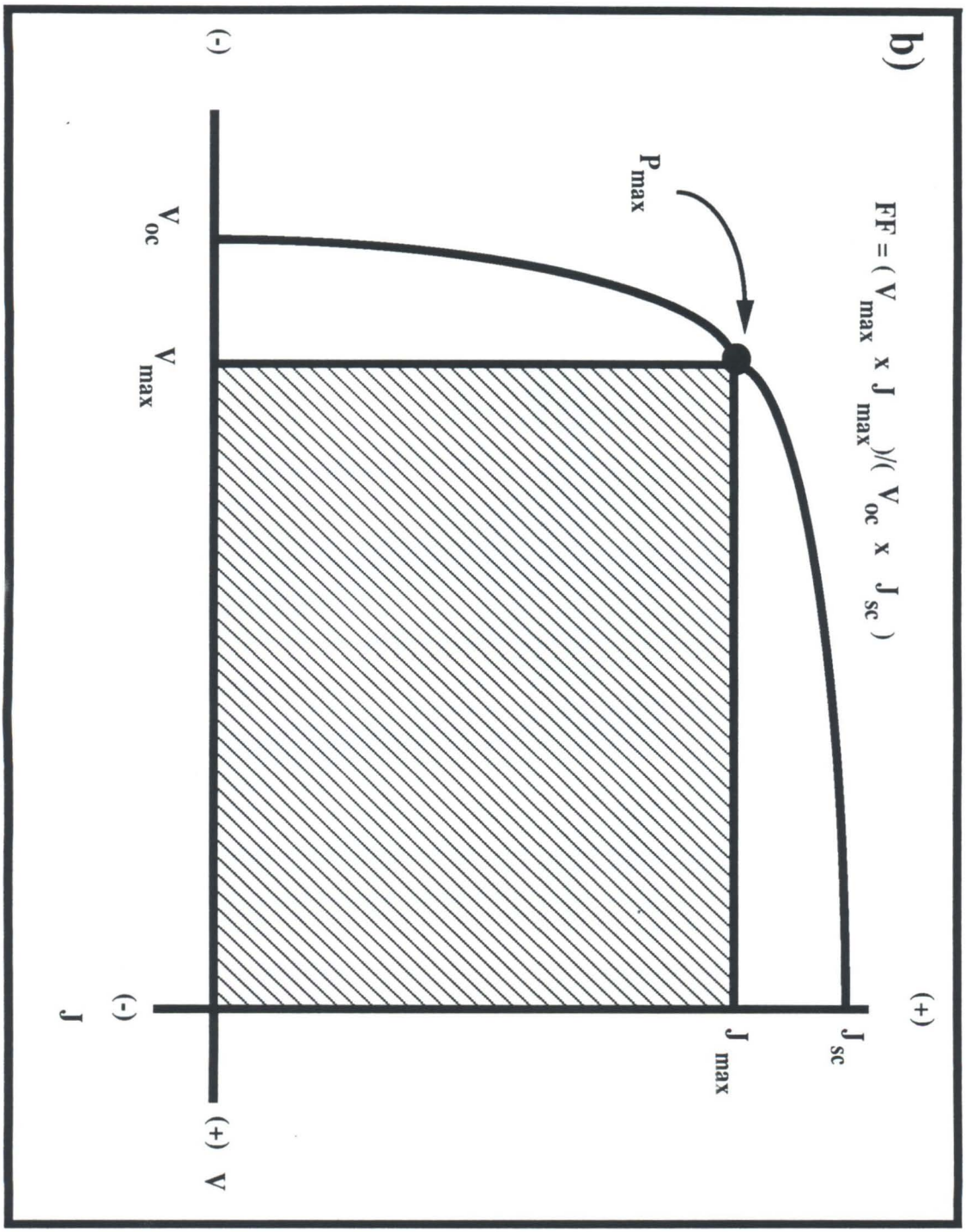
b)
FF = (V max x J max)/(V oc x J sc)
P max
V oc
V max
(-)
(+)
V
(-)
J
J max
J sc

Figure 4: Mechanisms contributing to the reverse saturation current. a) thermionic emission, b) tunneling through the barrier, c) surface-state recombination, d) recombination in the depletion layer, e) bulk-diffusion/ recombination.

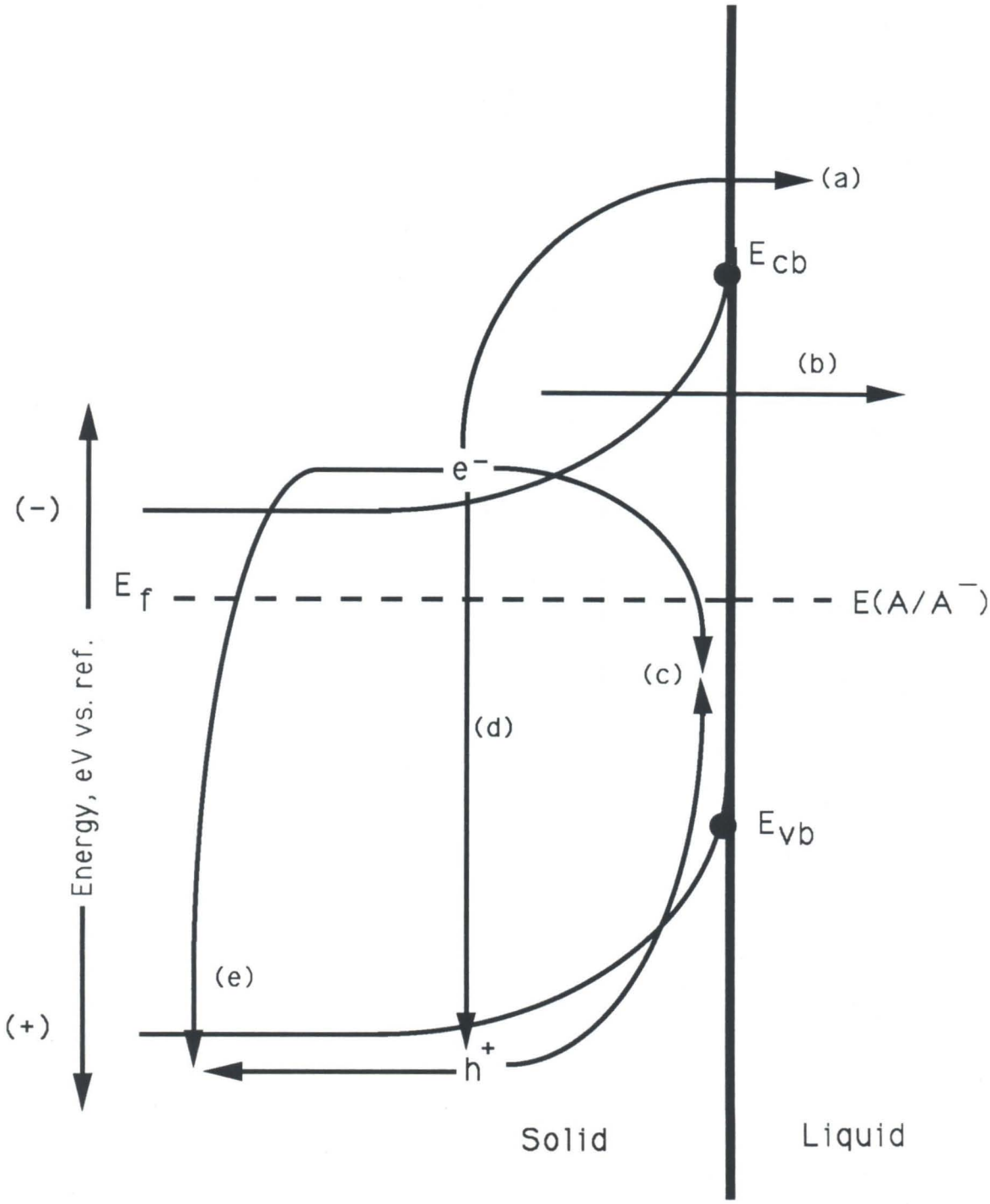
(a)
E_{cb}
(b)
e^-
(-)
E_f
$E(A/A^-)$
(c)
(d)
Energy, eV vs. ref.
E_{vb}
(e)
(+)
h^+
Solid
Liquid

Figure 5: Water photoelectrolysis cell. Upon carrier generation, the holes come to the semiconductor/liquid interface and oxidize water to oxygen. The electrons arrive at the Pt counter electrode and reduce water to hydrogen.

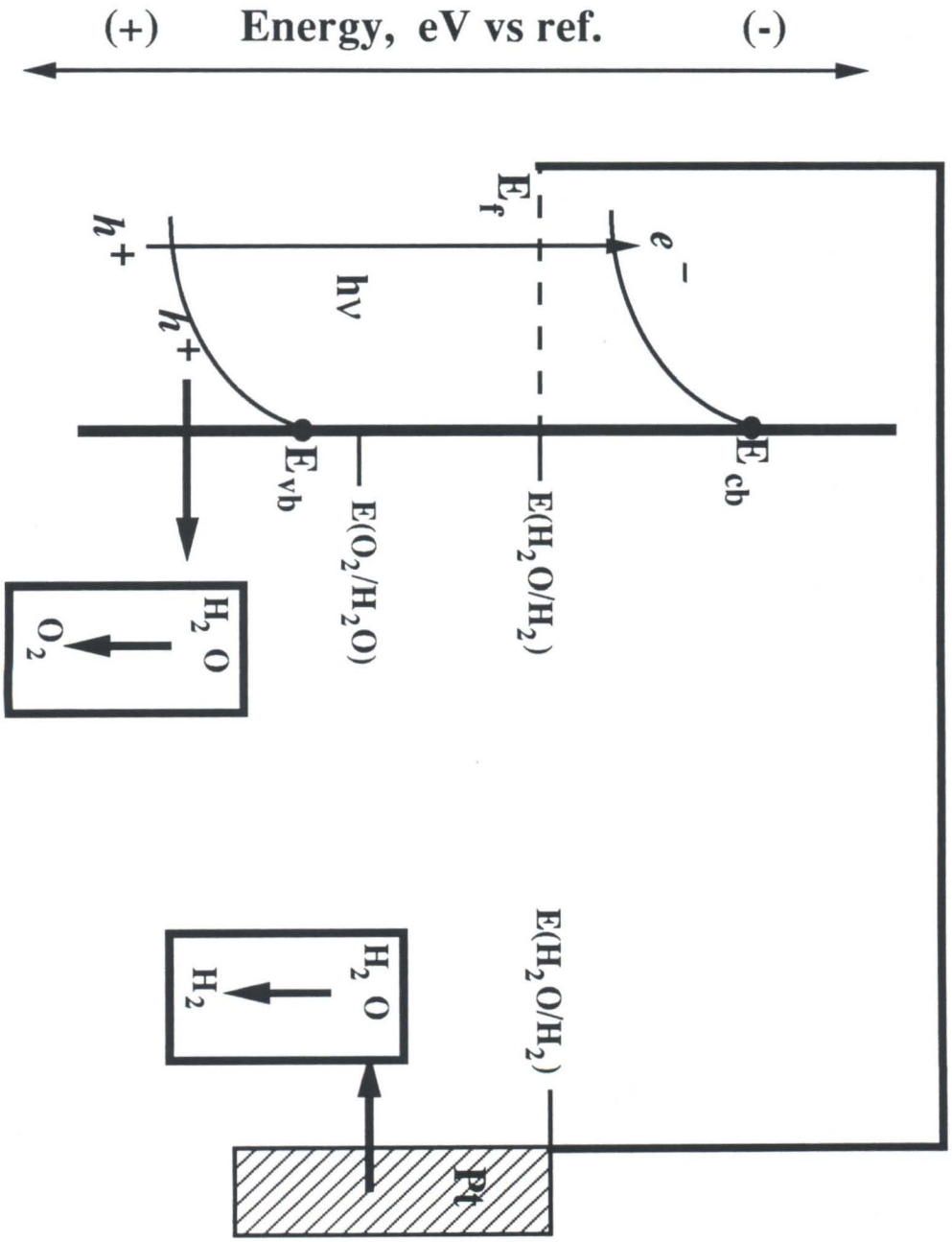
(+) Energy, eV vs ref. (-)
Solid
Liquid
h^+
h^+
hν
e^-
E_f
E_{vb}
E_{cb}
$E(O_2/H_2O)$
$E(H_2O/H_2)$
$E(H_2O/H_2)$
H_2O
O_2
H_2O
H_2
Pt

Figure 6: Gerischer model for charge transfer across a semiconductor/liquid junction. Overlap of the oxidized molecule and reduced molecule energy distributions with the appropriate bands are controlled by the reorganization energy, λ.

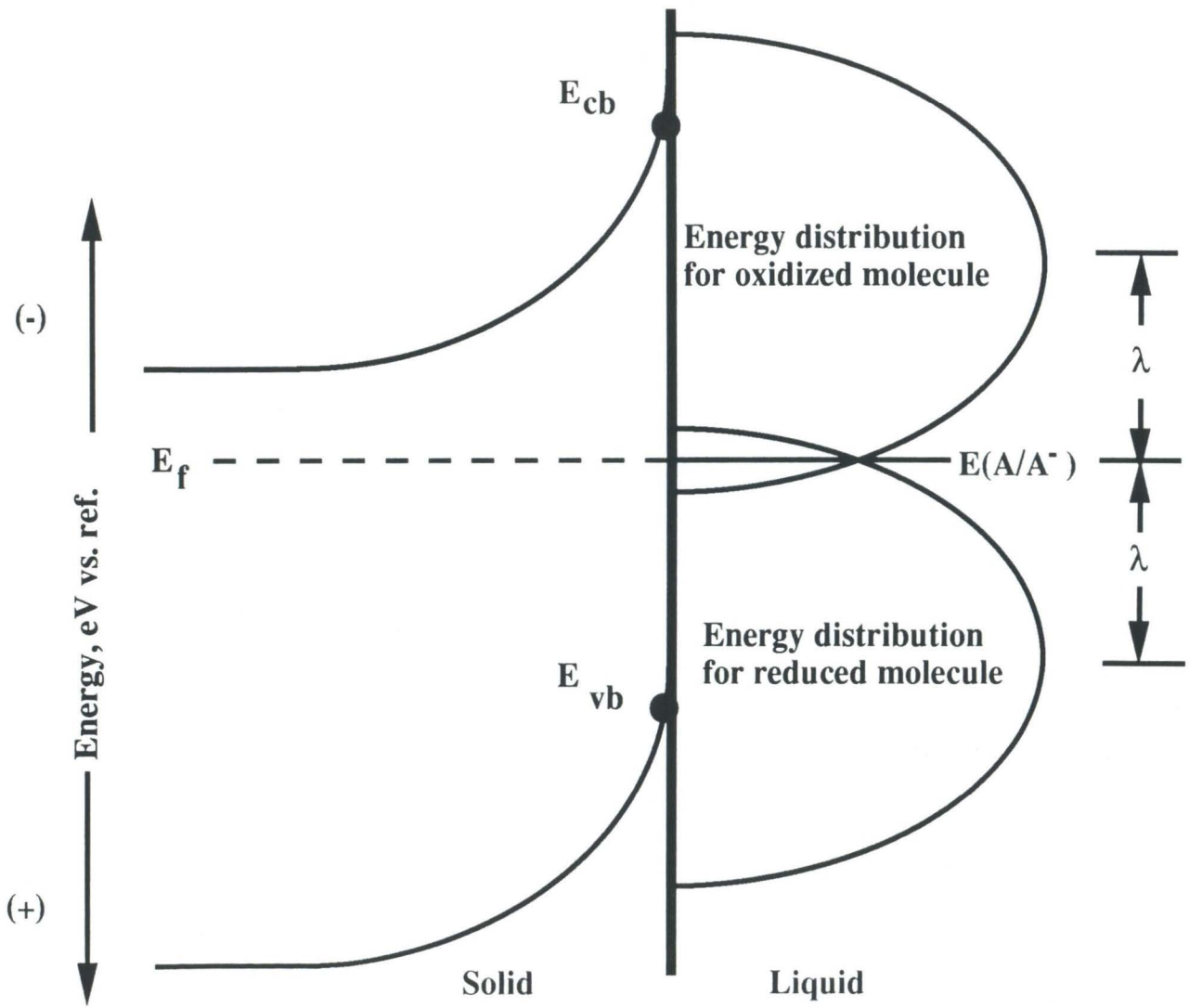
E cb
Energy distribution
for oxidized molecule
(-)
λ
E f
E(A/A-)
λ
Energy, eV vs. ref.
Energy distribution
for reduced molecule
E vb
(+)
Solid
Liquid

Charge Transfer Studies of Semiconductor Interfaces

Chapter 3: Short Wavelength Spectral Response Properties of Semiconductor/Liquid Junctions

Reprinted from The Journal of Physical Chemistry, 1990, 94.

Short-Wavelength Spectral Response Properties of Semiconductor/Liquid Junctions

Amit Kumar and Nathan S. Lewis*

Division of Chemistry and Chemical Engineering,† California Institute of Technology, Pasadena, California 91125 *(Received: December 11, 1989)*

We report the first measurements of photocurrent quantum yields for semiconductor/liquid junctions in the short-wavelength region of the spectrum (200–600 nm). The key feature of this wavelength region is the short penetration depth for the absorbed photon (less than 100 Å), which allows measurement of the majority carrier collection velocity. Spectra have been obtained for semiconductor/liquid, semiconductor/metal, and semiconductor/insulator/metal junctions. For all semiconductors studied (n-Si, p-Si, n-GaAs, n-InP, a-Si:H), the spectral responses of the liquid junctions showed higher quantum yields than the metal junctions, indicating greater majority carrier losses at the metal junctions. This general trend was independent of redox species, solvent, supporting electrolyte, and metal overlayer. The spectral response data can also be used to distinguish Schottky barrier behavior from electrocatalytic behavior of metal overlayers, and this approach has been used to study several semiconductor/metal film junctions in contact with electrolytes.

I. Introduction

One of the most important, but least understood, processes at a semiconductor/liquid interface is the rate of interfacial charge transfer. This process is key to understanding the behavior of semiconductor electrodes in corrosion reactions, in photoelectrochemical cells, and in chemical sensing devices.[1,2] Theoretical treatments of such systems predict that the interfacial rates will be sensitive to the concentration of solution redox species, to the solvent reorganization energies, to the driving force for electron transfer, and to the distance distribution of the redox species relative to the interface.[1,3] However, little rate data is available to date, because many stable semiconductor/liquid junctions do not exhibit kinetics that have interfacial electron transfer as the rate-determining step.[4]

One method to circumvent this difficulty is to take advantage of the wavelength-dependent photocurrent responses of illuminated semiconductor/liquid junctions. Long-wavelength spectral response data, which is based on the collection properties of photogenerated *minority carriers*, has been shown previously to provide valuable information on the bulk properties of the semiconductor and on the dimensions of the space charge region (Figure 1).[5-7] However, this type of data is not satisfactory for analyzing interfacial kinetic processes, and other information must be used. In order to obtain such information, small photon penetration depths must be employed. At sufficiently short wavelengths, the photogenerated carriers will be influenced both by the electric field gradient in the space charge layer and by the concentration gradient at the semiconductor/liquid interface. This leads to a wavelength-dependent *majority carrier* photocurrent, which can yield information about the interfacial kinetic prop-

* Address correspondence to this author.
† Contribution No. 8085.

(1) Morrison, S. R. *Electrochemistry of Semiconductor and Oxidized Metal Electrodes*; Plenum Press: New York, 1967.
(2) Finklea, H. O. *Semiconductor Electrodes*; Elsevier: Amsterdam, 1988.
(3) (a) Gerischer, H. In *Physical Chemistry, An Advanced Treatise*; Eyring, H., Henderson, D., Jost, W., Eds.; Academic Press: New York, 1973; Vol IXA, p 463. (b) Gerischer, H. *Adv. Electrochem. Electrochem. Eng.* **1961**, *1*, 139.
(4) Lewis, N. S. *Annu. Rev. Mater. Sci.* **1984**, *14*, 95.
(5) Gartner, W. W. *Phys. Rev.* **1959**, *116*, 84.
(6) (a) Tubbesing, K.; Meissner, D.; Memming, R.; Kastening, B. *J. Electroanal. Chem.* **1986**, *214*, 685. (b) Kautek, W.; Gerischer, H.; Tributsch, H. *J. Electrochem. Soc.* **1980**, *127*, 2491.
(7) Lastras-Martinez, A.; Raccah, P. M.; Triboulet, R. *Appl. Phys. Lett.* **1980**, *36*, 469.

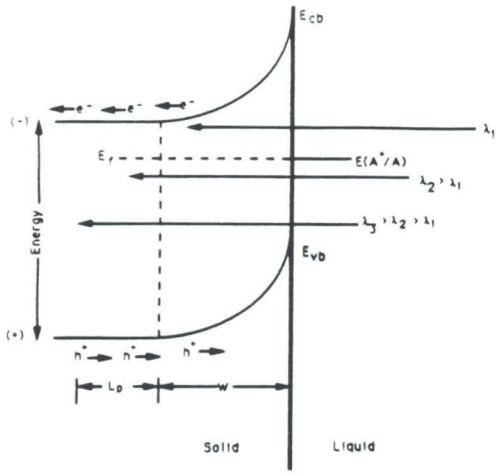

Figure 1. Schematic diagram of minority carrier collection at an illuminated semiconductor/liquid junction. When considering minority carrier photocurrents, the two most important quantities are the depletion width, W, and the minority carrier diffusion length, L_p. The minority carrier quantum yield vs wavelength data yields information about the magnitudes of W and L_p. No direct information regarding the interfacial properties is obtained.

erties.[8-10] This regime is the focus of the measurements described below.

To quantify these effects, we have collected short-wavelength spectral response data for a series of semiconductor junctions. Numerous differences in the steady-state current-voltage behavior of semiconductor/liquid, semiconductor/metal, and semiconductor/insulator/metal contacts have been proposed to arise from their differing majority carrier collection properties,[1-3,8-10] and the short-wavelength spectral response data should allow a direct assessment of this hypothesis. Additionally, the ability to quantify majority carrier collection rates should be useful in studies of semiconductor electrodes covered with thin metal films, in which ongoing controversy exists concerning the role of the metal overlayer in charge transport reactions.[11,12] We first describe the theory necessary to fit the experimental data and then present the results of our short-wavelength spectral response studies.

II. Theory

Spectral response measurements at small photon penetration depths differ in many respects from the conventional long-wavelength experiments. Generally, minority carriers produce the observed wavelength variation in the photocurrent properties, while currents due to photogenerated majority carriers are assumed to be negligible. The expression for the collected short circuit minority carrier photocurrent quantum yield, for an n-type semiconductor irradiated with light of wavelength λ, is given by the Gartner equation:[5]

$$\eta_{(\lambda),min} = 1 - \exp(-\alpha_{(\lambda)}W)/(1 + \alpha_{(\lambda)}L_p) \qquad (1)$$

In this equation $\eta_{(\lambda),min}$ is the internal quantum efficiency for minority carrier current flow at wavelength λ (i.e., the quantum yield based on collected minority carriers per absorbed photon),

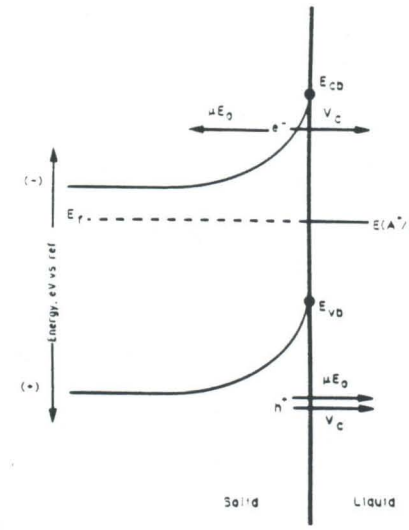

Figure 2. Schematic diagram depicting the processes affecting minority and majority carrier collection. At a depleted semiconductor junction, minority carriers are driven toward the interface both by the junction electric field and by the concentration gradient. Thus, the individual contributions of these two processes to the photocurrent cannot be resolved. For majority carriers, the electric field (μE_0) will drive majority carriers toward the bulk of the semiconductor, while the near-surface concentration gradient will drive them toward the interface where they may be collected with a velocity, v_c. The competition between these opposing effects can be determined by observing the decline in total quantum yield at short wavelengths.

$\alpha_{(\lambda)}$ is the absorption coefficient at wavelength λ, W is the depletion width, and L_p is the diffusion length of minority carriers (holes, in our n-type semiconductor example). Within this framework, use of smaller photon penetration depths, $1/\alpha_{(\lambda)}$, will yield increased collection of minority carriers and a consequent increase in internal quantum yield. However, no information regarding the minority or majority carrier interfacial kinetics is contained in the above treatment.

A closer examination of the photocurrent collection process reveals that the minority carrier concentration at the interface is influenced by two factors: the electric field at the interface, and the minority carrier concentration gradient at the interface. At a depleted semiconductor junction, the junction electric field and the carrier concentration gradient both tend to drive minority carriers toward the interface (Figure 2). Thus, the relative contributions of these two minority carrier collection processes cannot be separated by using the Gartner analysis of the spectral response vs wavelength data.

In contrast, for majority carriers, the electric field at a depleted interface will force the photogenerated carriers into the bulk of the semiconductor, while the near-surface carrier concentration gradient will tend to drive these carriers toward the junction (Figure 2). The competition between these opposing effects will produce a decline in internal quantum yield at very short photon penetration depths. Therefore, the short-wavelength spectral response properties of the majority carrier photocurrent should provide information regarding interfacial charge collection rates.

A quantitative derivation of this competition between the majority carrier electric potential and chemical potential gradients has been presented independently by Reichman[8] and by Green.[9,10] Both treatments resulted in an expression of the following form for the quantum yield of majority carriers moving across the interface, $\eta_{(\lambda),maj}$

$$\eta_{(\lambda),maj} = 1/|[1 + (v_d/v_c)][1 + (E_0/\alpha_{(\lambda)}V_t)]| \qquad (2)$$

where $v_d = \mu E_0$ is the majority carrier drift velocity, μ is the majority carrier mobility, E_0 is the maximum electric field strength

(8) Reichman, J. *Appl. Phys. Lett.* **1981**, *38*, 251.
(9) Shewchun, J.; Singh, R.; Green, M. A. *J. Appl. Phys.* **1981**, *52*, 5370.
(10) Green, M. A. *J. Appl. Phys.* **1976**, *47*, 547.
(11) (a) Degani, Y.; Sheng, T. T.; Heller, A.; Aspnes, D. E.; Studna, A. A.; Porter, J. D. *J. Electroanal. Chem.* **1989**, *228*, 167. (b) Heller, A.; Aharon-Shalom, E.; Bonner, W. A.; Miller, B. *J. Am. Chem. Soc.* **1982**, *104*, 6942.
(12) (a) Heller, A. *J. Phys. Chem.* **1985**, *89*, 2963. (b) Bockris, J. O'M.; Kainthla, R. C. *J. Phys. Chem.* **1985**, *89*, 2964. (c) Szklarczyk, M.; Bockris, J. O'M. *J. Phys. Chem.* **1984**, *88*, 1808. (d) Szklarczyk, M.; Bockris, J. O'M. *J. Phys. Chem.* **1984**, *88*, 5241.

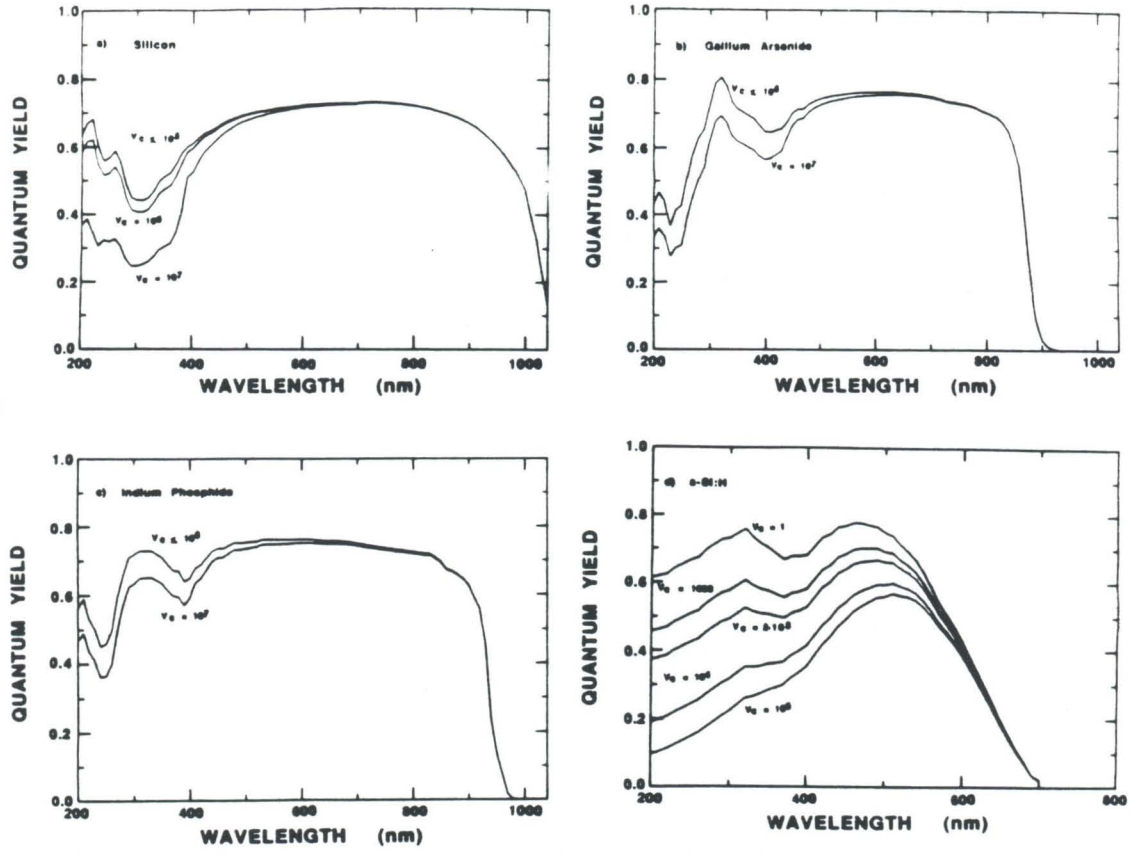

Figure 3. Simulated spectral responses as a function of collection velocity. The curves in this figure, and all subsequent curves, are based on eq 3 multiplied by $(1 - R_{(\lambda)})$, where $R_{(\lambda)}$ is the reflectivity at wavelength λ. Parameters used for these simulations are listed in Table I. Collection velocities are in units of cm/s. Note that the quantum yields as a function of collection velocity vary only in the short-wavelength regions. Also, for the high-mobility materials (Figure 3a–c), a large range in collection velocities is not distinguishable. For the low mobility material (Figure 3d), greater resolution of collection velocities is possible.

at the interface, and V_t is the thermal voltage ($V_t = kT/q$). The majority carrier collection velocity, v_c, is a direct quantitative measure of the interfacial majority carrier collection kinetics.

As defined above, the majority carrier photocurrent opposes the minority carrier photocurrent, so that the internal quantum yield for net photocurrent flow, $\eta_{(\lambda)}$, is obtained by subtracting eq 2 from eq 1:

$$\eta_{(\lambda)} = 1 - \exp(-\alpha_{(\lambda)}W)/(1 + \alpha_{(\lambda)}L_p) - 1/\{[1 + (v_d/v_c)][(1 + (E_0/\alpha_{(\lambda)}V_t)]\} \quad (3)$$

Note that the majority carrier internal quantum yield will become substantial only when $v_d \ll v_c$ and $E_0 \ll \alpha_{(\lambda)}V_t$. For semiconductors with a low majority carrier mobility (small v_d) and junctions with a high interfacial collection velocity, these conditions can be met by ensuring that the photon penetration depth in the semiconductor is small enough that $E_0/\alpha_{(\lambda)}V_t \ll 1$. Under these conditions, if the optical absorption and reflection properties of the semiconductor are known, and if the electric field in the semiconductor can be estimated, the variation in η with wavelength can be used to extract a value for v_c.

Figure 3a–d displays several predicted external quantum yield vs wavelength spectral response curves. These curves have been calculated by using a specific value of v_c in eq 3 and then converting the resultant internal quantum yield into an external quantum yield through multiplication by the factor $(1 - R_{(\lambda)})$, where $R_{(\lambda)}$ is the monochromatic reflectivity of the system at wavelength λ. In compiling these curves, known values for the absorption coefficient and majority carrier mobilities were taken from the literature.[13-16] Additionally, the monochromatic reflectivities for Si and a-Si:H were measured experimentally, while those for InP and GaAs were taken from the literature.[13,17,18] The structure observed in the short-wavelength region is due to the wavelength-dependent reflectivities of the particular interfaces.

TABLE I: Parameters Used for Spectral Response Simulations[a]

material	W, cm	L_p, cm	E_0, V/cm	v_d, cm/s
n-Si	7.8×10^{-5}	0.02	2.0×10^4	10^7
p-Si	4.4×10^{-5}	0.02	3.9×10^4	10^7
n-GaAs	8.7×10^{-4}	5.0×10^{-4}	2.3×10^3	6×10^6
n-InP	9.0×10^{-4}	2.0×10^{-4}	2.2×10^3	6×10^6
a-Si:H	6.0×10^{-4}	2.0×10^{-5}	5.0×10^4	2.3×10^3

[a] W, depletion width, calculated by using known dopant densities and assuming a barrier height of 1.0 V. L_p, hole diffusion length. E_0 maximum electric field strength, calculated by using known dopant densities and assuming a barrier height of 1.0 V. v_d, drift velocity.

(13) Aspnes, D. E.; Studna, A. A. *Phys. Rev. B* **1983**, *27*, 985.
(14) (a) Cody, G. D.; Wronski, C. R.; Abeles, B.; Stephens, R. B.; Brooks, B. *Solar Cells* **1980**, *2*, 227. (b) Abeles, B.; Wronski, C. R.; Tiedje, T.; Cody, G. D. *Solid State Commun.* **1980**, *36*, 537.
(15) Phillip, H. R.; Taft, E. A. *Phys. Rev.* **1960**, *120*, 37.
(16) Dash, W. C.; Newman, R. *Phys. Rev.* **1955**, *99*, 1151.
(17) Davey, J. E.; Pankey, T. *J. Appl. Phys.* **1964**, *35*, 2203.
(18) (a) Phillip, H. R.; Ehrenreich, H. *Phys. Rev.* **1963**, *129*, 1550. (b) Sturge, M. D. *Phys. Rev.* **1962**, *127*, 768. (c) Burkhard, H.; Dinges, H. W.; Kuphal, E. *J. Appl. Phys.* **1982**, *53*, 655.

Maximum electric field strengths were estimated based on known dopant concentrations and by using a barrier height at the interface of 1.0 V. This approximation does not significantly affect the value of v_c, since the maximum electric field is relatively insensitive to the value of the barrier height, and the ratio v_c/v_d is the quantity that is directly obtained from the short-wavelength spectral response fitting procedure. Further information regarding the values of the parameters used to simulate the curves of Figure 3 is given in Table I.

From the predictions of Figure 3, it is seen that, even at very small photon penetration depths, the decline in internal quantum yield is expected to be modest for high mobility ($\mu > 1 \times 10^3$ cm^2/(V·s)) semiconductors. This situation applies to samples of n-Si, p-Si, n-GaAs, and n-InP, where $v_d > 10^6$ cm/s at 300 K; thus the condition $v_d < v_c$ holds only when $v_c > 10^6$ cm/s. For $v_c < 10^6$ cm/s, no decline in external quantum yield is predicted, and the spectral response method only yields an upper limit on the value of the collection velocity. Physically, this can be understood by realizing that, for high mobility semiconductors, the driving force for movement of majority carriers into the bulk is so large that very few majority carriers reach the interface. Consequently, only when a large number of the carriers reaching the interface are collected will there be an observable perturbation on the total internal quantum yield. In contrast, for semiconductors with lower majority carrier mobilities, e.g., the a-Si:H alloys,[19] the spectral response method results in a larger range over which v_c can be determined quantitatively, because a significantly larger number of carriers reach the interface, and moderate collection results in observable perturbations on the total quantum yield. In a-$Si_{0.9}$:$H_{0.1}$, $v_d \approx 2 \times 10^3$ cm/s; therefore, collection velocities as low as 10^3 cm/s can be quantitatively determined for this semiconductor.

III. Experimental Section

A. Electrode Materials and Preparation. Silicon electrodes were fashioned from polished wafers of phosphorus-doped, 3 ohm-cm resistivity n-type Si or 2.45 ohm-cm boron-doped p-type Si. The wafers were single-crystal, (100)-oriented material from Monsanto Corp. Ohmic contact to the back surface of the n-type material was made by rubbing Ga:In eutectic onto the sample. Ohmic contact to the p-Si was made by a 1000-Å Au evaporation followed by a forming gas anneal for 10 min at 500 °C. n-GaAs samples were 10–15 μm thick epilayers, doped with 2×10^{17} cm^{-3} Se, on an n$^+$-GaAs substrate (oriented 2° off of (100)). The samples were grown by MOCVD at Varian Associates (Palo Alto, CA). Ohmic contact to the back surface was made by thermal evaporation of 1000 Å of 4% Ge–96% Au alloy, followed by an anneal under forming gas at 475 °C for 5 min. Sn-doped (1.7×10^{17} cm^{-3}) (100) oriented n-InP samples were obtained from Crysta Comm. Inc. (Mountain View, CA). Ohmic contacts were made by rubbing Ga:In eutectic onto the back of the electrode surface. The a-Si:H samples consisted of a 200-Å n$^+$ amorphous Si:H layer deposited on a stainless steel substrate, followed by a 0.6-μm layer of undoped a-$Si_{0.9}$:$H_{0.1}$ The samples were prepared by rf decomposition at HT Products, Inc. by H. Wiesmann, and have been described in more detail previously.[20] All electrodes were cut into squares approximately 4 mm on each side and attached to a Cu wire with Ag epoxy, and all metal surfaces were insulated from the electrolytes with ordinary epoxy.

Si and a-Si:H electrodes were etched for 10 s in 49% aqueous HF (semiconductor grade), washed with H_2O, then washed with CH_3OH, and dried in a stream of N_2. For GaAs and InP electrodes, the etching procedure consisted of a repetitive cycle as prescribed by Aspnes and Studna.[21] In each cycle, the GaAs or InP was exposed to 1.0 M KOH for 15 s, rinsed with H_2O, dried with N_2, exposed to 0.05% Br_2–CH_3OH for 15 s, rinsed with CH_3OH, and then dried with N_2. This cycle was repeated three times and was concluded with a 15-s immersion in 1.0 M KOH followed by a rinse with H_2O and drying in a stream of nitrogen.

Schottky diodes were fabricated by thermal evaporation of the metal from a W filament. Sources consisted of 99.999% Au, 99.99% Pd, and 99.99% Ni. Approximately 100 Å of the desired metal (as determined by a quartz crystal thickness monitor) was deposited, at a base pressure of $<5 \times 10^{-6}$ Torr, onto the appropriate semiconductor sample. For measurement of the absorption and reflection properties of the metal overlayer, an equivalent amount of metal was evaporated simultaneously onto a quartz slide, which was used for subsequent optical transmission and reflectance studies.

The n-type Si and a-Si:H MIS devices were fabricated by electrochemically cycling the silicon sample in a solution of 50 mM dimethylferrocene, 5 mM dimethylferrocenium, and 1.0 M $LiClO_4$ in CH_3OH.[22] During potentiostatic cycling, a few milliliters of 0.1 M $LiOCH_3$ (dissolved in CH_3OH solvent) was added to the electrolyte. The electrode was held at short circuit vs a Pt reference electrode in the cell solution. Short circuit photocurrent densities were in the range of 10–20 mA/cm^2. The open circuit voltage was monitored periodically until it had decreased by 0.12 V from its initial value. Rigorously dry solvent and electrolyte were not necessary for this procedure to be successful. The electrode was then removed, washed with CH_3OH, and dried under a stream of N_2. This was followed by evaporation of 100 Å of Au, as described above for Schottky barrier structures.

Pd overlayers on p-Si were photoelectrochemically plated from a deoxygenated solution of 10^{-5} M $Pd(NO_3)_2$ in 1.0 *M* aqueous perchloric acid. Care was taken to ensure that the solutions contained minimal concentrations of halide ions. Plating was conducted potentiostatically, without voltage scanning, at −1.55 V vs a mercuric nitrate reference electrode (−1.1 V vs SCE) and the illumination level was adjusted to maintain photocurrent densities of 25–70 μA/cm^2. At this current density no macroscopic bubbles of H_2 were observed. The amount of cathodic charge passed for different samples was 0.043 and 0.19 C/cm^2. Upon completion of plating, the electrode was removed from the solution and was immersed in a fresh 1.0 M $HClO_4$(aq) solution to examine the catalytic behavior of the overlayer. Typical reductions in overpotentials for hydrogen evolution were 0.4–0.6 V when compared to the *I–V* behavior of HF-etched p-Si electrodes in the same electrolyte.

B. Solvents and Materials. All solvents except CH_3CN were prepared and dried as described previously.[23] CH_3CN was pretreated with 3Å molecular sieves, dried over CaH_2, and then distilled from P_2O_5 under dry N_2. The collected solvent was stored over 3Å molecular sieves in an inert atmosphere glovebox. The preparation and purification of all redox couples and electrolytes used in this work have been described previously.[23] Except where described otherwise, all electrolytes were prevented from contact with ambient air by use of conventional Schlenk techniques.

C. Optical Techniques. Spectral response measurements were taken under potentiostatic control of the working electrode, which was held at short circuit vs the redox potential of the cell or held at a desired potential with respect to an SCE reference electrode. The cell was a Pyrex vessel with a quartz flat (Suprasil W) used as the bottom of the cell. Optical transmission through the quartz was determined to be 90–95% from 200 to 1040 nm. The distance between the flat and the electrode surface was as small as possible, and was always <1 mm. Under these conditions, the uncorrected optical transmittance losses through the cell and redox species

(19) (a) Swartz, G. A. *J. Appl. Phys.* **1982**, *53*, 712. (b) Gutkowicz-Krusin, D.; Wronski, C. R.; Tiedje, T. *Appl. Phys. Lett.* **1981**, *38*, 87. (c) Gutkowicz-Krusin, D. *J. Appl. Phys.* **1981**, *52*, 3370. (d) Wronski, C. R.; Abeles, B.; Cody, D. *Solar Cells* **1980**, *2*, 245.

(20) Gronet, C. M.; Lewis, N. S.; Cogan, G. W.; Gibbons, J. F.; Moddel, G. R.; Wiesmann, H. *J. Electrochem. Soc.* **1984**, *131*, 2873.

(21) Aspnes, D. E.; Studna, A. A. *Appl. Phys. Lett.* **1985**, *46*, 1071.

(22) (a) Gronet, C. M. Lewis, N. S.; Cogan, G.; Gibbons, J. *Proc. Natl. Acad. Sci. USA* **1983**, *80*, 1152. (b) Kumar, A.; Rosenblum, M. D.; Gilmore, D. L.; Tufts, B. J.; Rosenbluth, M. L.; Lewis, N. S. *Appl. Phys. Lett.* **1990**, *56*, 1919.

(23) (a) Rosenbluth, M. L.; Lewis, N. S. *J. Am. Chem. Soc.* **1986**, *108*, 4689. (b) Tufts, B. J.; Abrahams, I. L.; Casagrande, L. G.; Lewis, N. S. *J. Phys. Chem.* **1989**, *93*, 3260. (c) Lewis, N. S. *J. Electrochem. Soc.* **1984**, *131*, 2498. (d) Casagrande, L. G.; Lewis, N. S. *J. Am. Chem. Soc.* **1985**, *107*, 5793.

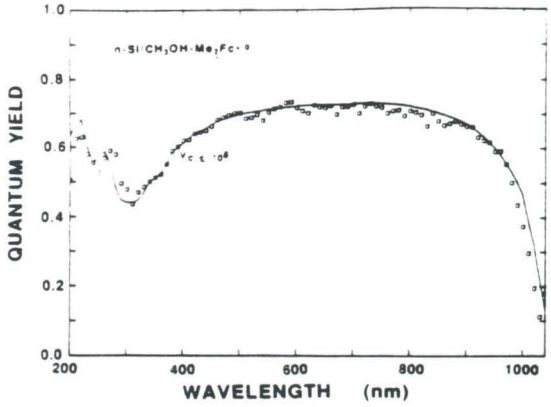

Figure 4. Spectral response of the n-Si/CH_3OH–1.0 M $LiClO_4$–dimethylferrocene$^{+/0}$ junction. The solid line is the best fit to eq 3, from which the collection velocity for these systems was extracted. Over the Me_2Fc^+ concentration range of 0.1–0.001 mM, no distinguishable differences were observed in the spectral response.

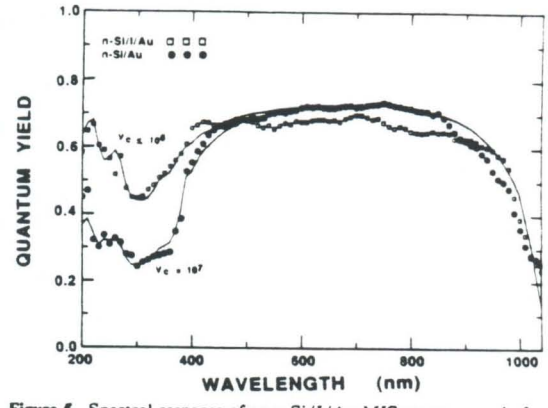

Figure 5. Spectral response of an n-Si/I/Au MIS structure and of an n-Si/Au Schottky diode. The response of the MIS junction was indistinguishable from that of the liquid junction in Figure 4. However, the Schottky structure displayed poor quantum yields in the UV, indicating higher majority carrier losses.

were less than 5% for all wavelengths and redox concentrations employed.

A three-electrode arrangement was used in all studies. The reference electrode was a Pt wire poised at the cell potential or was an SCE, and the counter electrode was a large area (2 cm^2) Pt foil. The spectral response system has been described earlier,[23b] except that the W lamp was replaced with a 150-W Xe arc lamp (Oriel Corporation, Stratford, CT) in order to obtain sufficient intensity in the short-wavelength region. Also, when using a calibrated photodiode to measure the monochromatic light intensities for runs involving the liquid junction cells, a Suprasil W window, identical with that at the bottom of the cell, was placed in front of the photodiode. This corrected for the absorption and reflection due to the optical window of the cell. Reflectance measurements for Si and a-Si:H were made using the same optical apparatus, by measuring the intensity of monochromatic light reflected off the appropriate surface.

IV. Results and Discussion

A. Silicon. Figure 4 displays the spectral response of the n-Si/CH_3OH–1.0 M $LiClO_4$–0.1 mM dimethylferrocene (Me_2Fc)–0.001 mM Me_2Fc^+ interface over the wavelength range 200–1040 nm. For comparison, Figure 5 depicts the spectral response of an n-Si/Au Schottky barrier and of an n-Si based MIS diode, respectively. The solid lines in Figures 4 and 5 represent best fits to the data by using the theory described in section II, with v_c the only adjustable parameter. The MIS and semiconductor/liquid junction data yielded excellent fits with $v_c \leq 10^6$ cm/s (i.e., $v_d \gg v_c$), while the n-Si/Au Schottky barrier data yielded $v_c = 10^7$ cm/s. A value of $v_c = 10^7$ cm/s was also obtained from the spectral response data for an n-Si/Ni Schottky diode. These data clearly show the differences in majority carrier collection properties of the various junctions.

The $v_c = 10^7$ cm/s value obtained for the n-Si/Au and n-Si/Ni junctions is in agreement with previous experimental results[24a] and with the well-documented electron collection velocity at n-Si/metal interfaces, as determined by conventional current–voltage methods.[24] This agreement provides a useful check on the validity of the spectral response analysis used in this work. This agreement between theory and experiment also indicates that the literature absorption coefficient data is accurate in this wavelength region and that the absorptivity of the semiconductor is not substantially altered by electroabsorption effects at the junctions of interest. The quantum yield data in Figures 4 and 5 indicate that the MIS and semiconductor/liquid interfaces both exhibit smaller majority carrier collection velocities than the Schottky barriers, and this observation is consistent with the superior I–V properties displayed by photovoltaic-type cells based on the non-Schottky systems.[22,23] Unfortunately, the high electron mobility for n-Si precludes a quantitative comparison of the collection velocities for these low v_d/v_c systems.

If interfacial electron transfer to dissolved redox species at the semiconductor/liquid junction were rate-determining for majority carrier collection, one might expect to observe increased currents as the majority carrier acceptor concentration is increased.[1] Therefore, a possible explanation for the low v_c in the n-Si/CH_3OH–$Me_2Fc^{+/0}$ system is the relatively low concentration of Me_2Fc^+ in the electrolyte. Variation in the concentration of Me_2Fc^+ from 0.001 to 0.1 mM yielded no change in spectral response properties of the n-Si/CH_3OH $Me_2Fc^{+/0}$ interface, and accurate quantum yield measurements at higher Me_2Fc^+ concentrations were not possible due to the intense optical absorption of Me_2Fc^+ in the 200–400-nm region. The lack of change in spectral response properties with increasing [Me_2Fc^+] either means that v_c did increase, but remained $\leq 10^6$ cm/s, or that the majority carrier capture process was not dominated by direct electron transfer to dissolved solution redox species. We cannot distinguish between these two possibilities from the spectral response data. Efforts to produce a lower equilibrium barrier height (and therefore lower E_0) by changing the redox system from $Me_2Fc^{+/0}$ to methylviologen$^{2+/+}$ also yielded no change in the internal quantum yield spectral response properties, indicating that v_c in this system was also $\leq 10^6$ cm/s. Similar behavior, with $v_c \leq 10^6$ cm/s, was also obtained from spectral response data on p-type Si photocathodes in the CH_3CN-0.70 M $LiClO_4$–0.001 mM cobaltocenium$^+$–0.0001 mM cobaltocene electrolyte. From this data, it is clear that the Si/liquid junction has a small short circuit majority carrier collection velocity under many experimental conditions, and this observation is consistent with the excellent open circuit voltages displayed by regenerative photoelectrochemical cells using these same liquid junctions.[25] We also note that, by taking advantage of the surface sensitivity of the short-wavelength photons, the n-Si/CH_3OH–$Me_2Fc^{+/0}$ data illustrates that the spectral response method can provide some information on magnitude of interfacial rate processes even when bulk recombination processes determine the steady-state current–voltage properties.[23]

B. n-GaAs and n-InP Junctions. Figures 6 and 7 depict the spectral response data for n-GaAs/1.0 M KOH–0.0003 mM

(24) (a) Gutkin, A. A.; Dmitriev, M. V.; Khait, V. M. *Sov. Phys. Semicond.* **1977**, *11*, 290. (b) Sze, S. M. *Physics of Semiconductor Devices*, 2nd ed.; Wiley: New York, 1981.

(25) (a) Gibbons, J. F.; Cogan, G. W.; Gronet, C. M.; Lewis, N. S. *Appl. Phys. Lett.* **1984**, *45*, 1095. (b) Lieber, C. M.; Gronet, C. M.; Lewis, N. S. *Nature (London)* **1984**, *307*, 533.

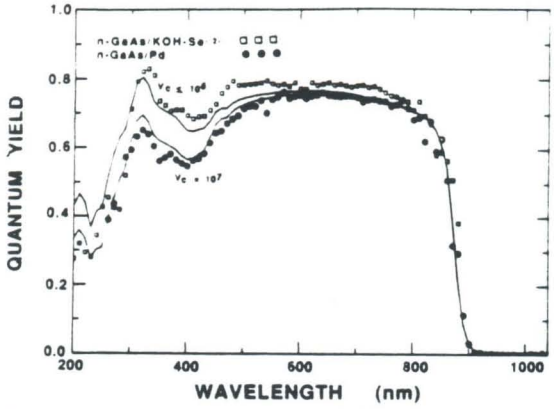

Figure 6. Spectral response of an n-GaAs/1.0 M KOH–1.0 M K_2Se–0.1 M K_2Se_2 system, along with that for an n-GaAs/Pd Schottky device. The lower quantum yields for the Schottky device indicate a much higher majority carrier collection velocity at the metal interface than at the liquid interface. Additionally, etched n-GaAs surfaces and Ru(III)-, Rh(III)-, Co(III)-, or Os(III)-treated n-GaAs electrodes in aqueous 1.0 M KOH–$Se^{-/2-}$ and etched or Ru(III) treated electrodes in 1.0 M KOH–$Te^{-/2-}$ yielded the same response as that of the n-GaAs/CH_3CN junction and the n-GaAs/KOH–$Se^{-/2-}$ junction.

Se^-–0.003 mM–Se^{2-}, n-GaAs/Pd, and n-InP/CH_3OH–$Me_2Fc^{+/0}$ junctions, respectively. As was the case for n-Si, the extremely high electron mobility in GaAs and InP severely limits the range over which v_c can be quantitatively determined. However, despite this restriction, clear distinctions can be seen between the collection properties of the semiconductor/metal junctions and the semiconductor/liquid interfaces. The n-GaAs/Pd Schottky barrier (Figure 6) yielded $v_c = 10^7$ cm/s, which is in agreement with the value expected from I–V measurements of such diodes.[24] Similar spectral response data, with $v_c = 10^7$ cm/s, was also observed for an n-GaAs/Au Schottky diode. In contrast, the data for the n-GaAs/liquid contact (Figure 6) and for the n-InP/liquid contact (Figure 7) yielded $v_c \leq 10^6$ cm/s. This data is again consistent with the improved photovoltaic performance of the n-GaAs and n-InP liquid junctions relative to that of Schottky contacts. No n-InP/metal contacts were examined by the spectral response method since they were found to be nonrectifying.[26]

Several redox systems were investigated in order to possibly obtain higher ($>10^6$ cm/s) majority carrier collection velocities; however, no suitable systems were found. n-GaAs/CH_3CN–$Fc^{+/0}$ junctions[23d] and etched and metal ion treated (Ru(III), Rh(III), Os(III), Co(III)) n-GaAs surfaces[23b] in aqueous 1.0 M KOH–0.003 mM K_2Se were found to display spectral response properties that were identical with those in Figure 6 for the n-GaAs/KOH–$Se^{-/2-}$ interface. Similar spectral response behavior was observed for both etched or Ru(III)-treated n-GaAs electrodes in aqueous 1.0 M KOH–0.001 mM K_2Te, and a response indistinguishable from that in Figure 7 was obtained for n-InP/CH_3CN–ferrocene$^{+/0}$ junctions. In contrast, both of the n-GaAs Schottky barriers investigated yielded $v_c = 10^7$ cm/s, underscoring the general differences between the two types of systems with respect to majority carrier collection properties.

C. a-Si:H Junctions. The low electron mobility in amorphous hydrogenated silicon is a well-documented drawback to fabrication of optimized p–n homojunction solar cells;[19d] however, this low μ_e makes a-Si:H quite useful for measurement of v_c in the range 10^3–10^7 cm/s. Figure 8 depicts the spectral response of the a-$Si_{0.9}$:$H_{0.1}$/CH_3OH–1.0 M $LiClO_4$–0.1 mM Me_2Fc–0.001 mM Me_2Fc^+ interface, along with the properties of an a-Si:H/Pd Schottky diode and an a-Si:H MIS diode.

The ability to distinguish between the responses of all three devices is due to the small drift velocity of electrons in the a-Si:H alloy. The spectral response of the a-Si:H/Pd Schottky barrier was fit by using $v_c = 10^6$ cm/s. The low quantum yields for the a-Si:H/Pd Schottky device are in agreement with previous measurements on similar devices.[19] The data for the MIS device yielded $v_c = 10^4$ cm/s, and the smallest collection velocity was obtained for the semiconductor/liquid junction, with the a-Si:H/CH_3OH–$Me_2Fc^{+/0}$ system yielding a best fit to $v_c = 2 \times 10^3$ cm/s. As was found for crystalline n-Si (vide supra), the spectral response showed no increase in v_c when the concentration of Me_2Fc^+ was changed from 0.001 to 0.1 mM. The lack of a concentration dependence indicates that the dominant interfacial charge transport mechanism for the a-Si:H/CH_3OH–$Me_2Fc^{+/0}$ junction is not simple electron transfer into the solution acceptor.

Although the fits for all three a-Si:H interfaces were excellent for $\lambda > 300$ nm, significant deviations between theory and experiment were found for shorter wavelengths in the a-Si:H/liquid system. This discrepancy was not due to the presence of uncorrected optical losses in the electrolyte/redox solution, because studies of n-Si and n-InP junctions in electrolytes of identical composition produced quantum yields that were in excellent agreement with theory over this same wavelength range (Figures 4 and 7). Possible reasons for the discrepancy between theory and experiment might include hot carrier effects,[27–29] inaccurate values of the absorption coefficient of the a-Si:H alloy,[14] or inefficient charge separation due to band tailing.[30] At present, we cannot distinguish between these alternatives. We note that unthermalized carriers might also be expected to contribute to an increased v_c for the n-Si system for $\lambda < 300$ nm, but no evidence for $v_c > 10^6$ cm/s was found in the analysis of the n-Si/CH_3OH–$Me_2Fc^{+/0}$ data (Figure 4). In view of the sensitivity of the calculated spectral response data to the value of v_c (Figures 2d and 8), and the general agreement between theory and experiment for $\lambda > 300$ nm, we take the data for $\lambda > 300$ nm with a-Si:H as indicative of the trends in majority carrier collection properties for the various a-Si:H interfaces.

D. Metal-Coated Si/Liquid Junctions. Controversy exists regarding the electronic characteristics of liquid junctions made from semiconductors with plated metal overlayers.[11,12] Some workers have suggested that these metal overlayers behave as electrocatalysts for minority carrier transfer,[11,12a] while others have claimed that the devices are merely buried Schottky junctions.[12b–d] On the basis of the measurements described above, in which v_c for the Schottky systems was always greater than v_c for the semiconductor/liquid junctions, the short-wavelength spectral response method should be able to distinguish between the two proposed situations. This can be done without resorting to changes in the electrolyte, metal overlayer, or other potentially confounding experimental variables.

To demonstrate this point, we have collected spectral response data on two different silicon-based semiconductor/metal systems. p-Si was photoelectrochemically plated with Pd according to a slight modification of literature methods[11] and was then examined in the CH_3CN–0.70 M $LiClO_4$–cobaltocene$^{+/0}$ electrolyte. This electrolyte was chosen because the spectral response properties of etched p-Si electrodes in this liquid junction clearly indicated lower collection velocities than for Schottky barriers (cf. section IVA). Unfortunately, thermally evaporated Pd could not be studied on p-Si because it is known to form poorly rectifying contacts,[31] which precludes use of the spectral response method.

(26) (a) Mead, C. A.; Spitzer, W. G. *Phys. Rev. A* **1964**, *134*, 713. (b) Newman, N.; Kendelewicz, T.; Bowman, L.; Spicer, W. E. *Appl. Phys. Lett.* **1985**, *46*, 1176. (c) Waldrop, J. R.; Kowalczyk, S. P.; Grant, R. W. *Appl. Phys. Lett.* **1983**, *42*, 454. (d) Brillson, L. J.; Brucker, C. F. *J. Vac. Sci. Technol.* **1982**, *21*, 564. (e) Heben, M. J.; Kumar, A.; Zheng, C.; Lewis, N. S. *Nature (London)* **1989**, *340*, 621.

(27) (a) Boudreaux, D. D.; Williams, F.; Nozik, A. J. *J. Appl. Phys.* **1980**, *51*, 2158. (b) Nozik, A. J.; Turner, J. A.; Peterson, M. W. *J. Phys. Chem.* **1988**, *92*, 2493. (c) Cooper, G.; Turner, J. A.; Parkinson, B. A.; Nozik, A. J. *J. Appl. Phys.* **1983**, *54*, 6463.

(28) Rothwarf, A. *Appl. Phys. Lett.* **1982**, *40*, 694.

(29) Koval, C. A.; Segar, P. *J. Am. Chem. Soc.* **1989**, *111*, 2004.

(30) Kanicki, J. *Mater. Res. Soc. Symp. Proc.* **1987**, *95*, 399.

(31) Anand, Y. *IEEE Trans., Electron. Devices* **1977**, *ED-24*, 1330.

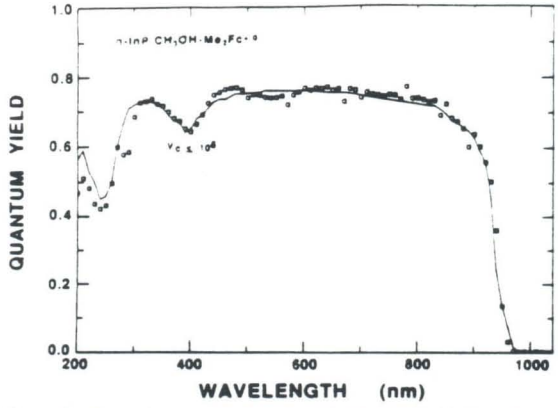

Figure 7. Spectral response of an n-InP/CH_3OH–1.0 M $LiClO_4$–dimethylferrocene$^{+/0}$ system. No n-InP Schottky barrier device was examined due to the nonrectifying behavior of n-InP/metal systems.[26] The n-InP/CH_3CN–0.70 M $LiClO_4$–ferrocene$^{+/0}$ junction yielded an indistinguishable response from that depicted in the figure.

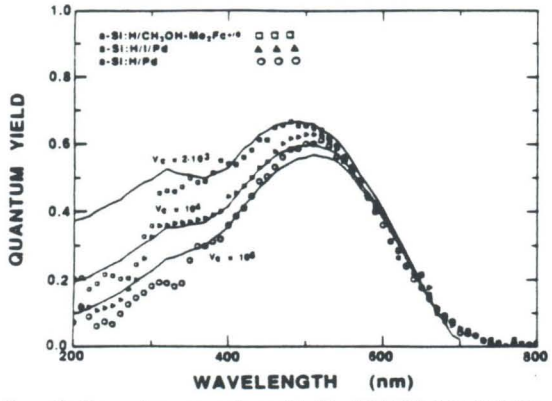

Figure 8. Spectral response of an a-$Si_{0.9}H_{0.1}$/CH_3OH–1.0 M $LiClO_4$–dimethylferrocene$^{+/0}$ liquid junction, along with the analogous a-Si:H MIS and Schottky contacts. The low drift velocity for electrons in this material allows measurement of the collection velocities for all these devices. No effect on the spectral response was observed over the Me_2Fe^+ concentration range of 0.1–0.001 mM. The poor agreement between the experimental and theoretical curves for wavelengths shorter than 300 nm is discussed in the text.

However, a suitable system for comparison was obtained from thermally evaporated Pd (9 Å) on n-Si in the CH_3OH–1.0 M $LiClO_4$–$Me_2Fc^{+/0}$ electrolyte.

Figure 9 shows the spectral response for the two Si/Pd systems. The p-type Si that had been photoelectrochemically plated with Pd displayed high quantum yields in the short-wavelength region, indicating $v_c \leq 10^6$ cm/s. In fact, after correction for the absorption properties of the Pd overlayer,[32] the response of this interface was indistinguishable from that of an HF-etched p-Si sample in this electrolyte. In contrast, the spectral response data for the thermally evaporated n-Si/Pd contact displayed low quantum yields at short wavelengths and gave excellent fits with $v_c = 10^7$ cm/s, as would be expected for a Schottky barrier.

In the above two specific cases chosen for study, the conclusions obtained from the spectral response analysis can be confirmed independently by examination of the steady-state current–voltage properties of these junctions. The p-Si/Pd surface was rectifying in the CH_3CN–cobaltocene$^{+/0}$ electrolyte, which clearly indicated

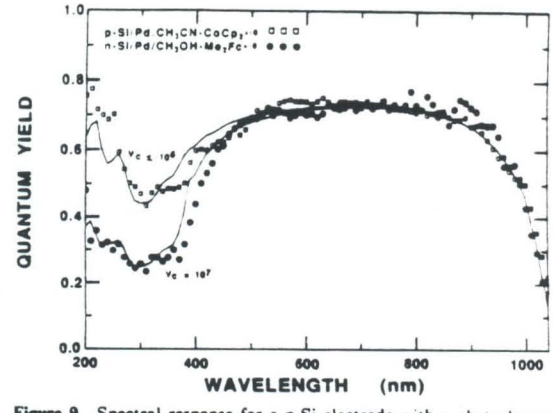

Figure 9. Spectral response for a p-Si electrode with a photoelectrochemically plated Pd overlayer (0.19 C/cm^2 cathodic charge), in CH_3CN–0.70 M $LiClO_4$–cobaltocene$^{+/0}$, along with the spectral response for an n-Si electrode with 9 Å of a thermally deposited overlayer, in contact with CH_3OH–1.0 M $LiClO_4$–dimethylferrocene$^{+/0}$. The spectral response for the p-Si/Pd electrode was indistinguishable from that of HF-etched p-Si in the same electrolyte.

that it was not a buried Schottky barrier (with a lower barrier height of 0.45 V[31]) in contact with the liquid. Similarly, the n-Si/Pd system only yielded open circuit voltages of 0.26–0.29 V at short circuit current densities of 20 mA/cm^2 in the CH_3OH–$Me_2Fc^{+/0}$ electrolyte, which contrasts to the bulk diffusion/recombination limited open circuit voltage of 0.566 V seen for 1.5 ohm-cm, HF-etched n-Si in this electrolyte.[33] The steady-state I–V behavior of these Si junctions thus is in accord with the conclusions obtained from the spectral response analysis.

For other metal-coated surfaces, the spectral response method can offer a valuable assessment of whether the interface of interest is a buried Schottky junction in contact with the liquid phase. For example, the spectral response data on the n-GaAs/M systems in KOH–$Se^{-/2-}$ electrolyte (M = Co(III), Rh(III), Os(III), Ru(III); see section IVB) were not consistent with the high majority carrier collection velocities that would be expected for direct semiconductor/metal contacts. Although we cannot explicitly rule out MIS-type behavior in these semiconductor/metal/liquid junction systems (resulting in $v_c \leq 10^6$ cm/s), we can conclude that the chemisorption of these metal ions on n-GaAs does not merely produce a buried Schottky junction in contact with the KOH–$Se^{-/2-}$ electrolyte. The spectral response method thus offers an alternative to the series of flat-band measurements suggested by Meissner et al. in order to ascertain whether a Schottky barrier has been formed[34] and has the advantage that it yields useful information in media such as aqueous 1.0 M KOH–$Se^{-/2-}$, where a series of comparable redox couples is not readily available.

V. Conclusions

Short-wavelength quantum yield measurements have been shown to yield information on the majority carrier collection velocities for a wide variety of semiconductor/metal, semiconductor/liquid, and semiconductor/insulator/metal interfaces. The Schottky diodes all exhibited spectral response properties that were consistent with high (10^7 cm/s) majority carrier collection velocities. In contrast, the semiconductor/liquid junctions and MIS systems showed reduced majority carrier losses. This qualitative trend in majority carrier collection velocities, and consequently in the rectification quality of the electrically active interface, appears to be general for the large number (>18) of systems studied in this work. Additionally, for junctions where the interfacial kinetics are known from other measurements not to be

(32) Moses, A. J. *Handbook of Electronic Materials Vol. 1: Optical Materials Properties*; Plenum: New York, 1971.

(33) Rosenbluth, M. L.; Lieber, C. M.; Lewis, N. S. *Appl. Phys. Lett.* **1984**, *45*, 423.

(34) Meissner, D.; Lauermann, I.; Memming, R.; Kastening, B. *J. Phys. Chem.* **1989**, *92*, 3484.

rate-determining, e.g., the n-Si/CH_3OH–dimethylferrocene$^{+/0}$ interface, the spectral response technique has been shown to provide the first available information on the magnitude of the interfacial majority carrier collection velocity. Finally, when metal overlayers have been used to modify the interfacial properties of semiconductor/liquid junctions, the short-wavelength spectral response method can be used to distinguish between Schottky-type behavior and electrocatalytic properties of the plated metal.

Acknowledgment. We thank the Department of Energy, Office of Basic Energy Sciences, for support of this work. We also acknowledge Mary L. Rosenbluth and Pat G. Santangelo for technical assistance with some of the experiments and for helpful discussions.

Charge Transfer Studies of Semiconductor Interfaces

Chapter 4: Further Mechanistic Studies of n-Type Si Photoelectrodes: Behavior in Contact with Methanol-Dimethylferrocene$^{+/0}$ and in Contact with Aqueous Electrolytes

Further Mechanistic Studies of n-type Si Photoelectrodes: Behavior in Contact with Methanol-Dimethylferrocene$^{+/0}$ and in Contact with Aqueous Electrolytes

ABSTRACT: Mechanistic studies of n-Si photoelectrodes have been conducted using aqueous and nonaqueous electrolytes. In contact with the CH_3OH-dimethylferrocene$^{+/0}$(Me_2Fc)$^{+/0}$ electrolyte, the dark current and open circuit voltage (V_{oc}) were not dependent on acceptor concentration for [Me_2Fc^+]≤0.010 **M**, and were only weakly dependent on acceptor concentration for [Me_2Fc^+]≥0.010 **M**. For [Me_2Fc^+] between 0.3 m**M** and 0.050 **M,** the temperature dependence of V_{oc} indicated that bulk-diffusion/recombination was the rate-limiting recombination process. In all of these experiments, conventional Shockley diode theory provided an excellent description of the solid/liquid junction properties. In a related set of experiments, HF-etched n-Si photoelectrodes ((100) and (111) oriented samples) and n-Si samples that had been metallized by several different methods all showed passivation in contact with $Fe(CN)_6^{3-/4-}{}_{(aq)}$ or $Br_2/Br^-{}_{(aq)}$ electrolytes. For several metallized Si samples, etches that had been reported to produce metal islands on the Si surface instead yielded Si surfaces free of metal. All Si samples that had been metallized by filament evaporation yielded I-V behavior in contact with the CH_3OH-$Me_2Fc^{+/0}$ redox system that was characteristic of a pinned surface Fermi level, even for coverages of metal as low as 9 Å. This indicates that proposed metal-insulator-semiconductor junctions with anomalously high barrier heights are difficult to obtain by such metallization and etching methods.

INTRODUCTION

Work in several laboratories has confirmed that n-type Si anodes in contact with $CH_3OH(l)$ can provide extremely stable and efficient photoelectrochemical interfaces.[1-4] Extensive mechanistic studies on the n-Si/dimethylferrocene $(Me_2Fc)^{+/0}$-CH_3OH system have shown that this solid/liquid interface is sufficiently free of electrical recombination sites that the rate-determining recombination process occurs in the bulk of the Si photoelectrode, and not at the solid/liquid interface.[5-7] The quantitative agreement between theoretical expectations based on the bulk-diffusion/recombination treatment of Shockley[8] and experimental data for the n-Si/$Me_2Fc^{+/0}$-CH_3OH interface[5-7] has led to the development of n-Si/liquid junctions that exhibit open-circuit photovoltages, V_{oc}, as high as 0.670 V at light intensities providing short-circuit photocurrent densities, J_{sc}, of 20.0 mA/cm^2 at 298 K.[6] Despite the accord between theory and experiment reported for this semiconductor/liquid system,[5-7] a recent report by Kobayashi *et al.*[3a] has claimed that a new, unprecedented, theory of the open circuit voltage in a photovoltaic device is required to explain some experimental observations[3] on the n-Si/CH_3OH-$Me_2Fc^{+/0}$ interface. Kobayashi and co-workers have also presented evidence that efficient thermionic emission of majority carriers over the n-Si/CH_3OH barrier is the dominant recombination step at low temperatures (<250 K) or at room temperature and high (>0.010 **M**) Me_2Fc^+ concentrations.[3b] This hypothesis appears to contradict previous studies indicating that bulk-diffusion/recombination is the rate-limiting step for temperatures as low as the freezing point (< 210 K) of the CH_3OH-$LiClO_4$ electrolyte and for a wide concentration range of Me_2Fc^+ (10^{-4} **M**-10^{-2} **M**).[5-7] In response to these claims, we present further mechanistic studies of the n-Si/CH_3OH-$Me_2Fc^{+/0}$ interface. These studies have been performed specifically to address the applicability of the Shockley diffusion/recombination theory in the n-Si/$Me_2Fc^{+/0}$-$LiClO_4$-CH_3OH system over a wider range of $Me_2Fc^{+/0}$ concentrations and cell temperatures.

A related set of findings described in the recent literature is concerned with the photoelectrochemical behavior of metal-coated n-Si electrodes in contact with aqueous electrolytes.[9,10] At moderate current densities (>0.1 mA/cm^2), it is well documented that unprotected n-Si photoanodes undergo photocorrosion or photopassivation processes in all aqueous solutions investigated to date.[11] Improved anode stability has been obtained after pinhole-free metallization of n-Si with Pt, Pd, Rh, Ru, and Ir,[12] but this process forms metal silicide layers and results in the formation of buried semiconductor/metal junctions. For such Si/metal/liquid junctions, the metallization process results in low V_{oc} values (V_{oc}=200-300 mV at J_{sc}=20 mA/cm^2 and 298 K)[12] due to Fermi level pinning at the Si/metal interface.[8b,13] In contrast, Nakato *et al.* have claimed that several methods of depositing Pt islands onto partially oxidized (100) and (111)-oriented n-Si anodes can yield stable, high V_{oc}, photoelectrode behavior in contact with aqueous solutions that would passivate or corrode HF-etched n-Si photoelectrodes.[9] In fact, the V_{oc} values reported in the work of Nakato *et al.* (V_{oc} = 0.685 V for J_{sc} = 25 mA/cm^2)[9] are superior to the open-circuit voltages obtained from Si/CH_3OH junctions[5-7] and from all known solid-state Si p-n junctions at comparable photocurrent densities.[8,13,14] The voltages observed by Nakato *et al.* and by Kobayashi *et al.*[3] are so large that they cannot be explained by conventional photovoltaic theory,[8,14] so a new model to explain photovoltaic action in semiconductor-surface barrier devices was developed and invoked to explain these novel results.[9,10] As part of this work, we have attempted to verify this interesting set of observations, and describe herein the results of our study of the photoelectrochemical behavior of various metallized n-Si samples in aqueous electrolytes.

EXPERIMENTAL

A. Materials and Preparation

The Czochralski grown samples were n-type (100) and (111) oriented, phosphorus-doped, single crystal Si obtained from Siltec Corp. or Monsanto Co. Float-

zone grown, n-type, (100)-oriented, 0.245 Ω-cm resistivity Si samples were supplied by Professor Richard Swanson of Stanford University. Four point probe measurements were made to determine the resistivity of all samples, and the dopant densities were then calculated using the data of Thurber *et al.*[15] The samples were cut into 4 mm by 4 mm squares, and were then fashioned into electrodes as described previously.[1] The photoelectrodes were etched in 49% HF(aq) for 10-15 seconds, rinsed with water, and dried in a stream of nitrogen immediately before immersion into the electrolyte. The minority carrier diffusion length of certain Si samples was determined by measuring photocurrent quantum yields in the CH_3OH-$Me_2Fc^{+/0}$ cell in the long wavelength region of the Si absorption spectrum, (700-1000 nm), as described previously.[6]

For metal island studies, thermal evaporation of the desired metal from a W filament was conducted in a chamber of base pressure < 5 x 10^{-6} Torr. Thicknesses were monitored using a quartz crystal oscillator purchased from R.D. Mathis Co. of Long Beach, CA. Metal evaporation sources consisted of > 99.999% Pd and >99.999% Pt.

For metal island formation by alkali etching,[10] the Pt-coated silicon samples were etched for 3 min in a solution of 4 **M** NaOH(aq) at 90 °C. This was followed by a 3 minute etch in a 0.25 **M** aqueous NaOH solution that contained 0.60 **M** 2-propanol and was held at 90 °C. Samples supplied by H. Tsubomura were coated at Osaka University, Japan, by placing a drop of an ethanolic solution of H_4PtCl_6 onto the sample. The solution was then dried and the Pt was reduced by heating under hydrogen.[10b]

B. SEM and EDX analysis

SEM data was obtained on a Camscan Series II instrument built by Cambridge Scanning (England). EDX analysis was conducted using a Tracor Northern (England) TN 5500 X-ray detector. The samples were not coated with metal because back-scattered

electron images and/or secondary electron images provided satisfactory data. The images were obtained at an accelerating voltage of 25 kV.

C. Electrochemical Cells and Techniques

All experiments were done in air-tight pyrex vessels, although anaerobic conditions were not necessary for the short term stability experiments performed in this study. I-V curves were measured potentiostatically in a three electrode configuration where the silicon was the working electrode, the counter electrode was a large area (> $2cm^2$) Pt electrode, and the reference electrode was either a Pt wire poised at the solution redox potential or a standard calomel electrode (SCE). The photoelectrode was positioned with the active surface oriented either vertically or horizontally. For the horizontal configuration, the electrode was illuminated through the bottom of the cell via reflection of light from a mirror. In the vertical configuration, the electrode was illuminated directly through the side wall of the cell. In all cells, the reference, counter and working electrodes were positioned approximately 1.5 cm apart from each other in a triangular configuration. When a Pt wire reference was used, the cell potentials were independently measured *vs* an SCE to verify that changes in the equilibrium potential of the solution were in accord with the Nernst equation. In accord with the IUPAC electrochemical convention, negative voltages reported in this work correspond to more reducing applied potentials, *i.e.* forward biases at an n-type semiconductor are negative applied voltages with respect to the short circuit condition.[16] The supporting electrolyte for all non-aqueous cells operated at room temperature was 1.0 **M** $LiClO_4$.

The solutions were stirred with a magnetic stir bar, and I-V data was collected up to the mass transport limited cathodic current. Mass transport restrictions on the current density for semiconductor electrodes were determined by scanning the silicon electrode into forward bias (negative voltages) until a limiting current density was observed. This was

confirmed by determining mass transport limitations at a Pt working electrode that was maintained in the same electrode geometry as that used for the Si photoelectrode measurements. The deviation from Nernstian behavior of the $Me_2Fc^{+/0}$ redox couple at the Pt working electrode was used to estimate the concentration overpotentials and uncompensated resistance losses for a particular cell configuration. Neither iR compensation nor a Luggin capillary electrode was used to reduce the effects of uncompensated resistance in any of the cells investigated in this work.

Illumination for all experiments was provided by an ELH type tungsten-halogen lamp (3250 K color temperature, dichroic rear reflector).[17] For variable temperature experiments, the $LiClO_4$ concentration was reduced to 0.1 **M**, to eliminate precipitation of the electrolyte. Additionally, lower concentrations of $Me_2Fc^{+/0}$ were used in these cells. Because the low concentration of redox couples required for variable temperature studies did not permit measurement of high light limited photocurrent densities (J_{ph}) in these cells, the illumination intensity for each cell composition was adjusted at 300 K to yield a V_{oc} value that was identical to the V_{oc} measured at J_{ph}=20.0 mA/cm^2 in contact with the CH_3OH-0.200 **M** Me_2Fc-0.1 m**M** Me_2Fc^+-1.0 **M** $LiClO_4$ electrolyte. After this light intensity was adjusted, it was maintained at a constant value throughout the experiment, and the desired V_{oc} *vs* temperature data were then acquired as described previously.[5]

D. Solvents and Materials

Most experiments used methanol (Fischer Scientific Inc., Fair Lawn, NJ) that had been dried over calcium hydride and then distilled from Mg, although identical I-V properties were obtained using CH_3OH as received from the supplier. Me_2Fc was purchased from Polysciences (Warrington, PA) and was purified by sublimation. To obtain Me_2Fc^+, the Me_2Fc was oxidized by a solution of benzoquinone and HBF_4 dissolved in diethyl ether. The resulting Me_2Fc^+ was precipitated as the BF_4^- salt. After

isolation as solids and subsequent purification, the two forms of the redox couple were added separately to the electrolytes to achieve the desired concentrations of redox reagents.

For studies in aqueous electrolytes,[9,10] concentrated $HBr_{(aq)}$ (8.6 **M**) was used as received (J.T Baker Inc., Phillipsburg, NJ), as were $K_4Fe(CN)_6$, $K_3Fe(CN)_6$ and KCl (J.T. Baker Inc., Phillipsburg, NJ). The water was obtained from a Barnstead Inc. deionizing column and was typically 18 MΩ-cm in resistivity .

RESULTS and DISCUSSION

I. HF-etched n-Si in Contact with the $Me_2Fc^{+/0}$-CH_3OH Electrolyte

A. Redox concentration effects on dark I-V properties

Figure 1 displays the dark I-V properties for a 0.245 Ω-cm resistivity, float-zone grown n-Si sample in contact with various concentrations of Me_2Fc^+ in the 0.050 **M** Me_2Fc-1.0 **M** $LiClO_4$-CH_3OH electrolyte. When the photoelectrode potential was measured with respect to the equilibrium potential of the solution, no detectable change in the I-V relationship was observed for Me_2Fc^+ concentrations 0.3 m**M** $<[Me_2Fc^+]\leq$0.010 **M** at biases of -0.4<V<0. Specifically, the forward bias voltage required to obtain any specific cathodic current density in the range ≤0.1 mA/cm^2 was observed to be constant to within 2-5 mV (Figure 1). At Me_2Fc^+ concentrations greater than 0.010 **M**, small shifts in I-V behavior were observed, but the maximum shift in voltage required to produce a specific current density (≤0.1 mA/cm^2) was 20 mV for the 10-fold increase in Me_2Fc^+ concentration from 0.010 **M** to 0.100 **M**. Similar behavior was observed for 3 separate cells with a total 5 different Si electrodes in contact with the CH_3OH-$Me_2Fc^{+/0}$-$LiClO_4$ electrolyte.

Under large forward bias (V≤ -0.5 V), the cathodic currents at a given voltage depended strongly on the concentration of Me_2Fc^+ and on the solution stir rate (Figure 1b).

Measurements of the limiting current density at Pt electrodes and n-Si electrodes (Table I) confirmed the assignment of the limiting Si cathodic current density to mass transport effects, as opposed to charge transfer resistances across the semiconductor/liquid junction. Such measurements enabled calculation of the concentration overpotentials for all I-V data collected in our work, and representative concentration overpotential values for selected cells have been included in Table I. For the range of Me_2Fc^+ concentrations used in this work, only data for V >-0.4 V (J<0.1 mA/cm^2) and [Me_2Fc^+]>0.010 **M** were not subject to large concentration overpotential corrections, and we only used this unambiguous I-V data to analyze the interfacial charge transfer kinetics of the n-Si/CH_3OH-$Me_2Fc^{+/0}$ interface.

In the data of Figure 1a,b, an additional factor influencing the shape of the I-V relationship in the high current region was the uncompensated ohmic resistance of the CH_3OH-$LiClO_4$ cells.[1] From measurements at a Pt electrode, the uncompensated resistance was determined to be (159±4) Ω in a typical cell used in this work. Thus, even when high concentrations of Me_2Fc^+ were present to minimize the concentration overpotentials, I-V data for V<-0.5 V (J>1 mA/cm^2) could not directly be interpreted in terms of interfacial charge transfer rate constants without substantial correction for cell iR drops. Specifically, for V<-0.5 V and [Me_2Fc^+]<0.10 **M,** the corrections for concentration overpotentials, combined with those for uncompensated iR losses, were so large that extraction of the dark I-V dependence of the semiconductor/liquid junction was unreliable (Table I).

Using a similar cell design, the I-V properties at low Me_2Fc^+ concentrations (<0.050 **M**) were analyzed for the high forward bias (V<-0.5 V) region by Kobayashi *et al*[3]. From the substantial Me_2Fc^+ concentration dependence of the I-V data obtained in this regime, Kobayashi *et al.* concluded that thermionic emission was the rate-determining reaction step for this system.[3] In contrast, the data presented above in Figure 1 and Table I

strongly indicate that this concentration dependence does not reflect the fundamental behavior of this semiconductor/liquid interface, but that the Me_2Fc^+ concentration dependence observed by Kobayashi *et al.*[3] was due to concentration overpotential losses and uncompensated resistance losses. Our dark I-V data, collected at lower current densities (where mass transport and series resistance corrections became negligible), clearly indicates that the cathodic I-V properties of the n-Si/$Me_2Fc^{+/0}$-$LiClO_4$-CH_3OH junction are strictly independent of redox concentration for [Me_2Fc^+] ≤0.010 **M**.

When the concentration overpotentials and iR losses were minimized, the I-V data of Figure 1 did show a weak Me_2Fc^+ concentration dependence, but only under certain low bias, high [Me_2Fc^+] conditions that had not been investigated in previous studies. For the highest Me_2Fc^+ concentrations used in our experiments, and V > -0.4 V, the small but significant dependence of the cathodic current on the concentration of Me_2Fc^+ (Figure 1a) could indicate that direct charge transfer from electrons in the Si conduction band to the acceptor ions in the electrolyte was starting to contribute to the rate determining charge transport process.[18,19] Unfortunately, solubility constraints limited the accessible Me_2Fc^+ concentration range to ≤0.200 **M**, and a strict linearity between log(current density) and [Me_2Fc^+], with the expected slope of RT/F, was not observed in our work for the concentrations available with this solvent/redox ion combination. Also, at the very low bias voltages for which unambiguous I-V data were available, the diode quality factor deviated from the value of 1.0 measured from V_{oc} *vs* J_{sc} experiments at high light intensities. The non-ideal quality factor, combined with the large contribution of bulk-diffusion/recombination to the n-Si/$Me_2Fc^{+/0}$-CH_3OH forward bias current density even at low bias conditions, precluded obtaining a quantitative estimate for the direct charge transfer process to the Me_2Fc^+ acceptor in this semiconductor/liquid junction system. Use of a redox species with a more negative formal potential,[6] combined with an optimized cell design,[20-22] would be required to study these effects in more detail.

An additional aspect of the I-V properties reported in Figure 1 relates to the work of Fantini *et al.*[2], who have proposed that surface states are present at the n-Si/$Me_2Fc^{+/0}$-CH_3OH interface and that these states serve to pin the surface Fermi level of the n-Si/liquid junction. Evidence for these surface states was obtained from an anomalous (approximately +10% relative to background) increase in cathodic current at -0.5 V *vs* the cell potential (*i.e.* at a voltage of -0.362 *vs* SCE). For typical Si electrodes, we observed no anomalous increases in current in this voltage range (Figure 1), however, we observed that when there was obvious physical damage to the photoelectrode (such as a visible scratch on the active surface area), or when there was a leak in the electrode insulation, anomalies in I-V behavior that were similar to those reported by Fantini *et al.* were sometimes observed. The data of Figure 1 clearly indicates that these features are not an intrinsic property of the n-Si/CH_3OH interface, and indicates that junctions displaying no current anomalies for V≥-0.6 V can be obtained from these semiconductor/liquid interfaces under our experimental conditions.[23]

B. Redox concentration effects on V_{oc}

An alternative method for examining the concentration dependence of the dominant recombination rate is to determine the response of V_{oc} to changes in acceptor concentration. In general, V_{oc} can be related to the recombination current density through equation (1):

$$V_{oc} = (AkT/q)\ln (J_{ph}/J_o) \qquad (1),$$

where A is the diode quality factor, k is Boltzmann's constant, T is the absolute temperature, q is the charge on an electron, J_{ph} is the light-limited photocurrent density, and J_o is the exchange current density for recombination.[8] In contrast to a dark I-V analysis, measurement of V_{oc} is not sensitive to the presence of concentration polarization or series resistance losses, because the measurement is performed without net current flowing through the photoelectrochemical circuit. If the magnitude of the rate-determining

recombination process depends on the Me_2Fc^+ concentration, then V_{oc} should be affected by a variation in $[Me_2Fc^+]$ provided that the illumination and cell temperature are held constant.

Table II displays V_{oc} values measured for a 0.245 Ω-cm resistivity, float zone, n-Si sample in contact with the CH_3OH-Me_2Fc-$LiClO_4$ electrolyte. At constant J_{ph} and T, V_{oc} was observed to be constant (to within 3 mV) for Me_2Fc^+ concentrations from 10^{-4} **M** to 0.050 **M**. For higher Me_2Fc^+ concentrations, a slight change (10 mV) in V_{oc} was observed when $[Me_2Fc^+]$ was increased from 0.050 **M** to 0.200 **M**. These observations are entirely consistent with the slight dependence of the dark I-V properties on the Me_2Fc^+ concentration and with previous studies of the behavior of V_{oc} *vs* $[Me_2Fc^+]$ at n-Si/CH_3OH-$Me_2Fc^{+/0}$ contacts for a more limited range of Me_2Fc^+ concentrations.[5,6]

For $[Me_2Fc^+] \leq 0.050$ **M**, the experimental value of V_{oc} reported in Table II can be predicted quantitatively based on bulk-diffusion/recombination kinetics. As derived by Shockley,[8a] the bulk-diffusion/recombination limited V_{oc} can be expressed by equation (2):

$$V_{oc} = (AkT/q)\ln (J_{ph}L_pN_d)/(qD_pn_i^2) \qquad (2),$$

where L_p is the minority carrier (hole) diffusion length for this n-type semiconductor sample, N_d is the majority carrier dopant density, D_p is the diffusion coefficient of the minority carriers, and n_i is the intrinsic carrier concentration of the semiconductor. This equation has been shown to provide quantitative predictions of V_{oc} for the n-Si/CH_3OH-$Me_2Fc_{+/0}$ junction over a variety of different values of L_p, N_d, T, J_{ph}, $[Me_2Fc]$, and $[Me_2Fc^+]$.[5-7] The V_{oc} of 635 mV obtained for the 0.245 Ω-cm resistivity n-Si sample of Table II (N_d=2.46 x 10^{16} cm^{-3}; L_p=195 μm) is also in accord with this general correlation when the accepted value for n_i=1.45x10^{10} cm^{-3} of Si is used in Eq. 2. The V_{oc} predicted by equation (2) is the highest possible V_{oc} obtainable from a given sample under the specified conditions of J_{ph}, and T, because the presence of any additional recombination

pathway could only act to lower the voltage from its bulk-diffusion/recombination limited value.[7,8]

At higher Me_2Fc^+ concentrations, (> 0.050 **M**), the drop in V_{oc} by 10 mV for a 4-fold increase in $[Me_2Fc^+]$ was a significant deviation from equation (2), since for the low Me_2Fc^+ concentrations, the experimental and calculated V_{oc} values differed by at most 3 mV for a range of Si samples. This deviation is consistent with the slight increase in dark current observed at high Me_2Fc^+ concentrations *(vide supra)*, and is an indication that conduction band processes start to contribute to the overall recombination rate at the highest solution acceptor concentrations. Data at higher Me_2Fc^+ concentrations would have been useful to quantify the extent of this effect, but such were not attainable due to Me_2Fc^+ solubility limitations. A quantitative exploration of the majority carrier concentration dependence would require the use of redox couples with more negative formal potentials, and the results of such studies on the n-Si/CH_3OH system will be reported separately.

For the n-Si/CH_3OH-$Me_2Fc^{+/0}$ interface, the highest V_{oc} value measured under ≈air mass 2 illumination conditions (J_{ph} = 20 mA/cm^2, cell temperature = 300 K) was 0.670 V for a sample with $N_d = 2.2 \times 10^{18}$ cm^{-3} and L_p = 0.0017 cm. Although use of equation (2) with $n_i = 1.45 \times 10^{10}$ cm^{-3} predicts that V_{oc} for this sample should be 0.712 V, a 40 mV reduction in V_{oc} is predicted to occur from band gap narrowing at very high dopant densities.[24] Equation (2) can still be used to predict V_{oc} if a corrected value for n_i is used at these high dopant densities, and the 40 mV reduction in V_{oc} is in accord with the increase in n_i at these N_d values. Experimental attempts to further maximize V_{oc} via additional increases in N_d resulted either in severe degradation of L_p, decreases in the band gap (i.e., increases in n_i), or the onset of non-rectifying properties due to degenerate doping of the semiconductor. However, no Si sample investigated in any of our prior or current work yielded V_{oc} values that were higher than those predicted by equation (2).[5,6]

A recent report of V_{oc} = 0.695 V for an n-Si/CH_3OH-$Me_2Fc^{+/0}$ junction at J_{ph} = 16 mA/cm^2 has been touted as the highest photovoltage ever reported for a Si cell.[3] Furthermore, this result has been invoked to justify the development of a new, alternative theory to Equation (2) that will describe the photovoltage in all solid state photovoltaic systems and will explain the higher photovoltage in the Si/CH_3OH cell.[3] However, the report describing the measurement of the 0.695 V V_{oc} value contained no information concerning the values of L_p, N_d, T, or other related variables for the cell of interest. The rather low concentration of Me_2Fc (0.050 **M**) used in that study[3] suggests that mass transport limitations may have led to an artificially low measured value of J_{ph}, even though the light intensity was sufficient to provide a much higher true J_{ph} value (and therefore higher measured V_{oc} value). Given the excellent agreement observed between experiment and theory for the n-Si/CH_3OH system in our laboratory, the temperature coefficient for the n-Si/CH_3OH system of ≈ -2 mV/K, and considering quantitatively the importance of the other terms in equation (2), more definitive experiments would be needed to conclude unambiguously that equation (2), and the accompanying conventional bulk photovoltaic transport and recombination theory, does not apply rigorously to the n-Si/CH_3OH-$Me_2Fc^{+/0}$ system. Additionally, comparison of V_{oc} values for different electrochemical cells must be done under specified conditions of J_{ph}, temperature, *etc.* if the photoelectrode performance is to be compared with, and claimed to exceed, the 670 mV V_{oc} value reported for 0.015 Ω-cm resistivity n-Si samples observed at J_{ph}=20.0 mA/cm^2 (300 K) in contact with the CH_3OH-$LiClO_4$-$Me_2Fc^{+/0}$ electrolyte.[6]

C. Temperature dependence of V_{oc} for the n-Si/CH_3OH-$Me_2Fc^{+/0}$ system

Figure 2 displays the V_{oc} *vs* temperature behavior for a 0.245 Ω-cm resistivity, float-zone, n-Si electrode in contact with a CH_3OH solution containing 0.050 **M** Me_2Fc, 0.0002 **M** Me_2Fc^+, and 0.10 **M** $LiClO_4$. The T=0 K intercept of the V_{oc} *vs* T plot in Figure 2 is 1.18 V, and the slope is 1.85 mV/K. To investigate the effects of the acceptor

concentration on this behavior, a series of experiments was performed in which only the Me_2Fc^+ concentration was varied. For [Me_2Fc^+] ranging from 0.3 m**M** to 0.050 **M**, the intercepts of the V_{oc} *vs.* T plots were 1.19±0.01 V (Table III). All V_{oc} vs. T plots were linear, with correlation coefficients > 0.997 for each data set (typically containing 100-300 data points).

The intercept value of 1.19 V, which is slightly higher than the Si band gap energy at 300 K, has been shown previously to be consistent with expectations for a bulk-diffusion/recombination mechanism.[6] The lack of a [Me_2Fc^+] dependence on either the slope or intercept of such plots is also consistent with this interpretation, and supports the use of equation (2) to describe the V_{oc} values at all temperatures between 200 and 300 K.

A recent report by Kobayashi *et al.*[3b] indicated that V_{oc} vs. T plots for the n-Si/CH_3OH-$Me_2Fc^{+/0}$ interface were non-linear. These authors interpreted the deviation from linearity as lending support to the thermionic emission model for the n-Si/CH_3OH-$Me_2Fc^{+/0}$ interface that had been derived from the concentration dependence of the dark I-V curves at high forward bias (*vide supra* and ref. 3). For controlled sample/cell combinations, we never observed non-linearity in V_{oc} *vs* T plots. However, in poorly stirred solutions that contained high concentrations of either Me_2Fc, Me_2Fc^+ or $LiClO_4$, precipitation of solids was observed to occur at low temperatures. This precipitation decreased the light intensity available for absorption by the Si. The lower effective light intensity resulted in a decreased V_{oc} value at a given temperature, and consequently produced a spurious nonlinearity of the resulting V_{oc} *vs* T plot. This condition was readily avoided by adequate stirring and by use of relatively low concentrations of redox couples and supporting electrolytes. We also note that analysis of the linear range of the data reported by Kobayashi *et al.* (i.e., the high temperature range from 240-300 K)[3b] yields an intercept of 1.15 V, which is in excellent agreement with the experimental data of Figure 2

and of references 5-6, as well as with predictions based on the bulk-diffusion/recombination theory expressed by equation (2).

II. Metal Coated n-Silicon/Liquid Junctions

Although n-Si/liquid junctions can yield open circuit voltages that are described by the bulk-diffusion/recombination limit,[5-7] such high voltages are extremely rare for Schottky barrier (semiconductor/metal) devices fabricated with n-type Si.[8,12] Excluding metal/insulator/semiconductor[25] and conducting polymer/semiconductor[26] interfaces, the only reports to date describing large V_{oc} values for metallized n-Si surfaces involve photoanodes made from the controlled deposition of metal islands onto Si surfaces.[9,10] The nonuniform barrier height distribution at these hybrid semiconductor/metal/liquid interfaces has been postulated to yield high V_{oc} values while also suppressing deleterious corrosion, Fermi level pinning, and thermionic emission processes.[9,10] We have attempted to verify these reports, and have also attempted to compare the behavior of metallized n-type Si photoelectrodes to the behavior of HF-etched n-Si surfaces.

The $Me_2Fc^{+/0}$-CH_3OH electrolyte is convenient because of its inhibition of Si oxide growth and inhibition of Si corrosion processes.[1,25] Furthermore, the high V_{oc} of the HF-etched Si/CH_3OH-$Me_2Fc^{+/0}$ interface readily allows detection of any increased recombination that might result from junction metallization. To prepare the samples for study, various overlayers of Pd, ranging from 9 Å to 46 Å in nominal thickness, were deposited onto Si surfaces (1.68 Ω-cm resistivity, (100)-oriented, Syton polished, HF-etched Si) from a thermal filament evaporation system. The resulting samples were then immersed into the CH_3OH-$Me_2Fc^{+/0}$ electrolyte and their I-V properties were measured in a conventional fashion for a photoelectrochemical cell, as described previously.[1,5,6]

Figure 3 compares the I-V curves for a HF-etched n-Si electrode and an n-Si electrode on which 9 Å of Pd has been evaporated, in contact with the CH_3OH-1.0 **M**

$LiClO_4$-0.200 **M** Me_2Fc-0.001 **M** Me_2Fc^+ electrolyte. Electrodes with greater amounts of metallization (up to 120 Å) yielded behavior similar to those with 9 Å metallization. All of these metallized samples displayed poor I-V properties at light intensities sufficient to provide J_{ph} values of 20 mA/cm^2. The observed V_{oc} values were far lower than the 0.570 V_{oc} mV value obtained for the non-metallized, HF-etched samples, and were identical to the values obtained from n-Si/Pd Schottky barriers (with 120 Å thick Pd films) that were operated in air. Identical, low, V_{oc} values were also observed when n-Si/Au Schottky barriers (120 Å thick Au films) were immersed into the CH_3OH-$Me_2Fc^{+/0}$ electrolyte and used as photoelectrodes. This data clearly shows that the metal deposition step in the formation of the "island" devices resulted in pronounced increases in interfacial recombination, even at nominal metal thicknesses of 9 Å. It also demonstrates that the Si/metal Schottky barrier systems yield much lower V_{oc} values than those observed from n-Si/CH_3OH-$Me_2Fc^{+/0}$ interfaces.

Additional experiments were performed with metallized Si samples that had been exposed to a basic aqueous etching solution after the metal deposition step. Tsubomura and co-workers have reported that this alkali etch procedure yields a beneficial oxide layer that minimizes recombination at the solid/liquid interface.[9,10] These workers also reported that these alkali etched metal/oxide/semiconductor electrode structures were stable in several aqueous electrolytes, and that these anodes yielded high V_{oc} values despite the presence of metal at the Si interface.[9] To quantify these effects, the I-V properties of the alkali etched metal/oxide/Si samples were investigated in both aqueous and CH_3OH-based electrolytes.

Figure 4 shows the I-V behavior of an n-Si sample that had been etched, metallized, and then placed in contact with a 0.10 m**M** $K_3Fe(CN)_6$-0.100 **M** $K_4Fe(CN)_6$-1.0 **M** KCl(aq) solution. HF-etched Si samples, etched and metallized Si samples, and alkali etched Si samples converted into metal/oxide/Si structures all yielded similar behavior in contact with either the 8.6 **M** HBr(aq)-0.01 **M** Br_2(aq) or 0.10 m**M** $K_3Fe(CN)_6$-0.10 **M**

$K_4Fe(CN)_6$-1.0 **M** KCl(aq) electrolytes. In these aqueous electrolytes, all samples with metal overlayers from 9Å to 46 Å Pd exhibited low V_{oc} values, and also displayed time dependent I-V properties indicative of passivating behavior. The n-Si sample with a 120 Å Au overlayer showed low V_{oc} values but stable I-V properties in the ferri/ferrocyanide cell (Figure 5), as would be expected for a "buried" Schottky structure where the electrolyte makes an ohmic contact to the metal. To insure the reliability of the cells used in this work, an authentic metal/insulator/semiconductor[25] structure that displayed large V_{oc} values when operated in air was also investigated in contact with the $Fe(CN)_6^{3-/4-}$ electrolyte. This device yielded high V_{oc} values in the ferri/ferrocyanide cell, (Figure 5), as would be expected based on the I-V behavior of this device when operated in air. All other samples (alkali etched, and HF-etched Si surfaces) exhibited I-V curves that were characteristic of passivation in these aqueous electrolytes. Hysteresis and instability of the I-V curves were always observed for these samples in contact with the aqueous electrolytes (Figure 4). These observations are in agreement with prior results on the photoelectrochemistry of HF-etched Si in aqueous electrolytes, but are not in agreement with claims of high V_{oc} values and stable I-V properties for the alkali etched metal/oxide/Si overlayer samples. Some additional experiments were performed in our laboratory with metal/oxide/Si structures supplied by H. Tsubomura of Osaka University. Identical passivating behavior was observed for these samples in contact with the aqueous electrolytes of Figure 4.

Scanning electron microscopy and energy dispersive X-ray analyses (EDX) were performed on samples that had been only metallized and on samples that had been metallized and then alkali etched (See Experimental section). EDX measurements indicated that the alkaline etch used to form the hybrid metal/oxide/silicon structures completely removed the Pt layer, and SEM data indicated that the etch also removed some of the underlying silicon. The (111)-oriented Si surfaces showed complete loss of Pt in the EDX measurements and also displayed striations in the SEM images, whereas (100)-oriented Si

surfaces showed complete loss of Pt and patches of a very rough, matte-textured, surface layer. Neither orientation of Si yielded SEM or EDX data that was consistent with a Pt/oxide/Si structure.

Although we never observed stable I-V behavior for these samples in aqueous electrolytes, transient measurements of the open circuit voltage yielded values in excess of 0.8 V under some irreproducible conditions. We ascribe these anomalously high V_{oc} values to the presence of passivation and/or corrosion processes that are acting in series with the photovoltage developed by the reversible redox system. The presence of a corrosion current would also lead to stable I-V behavior until a substantial portion of the Si crystal dissolves, so short term photocurrent stability does not provide conclusive evidence for regenerative photoelectrochemical operation under such conditions. When corrosion and/or passivation potentials are included with the value of the photopotential, it is possible for the experimentally measured V_{oc} value to be significantly higher than the actual light-induced photovoltage obtained in a truly regenerative photoelectrochemical cell. This could be an explanation for the large (0.685 V) V_{oc} value reported by Nakato *et al* for Pt-coated n-Si anodes in the 8.6 **M** HBr(aq) electrolyte. We note that for 0.4 Ω-cm resistivity Si samples, within the framework of equation (2), a V_{oc} of 0.685 V at J_{ph} = 25 mA/cm^2 requires an effective diffusion length of >0.2 cm at 300 K. For electrodes with ohmic contacts on the back side of the Si sample, this requires bulk Si with minority carrier lifetimes greater than 2 ms and requires samples thicker than 4 mm. Unless such unusual Si samples were used in the work of Tsubomura and coworkers,[10a] the V_{oc} value of 0.685 V is in excess of the thermodynamic limit, within conventional photovoltaic theory, unless a corrosion or passivation potential is adding to the true photopotential.

The behavior of the alkali etched electrodes in the CH_3OH-$Me_2Fc^{+/0}$ electrolyte offers an opportunity to evaluate the junction behavior of these systems without complications from passivation or corrosion processes. The I-V behavior of the alkali

etched electrodes in contact with CH_3OH-$Me_2Fc^{+/0}$ was similar to HF-etched samples. This is consistent with the lack of detectable Pt after the aqueous basic etching procedure, since the presence of low coverages of metal was observed to effect dramatic decreases in V_{oc} of the CH_3OH-$Me_2Fc^{+/0}$ system. The measured V_{oc} values were 15 to 20 mV lower than the bulk-diffusion/recombination limited values for HF-etched samples. This discrepancy between experimental and theoretical values was presumably due to increased interfacial recombination induced by the vigorous etching procedure, because similar behavior was observed for a set of alkali-etched n-Si samples that had not been exposed to any metal deposition steps.

The quantitative agreement between the V_{oc} of metallized photoelectrodes in CH_3OH-$Me_2Fc^{+/0}$ with values measured for n-Si/metal Schottky barriers operated in air strongly indicates that the current transport properties of metal island modified junctions are controlled by thermionic emission of majority carriers. This is consistent with previous work which has shown that metal overlayers on n-Si pin the surface Fermi level at 0.7-0.9 eV below the conduction band, and that thermionic emission controls the current transport properties of Schottky barrier type metallized Si devices. The metallized Si systems thus appear to exhibit predictable and normal I-V properties that fit within the established framework of conventional majority carrier thermionic emission theory, and the stable n-Si/CH_3OH junctions conform to the predictions of conventional bulk-diffusion/recombination theory over a wide range of experimental conditions.

In summary, no metallized Si sample prepared or investigated in our laboratory has shown the high voltages characteristic of the n-Si/CH_3OH-$Me_2Fc^{+/0}$ contact. Metallization sufficient to prevent corrosion in aqueous electrolytes yielded Schottky barrier behavior and resulted low V_{oc} values that were consistent with pinning of the surface Fermi level. Metallization followed by alkali etching to form hybrid metal/oxide/semiconductor structures removed all metal from the semiconductor surface, and yielded electrodes that

behaved similarly to HF-etched Si samples. The n-Si/CH_3OH-$Me_2Fc^{+/0}$ interface showed a small contribution from majority carrier-based processes at the highest accessible Me_2Fc^+ concentrations, but at lower concentrations, minority carrier dominated bulk-diffusion/recombination processes were observed to dominate the junction behavior under all accessible conditions of cell temperature and acceptor concentration. At present, the Shockley diode treatment appears to be quite adequate to describe the behavior of this class of photovoltaic devices, and the 670 mV V_{oc} value obtained from 0.015 Ω-cm resistivity n-Si samples (J_{ph}=20.0 mA/cm^2, T=300 K) remains the highest reported photovoltage measured under controlled conditions in a regenerative-type Si/liquid photoelectrochemical cell. The small deviations from bulk-diffusion/recombination behavior at high acceptor concentrations could signify the onset of majority carrier processes, and the magnitude of these effects will be quantified in subsequent reports describing the photoelectrochemical properties of n-Si/CH_3OH junctions in the presence of redox couples that produce lower V_{oc} values than those exhibited by the $Me_2Fc^{+/0}$ system.

ACKNOWLEDGEMENTS

We acknowledge the National Science Foundation, grant CHE-8814694, for support of this work. A.K. acknowledges the Department of Education for a research fellowship, and the authors are grateful to Prof. H. Tsubomura for helpful discussions and for generously providing a metallized Si sample for use in our work.

REFERENCES

1. Gronet, C.M.; Lewis, N.S.; Cogan, G.; Gibbons, J. *Proc. Natl. Acad. Sci. U.S.A.* **1983**, *80*, 1152.

2. a) Fantini, M.C.A.; Shen, W.; Tomkiewicz, M.; Gambino, J.P. *J. Appl. Phys.* **1989**, *15*, 4884. b) Shen, W.; Fantini, M.C.A.; Tomkiewicz, M.; Gambino, J.P. *J. Appl. Phys.* **1989**, *66*, 1759.

3. a) Kobayashi, H.; Tsubomura, H.; *J. Electroanal. Chem.* **1989**, *272*, 37. b) Kobayashi, H.; Chigami, A.; Takeda, N.; Tsubomura, H. *J. Electroanal. Chem.* **1990**, *287*, 239.

4. Rosamilia, J.M.; Miller, B. *J. Electrochem. Soc.* ***1985***, *132*, 349.

5. Rosenbluth, M.L.; Lieber, C.M.; Lewis, N.S. *Appl. Phys. Lett.* **1984**, *45*, 423.

6. Rosenbluth, M.L.; Lewis, N.S. *J. Am. Chem. Soc.* **1986**, *108*, 4689.

7. Lewis, N.S. *Acc. Chem. Res.* **1990**, *23*, 176.

8. a) Shockley, W. *Bell. Syst. Tech. J.* **1949**, *28*, 435. b) Fahrenbruch, A.L.; Bube, R.H. *Fundamentals of Solar Cells*; Academic: New York, 1983. c) Fonash, S.J. *Solar Cell Device Physics*; Academic: New York, 1981.

9. a) Nakato, Y.; Yano, H.; Tsubomura, H. *Chem. Lett.* **1986**, 987. b) Nakato, Y.; Tsubomura, H. *Ber. Bunsenges. Phys. Chem.* **1987**, *91*, 405.

10. a) Nakato, Y.; Ueda, K.; Yano, Y.; Tsubomura, H. *J. Phys. Chem.* **1988**, *92*, 2316. b) Tsubomura, H., personal communication.

11. a) Myamlin, V.A.; Pleskov, Y.V. *Electrochemistry of Semiconductors*, Plenum: New York, 1967. b) Brattain, W.H.; Garret, C.G.B. *Bell Syst. Tech. J.*, **1955**, *34*, 129.

12. a) Fan, F.R.F.; Keil, G.; Bard, A.J. *J. Am. Chem. Soc.* **1983**, *105*, 220. b) Fan, F.R.F.; Shea, T.V.; Bard, A.J. *J. Electrochem. Soc.* **1984**, *131*, 828.

13. Sharma, B.L. *Metal-Semiconductor Schottky Barrier Junctions and Their Applications*; Plenum: New York, 1984.

14. a) Sze, S.M., *Physics of Semiconductor Devices*, 2nd Ed.; Wiley: New York, 1981. b) Green, M.A. *Solar Cells: Operating Principles, Technolgy, and System Applications*; Prentice Hall: New Jersey, 1982.

15. Thurber, W. R.; Mattis, R.L.; Liu, Y.M.; Filliben, J.J. *J. Electrochem. Soc.* **1980**, *127*, 1807.

16. Bard, A.J.; Faulkner, L.R. *Electrochemical Methods: Fundamental and Applications*; Wiley: New York, 1980.

17. a) Gronet, C.M.; Lewis, N.S. *J. Phys. Chem.* **1984**, *88*, 1310. b) Seaman, C.H.; Anspaugh, B.E.; Downing, R.G.; Esrey, R.S. *Conf. Rec. IEEE Photovoltaic Spec. Conf.* **1980**, *14*, 494.

18. a) Gerischer, H. In *Physical Chemistry, An Advanced Treatise*; Eyring, H; Henderson, D.; Jost, W. eds.; Academic: New York, **1970**, *Vol 9A*, 463. b) Memming, R. *Ber. Bunsenges. Phys. Chem.* **1987**, *91*, 353.

19. Koval, C.A.; Austermann, R.L. *J. Electrochem. Soc.*, **1985**, *132*, 2656.

20. Gibbons, J.F.; Cogan, G.W.; Gronet, C.M.; Lewis, N.S. *Appl. Phys. Lett.* **1984**, *45*, 1095.

21. Sawyer, D.T.; Roberts, J.L. *Experimental Electrochemistry for Chemists*, Wiley, New York, 1974.

22. Anderson, L.B.; Reilley, C.N. *J. Electroanal. Chem.*, **1965**, *10*, 295.

23. The fact that no photoeffect was observed in reference 2 at potentials negative of -0.5 V *vs* the cell potential has been advanced as support for the claim that surface states are responsible for the anomalous "bump" in the I-V curves. . However, the fact that no photoeffect is observed at more negative potentials is also consistent with V_{oc} being limited by a bulk-diffusion/recombination process for the particular sample (*vide supra*). It has also previously been shown that samples with superior bulk properties, (*i.e.* $N_d = 2.2 \times 10^{18}$ cm^{-3}, $L_p = 0.0017$ cm and $N_d = 2.5 \times 10^{16}$ cm^{-3}, $L_p = 0.0195$ cm and other such combinations of N_d and L_p) yield photoeffect onsets which are up to 200 mV negative of the proposed energy level of the surface states (see Ref. 6).

24. Lanyon, H.P.D.; Tuft, R.A. *IEEE Trans. Electron. Device* **1979**, *ED-26*, 1014.

25. Kumar, A.; Rosenblum, M.D.; Gilmore, D.L.; Tufts, B.J.; Rosenbluth, M.L.; Lewis, N.S. *Appl. Phys. Lett.* **1990**, *56*, 1919.

26. Sailor, M.J.; Ginsburg, C.B.; Kumar, A.; Grubbs, R.H.; Lewis, N.S. *Science*, **1990**, *249*, 1146.

Table I. Concentration Overpotential and Uncompensated Resistance Data

$[Me_2Fc^+]$ (M)	$J_{l,c}$[a] (mA/cm^2)	$J_{l,c}$[b] (mA/cm^2)	η^c(0.2 mA/cm^2) (mV)	η^c(2.0 mA/cm^2) (mV)
0.0003	0.080	0.080	NA	NA
0.002	0.52	0.50	-130	NA
0.010	2.68	2.68	-77	-110
0.050	11.2	11.7	-39	-44
0.100	26.8	26.2	-16	-18
0.200	48.1	49.6	-0.3	-2.3

[a]Cathodic limiting current at the n-Si working electrode under forward bias conditions. [b]Cathodic limiting current at a Pt working electrode oriented in the same geometry as the Si electrode. [c]Concentration overpotential. The anodic limiting current for all cases was 48.3 mA/cm^2 at a Pt working electrode oriented in the same geometry as that of the silicon working electrode. The concentration overpotentials for 0.2 mA/cm^2 and 2.0 mA/cm^2 were calculated using $\eta = (RT/nF)\ln((J_{l,c}-J)/(J-J_{l,a}))$ (ref. 16). These two current density values were chosen arbitrarily to demonstrate the magnitude of the concentration overpotentials. R is the ideal gas constant, T is the absolute temperature, n is the number of electrons in the redox reaction, F is the Faraday constant, $J_{l,c}$ and $J_{l,a}$ are the cathodic and anodic limiting current densities respectively. The limiting current values used for these calculations were those obtained at the Pt electrode. As a comparison to the concentration overpotential losses, the IR losses at 0.2 mA/cm^2 and at 2.0 mA/cm^2 for typical silicon electrode areas were 1 and 20 mV respectively. These values were calculated assuming an uncompensated resistance of 159 ohms.

Table II. V_{oc} vs Concentration of Me_2Fc^+

$[Me_2Fc^+]$ (M)	V_{oc}(20.0 mA/cm^2) (V)	V_{oc}(10.0 mA/cm^2) (V)	V_{oc}(1.0 mA/cm^2) (V)
0.0001	0.635	0.616	0.548
0.001	0.635	0.617	0.551
0.010	0.635	0.616	0.549
0.050	0.634	0.614	0.551
0.100	0.625	0.604	-------
0.200	0.625	0.604	-------

The concentration of Me_2Fc was 0.200 **M** in all cases, with a cell temperature of 298 K. Measurements were made on three samples with a variation in V_{oc} of < 3 mV from sample to sample.

Table III. V_{oc} *vs* Temperature for n-Si/CH_3OH-$Me_2Fc^{+/0}$

$[Me_2Fc^+]$ (M)	T Range (K)	J_{ph} (mA/cm^2)	V_{oc}(0.0K)intercept (V)	$-dV/dT$(theory) (mV/K)	$-dV/dT$(expt.) (mV/K)
0.0003	210-300	20	1.18	1.89	1.85
0.0003	210-300	5	1.21	2.03	2.09
0.002	210-300	20	1.18	1.89	1.85
0.010	210-300	20	1.19	1.89	1.90
0.050	260-300	20	1.20	1.89	1.95
0.005	230-300	20	1.20	1.89	1.93

The concentration of Me_2Fc was 0.05 **M** in all cells except the last row where it was 0.005 **M**. The concentration of $LiClO_4$ supporting electrolyte was 0.10 **M** in all cases except the very last row, where it was 1.0 **M**. V_{oc}(0.0 K) was determined from the extrapolated T=0 intercept of the V_{oc} *vs* T data. This intercept overestimates the activation barrier by about 5% due to the weak temperature dependence of some parameters (Ref. 8b). $-dV/dT$(theory) was calculated from V_{oc}(theory) at 300 K and an intercept at 0 K of 1.18 V (Ref. 8b). The temperature range for the next to last row was limited by precipitation of Me_2Fc^+, and that for the very last row was limited by precipitation of the $LiClO_4$ supporting electrolyte.

Figure 1: Dark I-V curves of a 0.245 ohm-cm, (100) oriented, float zone grown n-type Si sample in contact with the CH_3OH-$Me_2Fc^{+/0}$ electrolyte at 298 K. The Me_2Fc concentration was 0.200 **M**, and the Me_2Fc^+ concentrations were as noted. The units accompanying the curves indicate the appropriate current density multiplication factor with reference to the axis labels. a) I-V behavior at small forward bias. Although solid curve is data with $[Me_2Fc^+]$=0.010 **M**, the dark curves for $[Me_2Fc^+] \leq 0.010$ **M** were indistinguishable in the voltage ranges where concentration overpotentials were not significant (0.0 V to -0.25 V for $[Me_2Fc^+]$ = 0.3 m**M**; 0.0 V to -0.35 V for $[Me_2Fc^+]$ = 0.002 **M**). b) I-V data for the samples of Figure 1a, but for higher current densities and larger forward bias voltages. At sufficient forward bias voltages (< -0.4 V), mass transport limited currents were reached for each Me_2Fc^+ concentration. The concentration dependence of the current for V<0.4 V was not due to an increase in thermionic current but was ascribable to concentration overpotentials and uncompensated resistance losses.

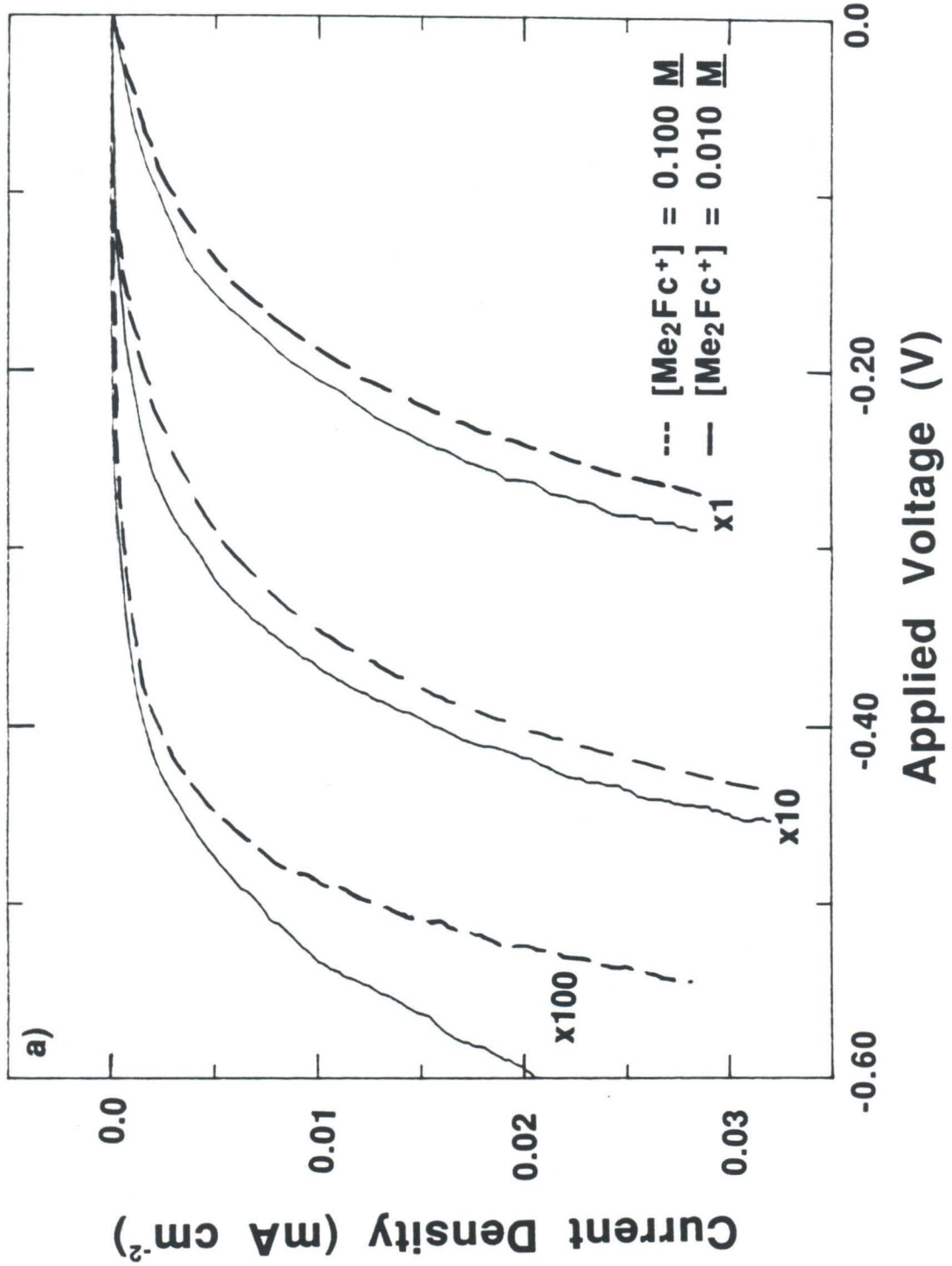
a)
0.0
0.01
0.02
0.03
Current Density (mA cm⁻²)
-0.60
-0.40
-0.20
0.0
Applied Voltage (V)
--- [Me2Fc+] = 0.100 M
— [Me2Fc+] = 0.010 M
x1
x10
x100

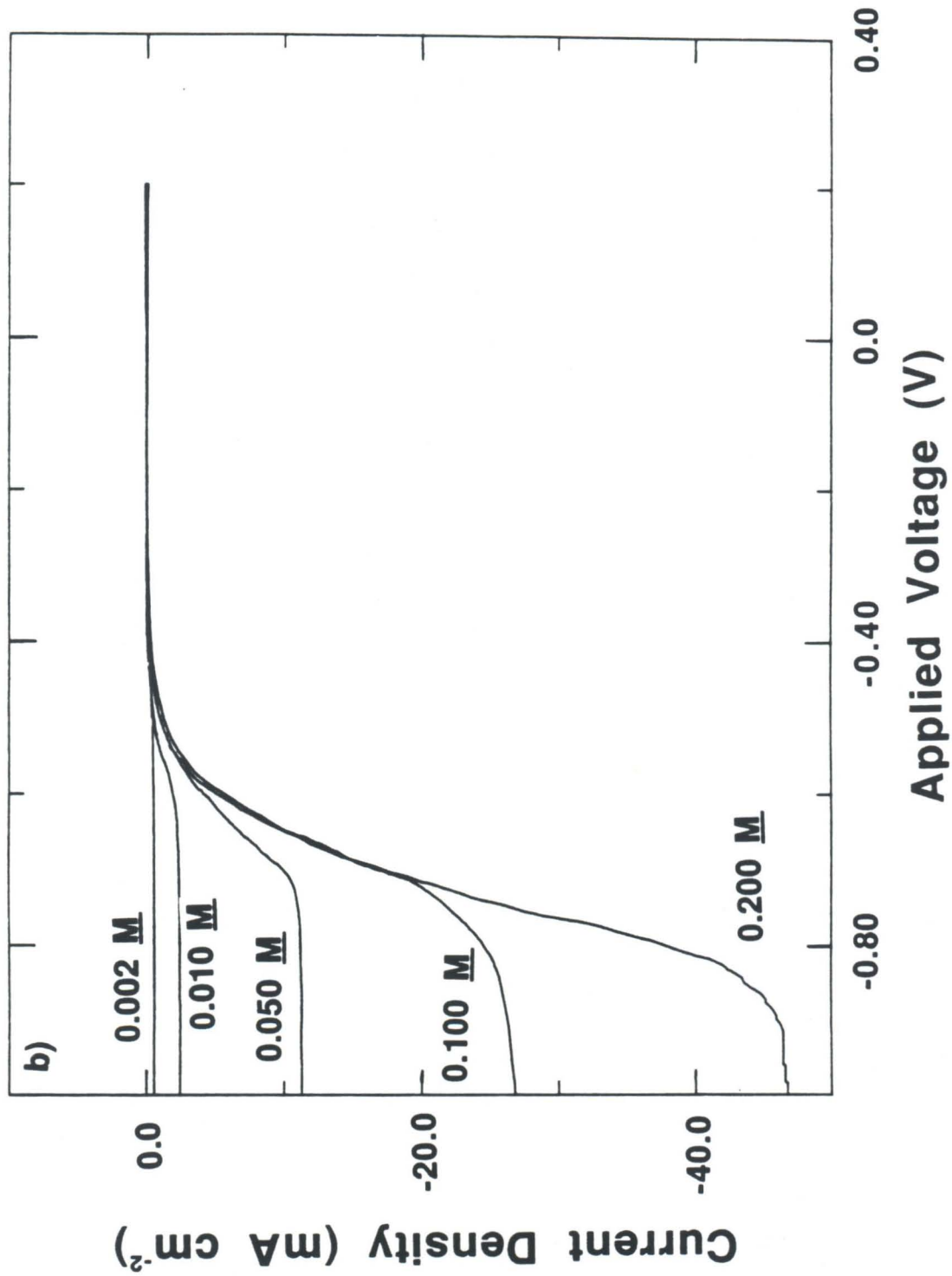
b)
0.002 M
0.010 M
0.050 M
0.100 M
0.200 M
0.0
-20.0
-40.0
Current Density (mA cm-2)
-0.80
-0.40
0.0
0.40
Applied Voltage (V)

Figure 2: Typical V_{oc} *vs* temperature data for a 0.245 ohm-cm, (100) oriented, float zone grown n-Si sample. The electrolyte was CH_3OH-0.0003 **M** Me_2Fc^+-0.050 **M** Me_2Fc-0.1 **M** $LiClO_4$. Me_2Fc^+ concentrations from 0.0003 **M** to 0.050 **M** all yielded linear responses, with extrapolated 0 K intercepts of (1.19 $\pm$ 0.01) V for Me_2Fc^+ concentrations of 0.0003 **M**, 0.002 **M**, 0.005 **M**, 0.010 **M**, and 0.050 **M.** The irradiation intensity was adjusted at 300 K to provide a V_{oc} = 0.635 V, which was the typical value for J_{ph}=20 mA/cm^2 at 300 K.

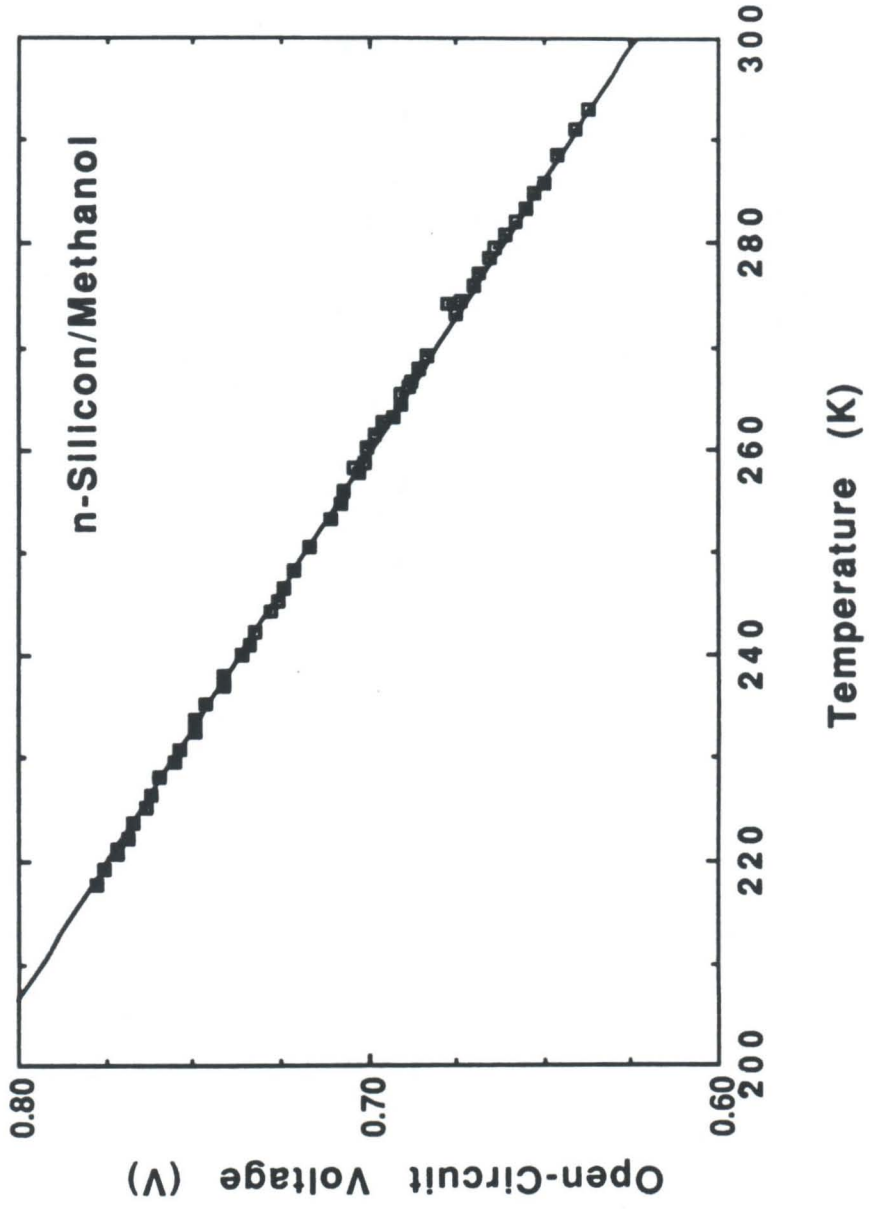
n-Silicon/Methanol
Open-Circuit Voltage (V)
0.80
0.70
0.60
200
220
240
260
280
300
Temperature (K)

Figure 3: Potentiostatic I-V curves for HF-etched and Pd covered (9Å) 1.68 ohm-cm (100) oriented n-Si in contact with CH_3OH-0.001 **M** Me_2Fc^+-0.200 **M** Me_2Fc-1.0 **M** $LiClO_4$. The solid curve is data for the HF-etched n-Si sample, where the V_{oc} of 0.570 V is in accord with the bulk-diffusion/recombination limited value (Eq. 2). The sample with 9Å of thermally evaporated Pd (dashed line) yielded a V_{oc} = 0.319 V. Seven samples consisting of various amounts of thermally evaporated Pd (9, 12, 24, 27, 30, 36 and 46 Å) yielded similar behavior, with open circuit voltages at photocurrent densities of 20 mA/cm^2 ranging from 0.273 to 0.319 V at 298 K.

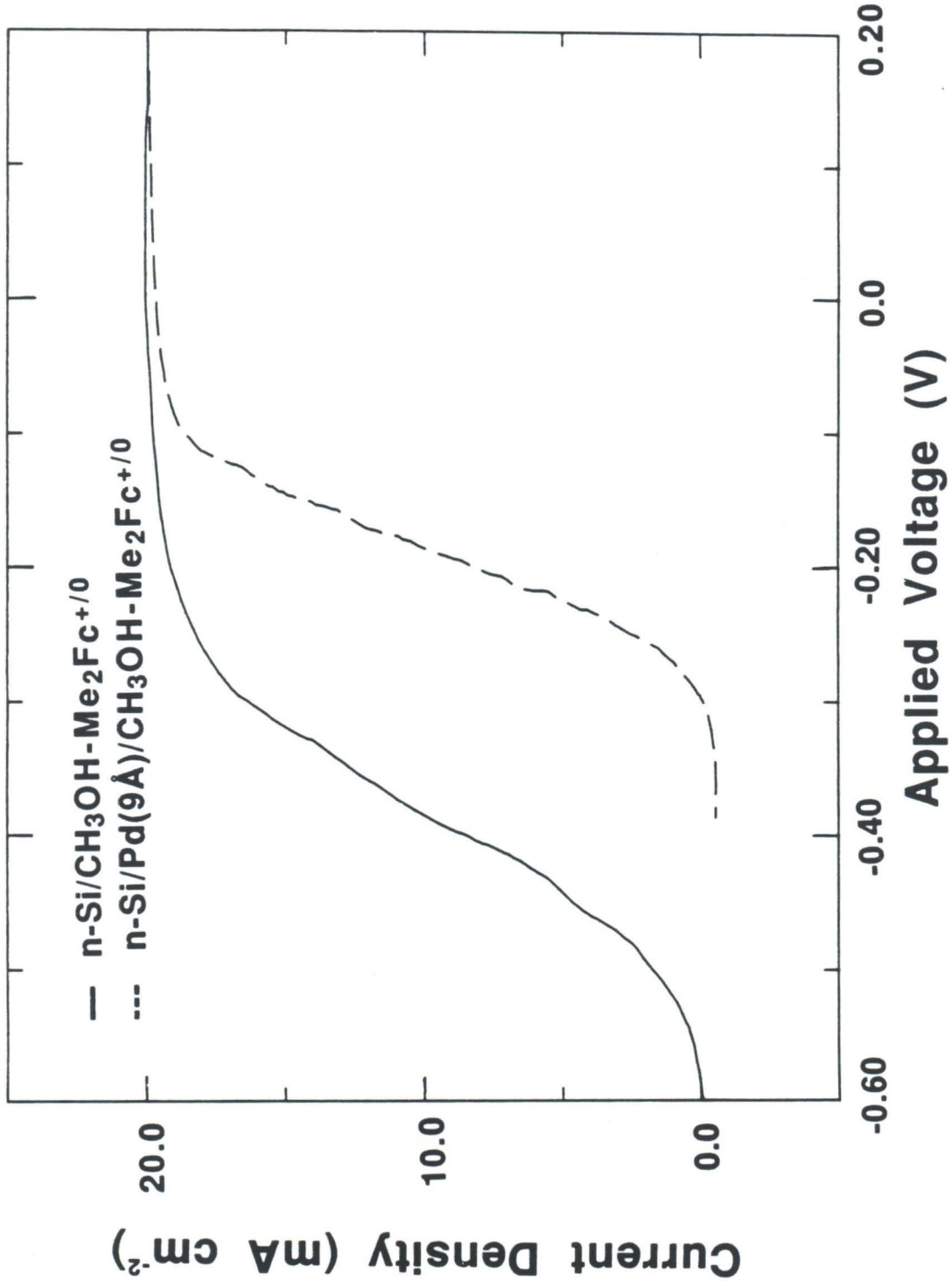
n-Si/CH3OH-Me2Fc+/0
n-Si/Pd(9Å)/CH3OH-Me2Fc+/0
Current Density (mA cm-2)
20.0
10.0
0.0
-0.60
-0.40
-0.20
0.0
0.20
Applied Voltage (V)

Figure 4: Potentiostatic I-V curves for a 0.61 Ω-cm, (111)-oriented Pt coated-alkali etched, n-Si photoelectrode in contact with 0.10 m**M** $K_3Fe(CN)_6$-0.100 **M** $K_4Fe(CN)_6$-1.0 **M** KCl(aq) (E_{cell} =+0.116 V *vs* SCE). The behavior in contact with 8.6 **M** HBr(aq)-0.01 **M** Br_2(aq) (E_{cell} =+0.590 V *vs* SCE) was similar. All samples including bare n-Si, Pt coated-alkali etched n-Si, and Pd metal island modified n-Si, and metal/oxide coated n-Si provided by H. Tsubomura exhibited similar behavior in both electrolytes. The surfaces were obviously passivating as indicated by successive scans under illumination. The light intensity was 80.0 mW/cm^2, however, the photocurrent densities were very low due to low quantum yields as a result of the passivation.

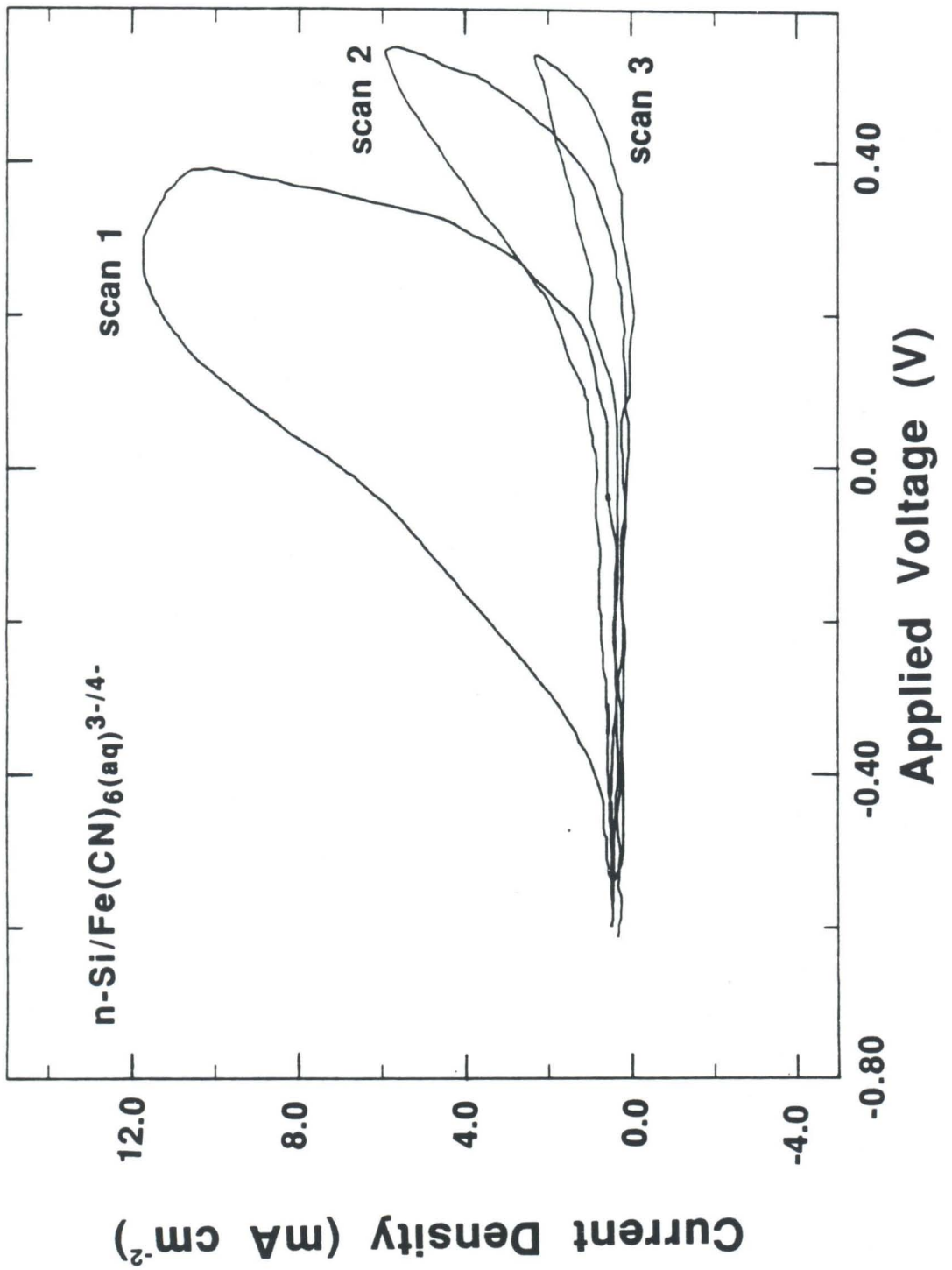
n-Si/Fe(CN)6(aq)3-/4-
scan 1
scan 2
scan 3
12.0
8.0
4.0
0.0
-4.0
-0.80
-0.40
0.0
0.40
Applied Voltage (V)
Current Density (mA cm-2)

Figure 5: Potentiostatic I-V curve of a 1.0 Ω–cm (100)-oriented n-Si sample covered with a continuous Au/insulator/semiconductor (solid curve) and of a 1.0 Ω–cm (100)-oriented n-Si/Au (120 Å Au) Schottky diode (dashed curve). Both curves were collected in contact with the 0.10 m**M** $K_3Fe(CN)_6$-0.100 **M** $K_4Fe(CN)_6$-1.0 **M** KCl(aq) electrolyte. In this experiment, for a thick continuous metal layer, the aqueous electrolyte acts as an ohmic contact for the "buried" MIS and Schottky diode.

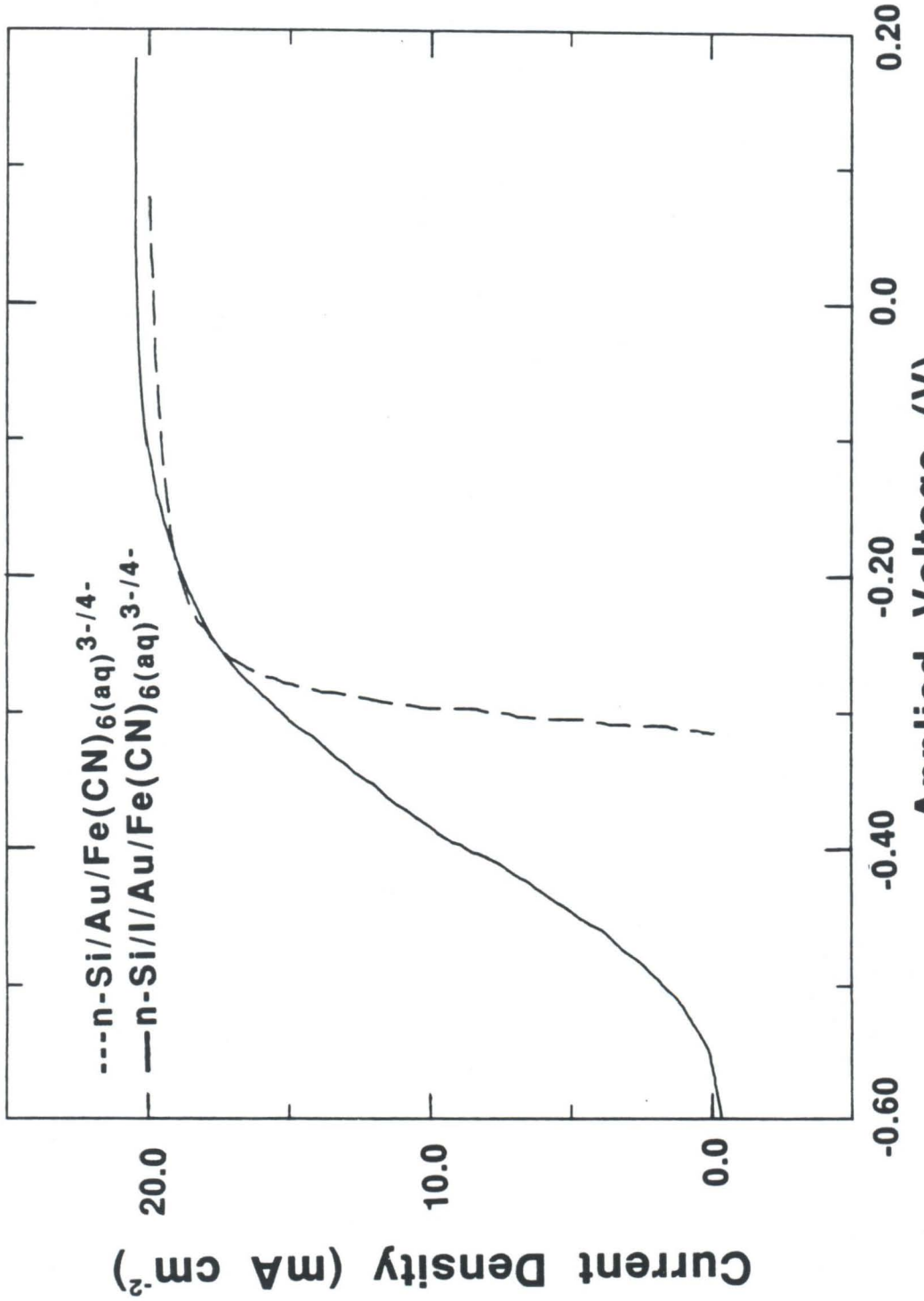
---n-Si/Au/Fe(CN)6(aq)3-/4-
—n-Si/I/Au/Fe(CN)6(aq)3-/4-
Current Density (mA cm-2)
20.0
10.0
0.0
-0.60
-0.40
-0.20
0.0
0.20
Applied Voltage (V)

Charge Transfer Studies of Semiconductor Interfaces

Chapter 5: Fabrication of Minority-Carrier-Limited n-Si/Insulator/Metal Diodes

Fabrication of minority-carrier-limited *n*-Si/insulator/metal diodes

Amit Kumar, Mark D. Rosenblum, Delwyn L. Gilmore, Bruce J. Tufts, Mary L. Rosenbluth, and Nathan S. Lewis[a)]
Division of Chemistry and Chemical Engineering, California Institute of Technology, Pasadena, California 91125

(Received 11 December 1989; accepted for publication 26 February 1990)

A photoelectrochemical anodization technique has been used to fabricate *n*-Si/insulator/metal (MIS) diodes with improved electrical properties. MIS structures fabricated with Au have provided the first experimental observation of a solid-state *n*-Si surface barrier device whose open circuit voltage V_{oc} is controlled by minority-carrier bulk diffusion/recombination processes. For these diodes, variation of the minority-carrier diffusion length and majority-carrier dopant density produced changes in V_{oc} that were in accord with bulk diffusion/recombination theory. Additionally, the variation in V_{oc} in response to changes in the work function of the metal overlayer indicated that these MIS devices were not subject to the Fermi level pinning restrictions observed for *n*-Si Schottky structures. X-ray photoelectron spectroscopic characterization of the anodically grown insulator indicated 8.2 ± 0.9 Å of a strained SiO_2 layer as the interfacial insulator resulting from the photoanodization process.

Although numerous studies of the semiconductor/liquid interface have addressed the design of efficient photoelectrochemical solar cells,[1,2] little attention has been devoted to the application of photoelectrochemistry to improve the performance of solid-state devices. Deposition of ultrathin dielectric layers is crucial to the fabrication of optimized metal-insulator-semiconductor (MIS) solar cells, chemically sensitive field-effect transistors, and tunnel-oxide based devices,[3] and photoelectrochemical techniques might afford controlled surface oxidation processes that are unavailable with thermal oxidation or other wet chemical methods. In particular, for *p*-type Si-based solar cells, Green and co-workers have obtained bulk diffusion/recombination limited performance with thermal oxidation techniques,[4] and have fabricated minority-carrier MIS systems which yield some of the highest open circuit voltages (V_{oc}) reported to date for any Si solar cell.[4,5] However, minority-carrier dominated behavior has not been reported for *n*-type Si-based MIS systems, because conventional oxidation techniques have resulted in *n*-Si/oxide/metal interfaces with large majority-carrier thermionic emission currents.[6,7] We report the use of photoelectrochemical oxidation techniques to prepare minority-carrier MIS systems with *n*-Si substrates, and report the preparation of *n*-Si MIS diodes that exhibit different electrical device properties with metals of different work functions.

The method of junction formation used in this work was based on the photoelectrochemistry of *n*-Si in alcohol solvents.[8] We have previously demonstrated that *n*-Si/methanol interfaces can produce liquid junctions which yield V_{oc} values in agreement with bulk diffusion/recombination theory.[8a] This system yields the theoretical V_{oc} value of 635 mV for 0.2 Ω cm *n*-Si samples at 20 mA/cm^2 photocurrent density, and more highly doped samples have produced photovoltages in excess of 670 mV at 300 K (at 20 mA/cm^2 photocurrent density) without any back surface field action.[8b] The high quality of this Si/liquid interface prompted us to apply these photoelectrochemical techniques to the formation of *n*-Si based MIS devices.

Device fabrication involved exposure of a HF etched, (100) oriented *n*-Si sample (typically 0.05–0.5 cm^2 in exposed area) to polychromatic illumination in a methanol solution which contained 50 m*M* of dimethylferrocene, 5m*M* of dimethylferricinium (BF_4^- or Cl^-), and 1.0 *M* of $LiClO_4$. The Si sample was maintained under potentiostatic control using conventional electrochemical cells and potentiostats,[8b] but dry, anaerobic conditions were not required for the success of the procedure. Short circuit photocurrent densities for separate runs varied from 16–20 mA/cm^2 depending upon the mass transport limit for the particular cell configuration, but in all cases, the photocurrent density was set to be 1–3 mA/cm^2 less than the mass transport limit for dimethylferrocene oxidation. After several potential scans of the *n*-Si electrode from short circuit to the open circuit potential, enough $LiOCH_3$ was added from a stock solution (1.0–2.5 *M* $LiOCH_3$ in methanol) to make the cell solution 0.02–0.08 *M* in methoxide ion. The *n*-Si electrode was then maintained under potentiostatic control at short circuit relative to the equilibrium solution potential of a Pt reference electrode in the cell solution. The desired oxide thickness was conveniently indicated by a decline in V_{oc} of 120 mV from its initial value (usually requiring 60–100 min of electrolysis at short circuit). This oxidation required up to 100 min, since the current efficiency for oxide formation is small relative to that for dimethylferrocene oxidation.[8a,b] A 10%–15% decrease in short circuit photocurrent and a degradation of the fill factor was observed to occur concurrently with the drop in V_{oc}. After overlayer growth, the *n*-Si sample was thoroughly rinsed with CH_3OH solvent, dried under nitrogen, and transferred to a filament evaporation system. A semitransparent metal film (100–125 Å) was then deposited by thermal evaporation of $> 99.99\%$ pure metal from a tungsten filament under a base pressure of $< 8 \times 10^{-6}$ Torr. The properties of the resulting MIS devices with a series of different barrier metals were then investigated by light *I-V*, dark *I-V*, and differential capacitance versus voltage techniques.

Figure 1 displays the improvement in *I-V* behavior of *n*-

a) Author to whom correspondence should be addressed.

 0003-6951/90/191919-03$02.00

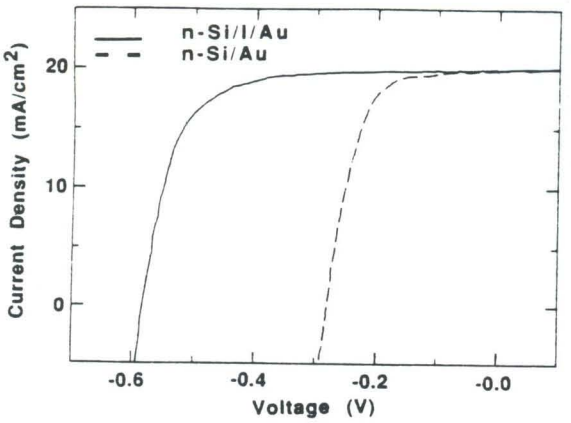

FIG. 1. Current-voltage properties under illumination of an n-Si/Au Schottky diode (dashed line) and of an n-Si/I/Au MIS (solid line) device at 25 °C (negative voltage is forward bias). The illumination intensities were adjusted to yield short circuit photocurrent densities of 20 mA/cm^2. The substrate material had a resistivity of 1.08 Ω cm.

Si/Au junctions after photoelectrochemical treatment, as compared to the behavior of n-Si/Au Schottky barriers. The photovoltage for the latter device, 0.29 V, is in agreement with expectations based on thermionic emission over a barrier height of 0.80 V for the n-Si/Au interface.[3a,5a] In contrast, the 0.58 V V_{oc} value obtained after anodization of this 1.08 Ω cm n-Si sample (370 μm thickness, effective hole diffusion length = 185 μm) indicates that the majority-carrier overbarrier recombination current had been suppressed in this system. The increased V_{oc} is in accord with a bulk diffusion/recombination process[3a,5a,8a] as expressed by Eq. (1):

$$V_{oc} = (kT/q)\ln(J_{ph}L_pN_D/qD_pn_i^2), \quad (1)$$

where J_{ph} is the photocurrent density, N_D is the dopant density, L_p is the effective minority-carrier diffusion length, D_p is the minority-carrier diffusion coefficient, and n_i is the intrinsic carrier concentration. Table I displays the correlation between theoretical open circuit voltages [based on Eq. (1)] and experimentally measured open circuit voltages for Au MIS devices fabricated on n-Si samples with varying dopant densities and hole diffusion lengths. The V_{oc} value of 0.62 V obtained with the 0.24 Ω cm n-Si sample is much larger than the 0.45–0.54 V values reported for previous n-Si based MIS devices at comparable injection levels.[3,5-7] The bulk recombination limited V_{oc} implies that, even at forward biases of 0.5–0.7 V with relatively low hole injection current densities, these MIS systems exhibit a ratio of hole injection current to electron injection current which is greater than 1.0 for all dopant densities and bulk lifetimes studied. This behavior contrasts with thermally oxidized n-Si MIS devices, in which Si samples with much higher hole injection current densities only exhibited hole/electron injection ratios of 10^{-3}–10^{-2} at forward biases of 1 V.[7b]

TABLE I. Variation in open circuit voltage (V_{oc}) for n-Si/I/Au devices. Theoretical voltages were calculated from Eq. (1), taking $n_i = 1.45\times10^{10}$ cm^{-3} (Ref. 3). All open circuit voltages were measured with W-halogen irradiation sufficient to provide short circuit photocurrent densities of 20 ± 2 mA/cm^2 at 298 K. The typical variation in V_{oc} among samples of the same resistivity and L_p was 0.02 V.

Resistivity (Ω cm)	Effective hole diffusion length L_p (μm)	V_{oc} (theory) (V)	V_{oc} (exptl.) (V)
0.24	195	0.63	0.62
0.77	200	0.59	0.60
1.08	185	0.58	0.58
1.35	175	0.57	0.57
1.5	200	0.57	0.57
1.59	13	0.50	0.50

The open circuit voltages of these MIS systems fabricated on 1.08–1.7 Ω cm n-Si with a series of metals are presented in Table II. Substantial frequency dispersion in the differential capacitance versus voltage plots generally prevented a rigorous measurement of the barrier heights using the $1/C^2$ vs V method, thus open circuit voltages are reported in Table II. For comparison, the open circuit voltages for analogous n-Si/M Schottky diodes were independently measured and have been included in the data set of Table II. The MIS systems exhibited a strong correlation of V_{oc} with the work function of the metal, as would be expected from the ideal Schottky barrier model. For instance, high work function metals such as Au, Pd, and Pt yielded MIS devices with larger V_{oc} values than Schottky contacts, whereas low work function metals produced lower V_{oc} values in the MIS structures than in the corresponding n-Si/M Schottky contacts.

Several experiments were performed with Au contacts in order to identify the chemical constituents necessary for successful MIS fabrication. Immersion of n-Si samples into the electrolyte in the presence of illumination, but with no faradaic current flow, yielded V_{oc} values of only 0.36 V, at photocurrent densities of 10–20 mA/cm^2, after deposition of

TABLE II. Comparison of V_{oc} for n-Si/metal contacts before and after photoelectrochemical anodization.[a]

Metal	Work function[b] (eV)	n-Si/M V_{oc} (V)	n-Si/I/M V_{oc} (V)
Pt	5.6 ± 0.1[c]	0.36	0.58
Pd	5.5 ± 0.1[c]	0.24	0.58
Au	5.1 ± 0.1[c]	0.29	0.58
Ag	5.1 ± 0.2[d]	0.25	0.52
Rh	5.0[e]	0.30	0.55
Co	5.0 ± 0.1[c]	0.18	0.44
Cu	4.7 ± 0.1[c]	0.06	0.38
Ni	4.6 ± 0.1[d]	0.10	0.35
Cr	4.5 ± 0.2[c]	0.09	0.00
Al	4.1[d]	0.24	0.00

[a] Substrates were n-Si (100) oriented samples of either 1.08 Ω cm or 1.7 Ω cm resistivity. The V_{oc} values were measured with W-halogen irradiation sufficient to provide short circuit photocurrent densities of 20 ± 2 mA/cm^2. The random variation in the V_{oc} values was typically ± 0.02 V.

[b] Where available, work functions for the polycrystalline metal on SiO_2 are listed.

[c] D. E. Eastman, Phys. Rev. B 2, 1 (1970).

[d] Reference 3a.

[e] B. E. Niewenhuys, R. Bouman, W. H. M. Sachtler, Thin Solid Films 21, 51 (1974).

a Au overlayer. Additionally, anodizations of *n*-Si in CH_3OH performed without the simultaneous presence of anodic photocurrent, $LiClO_4$, CH_3O^- (either generated electrochemically at the cathode or added chemically), dimethylferrocene, and dimethylferricinium failed to produce V_{oc} values with Au overlayers of greater than 360 mV. For example, samples that were maintained at short circuit current densities of 12–16 mA/cm^2 for 12–24 h, but without exposure to methoxide ion, yielded V_{oc} values of 0.34–0.38 V upon Au evaporation. These samples displayed peaks in the Si($2p$) region of the x-ray photoelectron spectrum (XPS) indicating the presence of only 3.1 ± 0.4 Å of a strained SiO_2 layer[9] [BeV = 103.85 relative to the Si($2p_{3/2}$) component of the Si substrate line at 99.70 BeV] on the silicon surface.

In contrast, XPS analysis of Si surfaces that produced satisfactory MIS behavior revealed the presence of 8.2 ± 0.9 Å of a strained SiO_2 layer. A wide scan XPS analysis of samples that had been removed from the anodization solution and rinsed with CH_3OH revealed that approximately 4.9 ± 1.5 Å of a ferricinium compound was on the surface, as indicated by the presence of a low spin Fe(III) compound, and also revealed an approximately equal amount of fluoride ion. However, the presence of Fe and F was not necessary to obtain the desired MIS device behavior, as evidenced by the high V_{oc} values of 0.56–0.58 mV that were obtained for Au MIS devices fabricated on 1.3 Ω cm *n*-Si samples that were rinsed with 0.016 *M* HCl(aq) prior to the metal evaporation step. Such acid rinsed samples exhibited significantly reduced XPS peaks attributable to Fe (0.3 ± 0.2Å) and F (0.8 ± 0.2 Å), but did display the 8.2 ± 0.9 Å of strained SiO_2 present in the other anodized *n*-Si samples. Thus, the important factor for MIS device fabrication is that the electrochemical process allows reproducible growth of ultrathin SiO_2 films, and that these oxide films are sufficiently uniform to prevent direct metal/Si contacts and are sufficiently nonporous to prevent interdiffusion of metal to the Si surface during the subsequent thermal metal deposition step.

In summary, we have shown that photoelectrochemical anodization can produce controllable amounts of oxide coatings that lead to novel *n*-Si MIS device properties. These MIS devices display improved V_{oc} values and exhibit an improved response to the work function of the contacting metal phase. A similar process may be occurring in a recent report describing the chemistry of WSe_2 surfaces, in which improved WSe_2/Au interface behavior was observed after electrochemical cycling of the WSe_2 anode in an aqueous I^-/I_3^- electrolyte.[10] Additionally, photowashing procedures have been recently advanced as a method for decreasing the surface recombination velocity of GaAs interfaces,[11] and suitable control over the electric potential and the chemical constituents of the GaAs/liquid interface might yield additional control and reproducibility for this passivation process. Clearly, photoelectrochemical processing of semiconductor surfaces can have beneficial effects that are not attainable through conventional thermal processing techniques, and other applications of these methods are being explored at present.

We thank the Department of Energy, Office of Basic Energy Sciences, for support of this work. Generous support for D. L. G. was provided by the SURF program at Caltech. We acknowledge F. J. Grunthaner, P. J. Grunthaner, R. P. Vasquez, and M. H. Hecht of the Jet Propulsion Laboratory, Pasadena, CA for access to the XPS instrument used in this study and for helpful discussions regarding this work. This work was performed at Division of Chemistry and Chemical Engineering, California Institute of Technology, contribution No. 8072.

[1] A. Heller, Acc. Chem. Res. **14**, 154 (1984).
[2] (a) K. Rajeshwar, J. Appl. Electrochem. **15**, 1 (1985); (b) N. S. Lewis, Ann. Rev. Mater. Sci. **14**, 95 (1984).
[3] (a) S. M. Sze, *Physics of Semiconductor Devices* (Wiley, New York, 1981); (b) J. Ruzyllo, IEEE Electron Device Lett. **EDL-1**, 197 (1980).
[4] (a) M. A. Green, A. W. Blakers, J. Shi, E. M. Keller, and S. R. Wenham, Appl. Phys. Lett. **44**, 1163 (1984); (b) A. W. Blakers, A. Wang, A. M. Milene, J. Zhao, and M. A. Green, Appl. Phys. Lett. **55**, 1363 (1989).
[5] (a) S. J. Fonash, *Solar Cell Device Physics* (Academic, New York, 1981); (b) R. R. King, R. A. Sinton, and R. M. Swanson, in *Conference Record, 20th IEEE Photovoltaic Specialists Conference* (IEEE, New York, 1989), p. 538.
[6] (a) D. R. Lillington and W. G. Townsend, Appl. Phys. Lett. **28**, 97 (1976); (b) J. P. Ponpon and P. Siffert, J. Appl. Phys. **47**, 3248 (1976); (c) T. E. Sullivan, R. B. Childs, J. M. Ruths, and S. J. Fonash, in *The Physics of SiO_2 and its Interfaces*, edited by S. T. Pantelides (Pergamon, New York, 1978), pp. 454–458; (d) H. Yamamoto, M. Moniwa, T. Sawada, and H. Hasegawa, Jpn. J. Appl. Phys. **87**, 20 (1981).
[7] (a) J. Shewchun and R. A. Clarke, Solid State Electron. **16**, 213 (1973); (b) H. C. Card and E. H. Rhoderick, Solid-State Electron. **16**, 365 (1973); (c) A. T. Howe and T. H. Fleisch, J. Electrochem. Soc. **134**, 72 (1987).
[8] (a) M. L. Rosenbluth, C. M. Lieber and N. S. Lewis, Appl. Phys. Lett. **45**, 423 (1984); (b) M. L. Rosenbluth and N. S. Lewis, J. Am. Chem. Soc. **108**, 4689 (1986); (c) M. C. A. Fantini, W. M. Shen and M. Tomkiewicz, J. Appl. Phys. **65**, 4884 (1989).
[9] (a) F. J. Grunthaner, P. J. Grunthaner, R. P. Vasquez, B. F. Lewis, and J. Maserjian, J. Vac. Sci. Technol. **16**, 1443 (1979); (b) S. I. Raider and R. Flitsch, IBM J. Res. Develop. **22**, 294 (1978); (c) A. Ishizaka and S. Iwata, Appl. Phys. Lett. **36**, 71 (1980); (d) J. Finster and D. Schulze, Phys. Status Solidi **68**, 505 (1981).
[10] G. Hodes, Appl. Phys. Lett. **54**, 2085 (1989).
[11] S. D. Offsey, J. M. Woodall, A. C. Warren, P. D. Kirchner, T. I. Chappell, and G. D. Pettit, Appl. Phys. Lett. **48**, 475 (1986).

Charge Transfer Studies of Semiconductor Interfaces

Chapter 6: Electrolysis of Water at $SrTiO_3$ Photoelectrodes: Distinguishing Between the Statistical and Stochastic Formalisms for Electron Transfer Processes in Fuel-Forming Photoelectrochemical Systems

ELECTROLYSIS OF WATER AT $SrTiO_3$ PHOTOELECTRODES: DISTINGUISHING BETWEEN THE STATISTICAL AND STOCHASTIC FORMALISMS FOR ELECTRON TRANSFER PROCESSES IN FUEL-FORMING PHOTOELECTROCHEMICAL SYSTEMS

ABSTRACT:

Conventional photoelectrochemical and photovoltaic theory predicts a light intensity threshold for sustaining the net electrolysis of water using semiconductor electrodes, but a stochastic charge transfer formalism for photoelectrolysis reactions does not predict such threshold behavior. This work examines the theoretical and experimental aspects of light-assisted water electrolysis using n-type $SrTiO_3/H_2O$ interfaces. A theoretical framework, based upon simple chemical kinetic considerations, has been formulated to describe the behavior of such photoelectrosynthetic cells. Experiments conducted on the n-$SrTiO_3$/5.0 **M** KOH(aq)/Pt photoelectrosynthetic cell have revealed a threshold in the short circuit electrolysis current at 0.02-0.03 mW/cm^2 of 325 nm illumination. Additional theory and experiments have provided insight into relationships between two-electrode regenerative photoelectrochemical cells, two-electrode photoelectrosynthetic cells, and three-electrode potentiostatic cells. These experiments and theory indicate that a conventional chemical kinetic treatment of interfacial electron transfer rates appears to be sufficient to describe the photoelectrochemical behavior of $SrTiO_3$ and TiO_2/aqueous junctions.

I. INTRODUCTION

Although one of the major advances in photoelectrochemical energy conversion was the 1977 "water splitting" experiment of Fujishima and Honda[1], 14 years later many fundamental questions still remain unanswered regarding the mechanism of water electrolysis at semiconductor electrodes.[2-7] One key issue, involving the thermodynamic limitations of water photoelectrolysis, is whether the charge transfer processes across semiconductor/liquid junctions should be viewed as irreversible stochastic events,[8] or whether these charge transfers should be treated within a statistical thermodynamic formalism.[9-11] This issue is the topic of the work presented below.

The stochastic approach to charge transfer has precedent in the theory of photoemission from solids into a vacuum.[12] Based on an analogy between semiconductor/vacuum and semiconductor/liquid contacts, Williams and Nozik[8a] formulated a stochastic framework for currents in the photoelectrolysis of water using TiO_2 and similar metal oxide electrodes. Their theory predicts that water photoelectrolysis currents should be observed at all light intensities, and implies that there should not be a light intensity threshold for the photoelectrolysis process. Such behavior is based on the premise that each electron-hole pair, at all illumination levels, delivers the full free energy required to sustain photoelectrolysis. In support of this theory, preliminary experiments with n-type TiO_2 electrodes have shown no evidence for a threshold in photoelectrolysis current for light intensities between $1x10^{-3}$ and $4x10^5$ mW/cm^2.[8b] Alternatively, conventional, statistical, solid-state photovoltaic theory for light-induced charge transfer reactions in regenerative and photoelectrosynthetic electrochemical cells does predict a threshold for photoelectrolysis,[3,9,10] because at very low light intensities, the photovoltage produced by the illuminated semiconductor electrode should not be sufficient to provide the free energy necessary to achieve the fuel-forming photoelectrolysis reaction.

Distinguishing between the predictions of these two formalisms is fundamentally important, because the ultimate upper bound on the performance of a photoelectrochemical energy conversion system is very different for the stochastic formalism relative to that obtained from the statistical thermodynamic approach. The focus of the work reported herein is to clarify the theory of each scenario, to develop criteria for differentiating between these two possible mechanisms, and to apply these criteria to experimental photoelectrolysis systems of current interest in solar energy conversion.

II. THEORETICAL EXPECTATIONS

A. General Kinetic Expressions

The basic problem can be expressed concisely, and in a straightforward formalism, by use of the kinetic framework of Figure 1. Consider an n-type semiconductor photoelectrode in contact with an aqueous electrolyte. The energies of the conduction band edge ($\mathbf{E}_{cb}$) and valence band edge ($\mathbf{E}_{vb}$) are as shown relative to the Nernstian redox energy $\mathbf{E}(A/A^-)$, and for simplicity, these band edge positions will be considered to be fixed in energy under the various conditions of light intensity, applied potential, *etc.* that will be encountered. Illumination of the semiconductor will produce photogenerated electrons and photogenerated holes, which will be separated by the electric potential gradient near the solid/liquid interface.[2,3,8-11,13] This charge separation ultimately will lead to a photocurrent through the external circuit, and to interfacial charge transfer events that will result in the formation of the fuels of interest in this work.

When a positive voltage is developed in the semiconductor electrode (Figure 1), the photogenerated minority carrier (hole) will be driven toward the interface, where it will undergo an interfacial charge transfer reaction with a donor, A^-, to yield the species A. Accompanying this process, the majority carrier proceeds into the ohmic contact and produces a photocurrent through the external circuit. Currents of the opposite sign are also

present, and these currents are responsible for "back reactions" in the system (so-called dark currents).[3,9,10] These "back reaction" processes can include electron transfer from the semiconductor conduction band to the acceptor, A, and hole transfer from the oxidized donor, A, back into the semiconductor valence band. The sum of the dark currents and photocurrents determines the total net current that will be measured in the external circuit at any particular applied potential.

A more quantitative treatment requires kinetic expressions for the interfacial charge transfer processes. In order to obtain a general expression for the behavior of the system at various light intensities, it is crucial to consider all of the possible forward and reverse currents in the complete electrochemical cell. The kinetic pathway for interfacial hole transfer can be expressed as follows:[9,14,15]

$$h^+ + A^- \underset{k_{ht}^{-1}}{\overset{k_{ht}}{\Longleftrightarrow}} A$$

The forward bimolecular rate expression is then:

$$\text{"anodic" hole flux} = k_{ht}\ p_s\ [A^-] \qquad (1)$$

and the reverse rate expression is:

$$\text{"cathodic" hole flux} = k_{ht}^{-1}\ [A] \qquad (2).$$

k_{ht} has units of cm^4/sec, because the "anodic" hole flux must be the product of the hole concentration at the semiconductor surface, p_s (in cm^{-3}), multiplied by k_{ht} and by the concentration of the donor $[A^-]$ (in cm^{-3}). k_{ht}^{-1} denotes the rate constant for injection of

holes into the valence band by the solution redox couple, and has units of cm/s (because the corresponding flux is simply $k_{ht}^{-1}[A]$).

k_{ht}^{-1} can be related to k_{ht} using detailed balance arguments.[3,10,16,17] At equilibrium, no net hole current passes through the interface, and we readily obtain $k_{ht}^{-1} = k_{ht}\, p_{so}\, [A^-]/[A]$, where p_{so} is the specific surface hole concentration at equilibrium. Substituting for k_{ht}^{-1} and subtracting equation (2) from equation (1), the net interfacial hole flux can then be expressed concisely as:

$$\text{"net" hole flux} = k_{ht}\,[A^-]\,(p_s - p_{so}) \qquad (3).$$

Note that a positive flux in this convention is holes flowing from the semiconductor into the liquid.

An analogous treatment can be applied to electron transfer from the semiconductor conduction band. The relationship between the forward and reverse electron transfer rate processes to the acceptor ion A is as follows:

$$e^- + A \underset{k_{et}^{-1}}{\overset{k_{et}}{\Leftrightarrow}} A^-$$

In this case, the electron flux is given as:

$$\text{"cathodic" electron flux} = k_{et}\, n_s\, [A] \qquad (4)$$

and

$$\text{"anodic" electron flux} = k_{et}^{-1}\, [A^-] \qquad (5).$$

Here, the bimolecular rate constant k_{et} relates the forward direction (cathodic) electron flux to the product of the surface electron concentration, n_s, and the dissolved acceptor concentration, [A]. The reverse rate constant, k_{et}^{-1}, describes the anodic electron injection current, and has units of cm/sec, as does k_{ht}^{-1}.

Detailed balance can also be used to obtain a relationship between k_{et}^{-1} and k_{et}. Denoting the equilibrium surface electron concentration by n_{so}, use of a procedure identical to that for holes yields:

$$\text{"net" electron flux} = k_{et}\,[A]\,(n_s - n_{so}) \qquad (6).$$

As for holes, our convention implies that a positive electron flux represents electrons leaving the solid into acceptors in the solution phase.

In photoelectrolysis systems, the only additional modification to these expressions is that more than one acceptor species can be present. In this situation, to properly describe the interfacial electron current, individual expressions corresponding to equations (4)-(5) would be required for each acceptor. An expression similar to equation (6) will then be obtained, but the factor multiplying the $(n_s - n_{so})$ term will reflect the sum of all the possible interfacial electron transfer kinetic pathways. As discussed below, equations analogous to (1)-(6) will suffice to describe the total interfacial current in any situation of interest in this work.

B. Simplifying Assumptions

To use equations (1)-(6), we need to solve for the surface electron and hole concentrations in response to changes in light intensity and bias applied to the semiconductor. The equations describing the general situation for the full semiconductor/liquid system, including diffusion, transport, and recombination, have been

presented by Reiss,[18] and are quite complicated. We will therefore adopt two simplifying assumptions in our treatment. As discussed below, these assumptions still faithfully preserve the overall behavior of the system, and will also preserve the differences between the stochastic and statistical formalisms. The simplifications are merely used to obtain closed form solutions for n_s and p_s without solving the full set of differential equations.

1. Hole continuity/hole capture

A photon flux of Γ_o (photons-cm^{-2}-sec^{-1}) striking the semiconductor electrode will produce a nonequilibrium concentration of electrons and holes in the solid. In a real system, only a fraction, ϕ, of the photogenerated minority carrier holes will survive to reach the electrode surface (Figure 2).[10,19] The surviving flux of minority carriers available to participate in interfacial charge transfer is therefore simply $\phi\Gamma_o$ (photons-cm^{-2}-sec^{-1}). Within this framework, $(1-\phi)\Gamma_o$ implicitly includes all of the optical reflection and kinetic recombination processes that can affect minority carriers, except for the interfacial charge transfer process.

To obtain an expression for p_s under illumination, continuity of the hole current at the interface must be invoked.[10,15,17,20] The net hole current, obtained by subtracting equation (2) from equation (1), must be equal to the arriving flux $\phi\Gamma_o$. This leads to the desired expression for p_s in terms of the system parameters of k_{ht}, $[A^-]$, and Γ_o:

$$p_s = (\phi\Gamma_o + k_{ht}[A^-]\,p_{so})/(k_{ht}[A^-]) \qquad (7).$$

Under conditions where $k_{ht} > \phi\Gamma_o/([A^-]\,p_{so})$, this expression simplifies to $p_s \approx p_{so}$. For these illumination and interfacial rate constant values, the minority carrier concentration at the surface does not vary greatly from the dark equilibrium minority carrier surface concentration. This lack of change in p_s relative to p_{so} is expected when the photogenerated minority carrier flux to the surface is much smaller than the interfacial flux

that can be supported by the heterogeneous charge transfer process. Under these conditions, continuity of the hole flux through the interface clearly implies that the net hole current is simply equal to $\phi\Gamma_O$.

In most of the discussion below, we will use this assumption that $p_S \approx p_{SO}$, and will write the net hole flux simply as $\phi\Gamma_O$. This assumption is certainly expected to be the case for the rapid charge transfers assumed in the stochastic treatment of solid/liquid junctions,[8] and would also be applicable at moderate light intensities in the statistical approach.[3,9,10] However, as discussed below, this assumption is not required in the general case represented by equations (1)-(7), as long as the more complex equations are used to solve for p_S and n_S.

2. Hole back reaction vs. electron back reaction

The other key assumption, made for simplicity, is that the dark current (back-reaction) is dominated by conduction band electrons interacting with acceptors in the solution, as opposed to injection of holes from the donor species back into the semiconductor valence band. The full expressions given in equations (1)-(7) do not require this assumption, but the resulting equations are greatly simplified when this kinetic situation applies. With this assumption, equation (6) can be used to describe the net electron flux through the solid/liquid interface.

3. Expression for the Total Interfacial Current

The total current is now readily obtained by combining the expressions for the interfacial flux of electrons and holes. Neglect of the hole back reaction, and assuming $p_S \approx p_{SO}$ as described above, implies that the net hole flux given by equation (3) can be replaced simply by the hole flux arriving at the solid/liquid interface, $\phi\Gamma_O$. Equation (6) yields the expression for the net electron flux. The total interfacial current is therefore

given by subtracting the electron flux (equation (6)) from the hole flux, $\phi\Gamma_o$, and multiplying the entire expression by the charge on an electron, q:

$$i = q \{\phi\Gamma_o - k_{et}[A](n_s - n_{so})\} \quad (8).$$

Equation (8) is the desired expression for the dependence of the total interfacial current on the incident photon flux. The only remaining variable that has not been explicitly solved for in the treatment at present is the surface electron concentration, n_s. It will be discussed below when the behavior of equation (8) for regenerative cells and photoelectrosynthetic cells in two electrode and three electrode potentiostatic configurations is explicitly considered.

C. Regenerative Electrochemical Cells

The regenerative cell is obtained when current flow yields no net change in the chemical composition of the liquid/electrolyte phase, *i.e.*, when only electrical energy is obtained as output from the illuminated semiconductor/liquid junction (Figure 3). In this cell, the reference potential is the Nernstian equilibrium cell potential of the redox couple/electrolyte/liquid phase. For simplicity, it is assumed that the kinetics and area of the counterelectrode are sufficient that the potential of this electrode does not deviate significantly from the Nernstian equilibrium potential of the solution, even when current flows through the cell. Under these conditions, the open circuit voltage measured between the illuminated semiconductor electrode and the metal counterelectrode is a measure of the free energy produced upon illumination of the semiconductor/liquid interface.[9,10,13]

1. Dependence of Current on Incident Photon Flux

For the regenerative cell, the relationship between the short circuit current and the incident photon flux is readily obtained from equation (8). At short circuit, no potential difference is present through the external circuit, implying that $n_s = n_{so}$. Using equation (8),

the total current is therefore $i=q\phi\Gamma_o$ (Figure 3b). This is the conventional conclusion for regenerative cells: the short circuit photocurrent is linearly related to the incident photon flux.[2,13,14] This conclusion will hold over a wide range of light intensity, provided that there is sufficient equilibrium band bending that $n_{so}<<n_{bulk}$, *i.e.*, that the junction acts as a good rectifier in the dark in response to a change in applied bias. For such cells, no threshold for photocurrent is predicted, due to the direct proportionality between i and Γ_o.

2. *Dependence of the Open Circuit Voltage on Incident Photon Flux*

At open circuit, no net current passes through the semiconductor/liquid interface. However, the individual electron and hole currents are generally non-zero, and must therefore exactly offset each other at open circuit. The open circuit expression is thus obtained from equation (8) by setting i=0:

$$\phi\Gamma_o = k_{et}[A](n_s-n_{so}) \qquad (9).$$

In order to have the electron current offset the photogenerated minority carrier flux, equation (9) indicates that n_s under illumination must exceed n_{so}. The quantitative expression for the open circuit voltage can be obtained from equation (9) by using the explicit expressions for n_s and n_{so}:

$$n_{so} = n_b\exp\{-q(V_{bi})/kT\} \qquad (10a)$$

$$n_s = n_b\exp\{-q(V_{bi}-V_{oc})/kT\} \qquad (10b).$$

These expressions merely represent the Boltzman relationship between the electric potential and the carrier concentrations.[2,3] n_b is the majority carrier concentration in the field-free bulk of the semiconductor, V_{bi} is the built in voltage (Figure 1), k is the Boltzman constant, and T is the absolute temperature. V_{oc}, the open-circuit voltage, is the extra voltage developed by the semiconductor in order to increase the surface electron

concentration from n_{so} to n_s so that the electron current will be increased and will offset the photocurrent ($\phi\Gamma_o$) to maintain zero net current flow (Figure 3c, 3d). Substituting equations (10a) and (10b) into equation (9) and solving for V_{oc} (assuming $V_{oc}>>kT/q$) yields:

$$V_{oc} = (kT/q) \ln \{\phi\Gamma_o/(n_{so} k_{et} [A])\} \quad (11).$$

This is the conventional form of the open circuit voltage in a photovoltaic[10,19] and regenerative photoelectrochemical system,[9,14,21] and shows the expected logarithmic dependence on the incident light intensity. A similar expression has been used previously by our group to elucidate the concentration dependence of V_{oc},[21] and has been presented earlier by others in identical form, but in somewhat different notation.[9,10,14]

There is no threshold dependence of V_{oc} on incident light intensity in a regenerative photoelectrochemical cell. Any finite illumination level will lead to development of a nonequilibrium concentration of carriers in the semiconductor, which will produce a steady-state potential difference between the solid phase and the liquid phase, as measured by the value of V_{oc}.[22] However, if fuels are to be formed by illumination of this junction, a certain light intensity will be required before the free energy per electron produced by the cell, qV_{oc}, exceeds the free energy per electron required to sustain the electrolysis current in the fuel-forming reaction. This condition is described in more detail in the next section.

D. Photoelectrosynthetic Cells

The photoelectrosynthetic cell[4,8b,9,13b,23] is obtained when chemical fuels are produced in addition to electricity, *i.e.*, when the reaction at the counterelectrode is not the exact opposite of the electron transfer reaction at the illuminated semiconductor electrode. In this case, at least two separate electrochemical potentials and electrode reactions must be considered to properly describe the cell operation (Figure 4a). In this cell, the two key

variables of interest are the light intensity dependence of the net current and the light intensity dependence of the open circuit voltage.

To apply the formalism of equations (1)-(6) to a photoelectrosynthetic cell, we again only need to calculate the net hole and electron fluxes through the semiconductor/liquid junction under the conditions of experimental interest. To avoid trivial solutions to the problem (*i.e.*, no current at any light intensity), we will assume that the band edges are located with respect to the two redox levels such that fuel production will occur under certain illumination conditions. This condition is met when $\mathbf{E}_{cb}<\mathbf{E}(C^+/C)$ and $\mathbf{E}_{vb}>\mathbf{E}(B^+/B)$, as shown in Figure 4a.[2]

The relevant redox potential energies are the Nernstian potential energies for the actual cell of interest (i.e., including activity effects and the actual concentrations of oxidized and reduced species), as opposed to the formal redox potential energies of a given system. To insure definite redox energies in the solution, we assume that the concentrations of B, B^+, C, and C^+ are maintained at defined values throughout the experiment, so that $\mathbf{E}(C^+/C)=\mathbf{E}^{o'}(C^+/C)+kT\ \ln\{[C^+]/[C])$, and $\mathbf{E}(B^+/B)=\mathbf{E}^{o'}(B^+/B)+kT\ \ln\{[B^+]/[B])$.[24] For water photoelectrolysis at an n-type semiconductor photoanode, this will simply correspond to maintaining the $H_2(g)$ pressure constant over the counterelectrode, and to maintaining a given $O_2(g)$ pressure over the semiconductor electrode.

We will also assume, for simplicity, that only C^+/C is present and/or electroactive at the counterelectrode, and will initially assume that only B^+/B is present in the working electrode compartment . This corresponds to the common situation for water electrolysis in which $H_2(g)$ is bubbled through the compartment containing a Pt or Pd counterelectrode, and $O_2(g)$ is being evolved at the semiconductor photoanode (Figure 4b).[8b]

The kinetic situation for this scenario can be readily described within the formalism of equations (1)-(6) (Figure 4a). k_{ht} will refer to the oxidation of B to form B^+. This again yields equation (7) to describe hole transfer processes at the semiconductor/liquid interface. In contrast to the regenerative photoelectrochemical cell, there are several possible pathways for interfacial electron transfer in the photoelectrosynthetic cell, because B^+ can be reduced to B (with rate constant $k_{et,\ B^+/B}$), or C^+ can be reduced to C (with rate constant $k_{et,\ C^+/C}$). In water photoelectrolysis, this scenario would correspond to oxidation of water to O_2 ($B=H_2O$; $B^+=O_2$) as the hole reaction, and to reduction of either O_2 (B^+) or of H_2O (C^+) as the electron reaction at the semiconductor electrode (Figure 4b).

At the counterelectrode, we will assume that the reaction consists entirely of charge exchange with species C^+ to form C (*i.e.*, $H_2O \Rightarrow H_2$), and that this reaction occurs with little overpotential (*i.e.*, the measured potential of the counterelectrode does not deviate significantly from the Nernstian equilibrium C^+/C potential). This is the common case for noble metal electrodes used in water photoelectrolysis.[25] The assumption that only C^+/C is electroactive at the counterelectrode has been adopted for several reasons: 1) species B^+ (*i.e.*, O_2 in our scenario) has been minimized in the counterelectrode compartment in order to insure that fuel can be formed from the reduction of C^+ to C; 2) if the entire cathode reaction exclusively involved the B^+/B ($O_2 \Rightarrow H_2O$) reduction, this would produce a regenerative cell (based on the O_2/H_2O redox system) whose characteristics have already been described above; and, 3) if a mixed reaction is assumed, only that portion of the current forming fuel differs in treatment from the regenerative cell. We do allow, however, for the possibility that conduction band electrons in the semiconductor can reduce either B^+ (O_2) or C^+(H_2O), because both species will be present simultaneously in this compartment and both will, in general, be electroactive at semiconductor surfaces.

Under these conditions, the equation for the net hole flux is identical to equation (3), with the general donor A^- replaced by the specific donor B (H_2O) of Figure 4. Continuity of interfacial hole flux again leads to equation (7), and again we will assume for simplicity that the hole transfer rate constant is sufficient that $p_s \approx p_{so}$.

The net electron flux in this photoelectrosynthetic cell is given by the sum of two terms:

$$\text{"net" electron flux} = k_{et,\, B^+/B}\,[B^+]\,(n_s - n_{so}) + k_{et,\, C^+/C}\,[C^+]\,(n_s - n_{so}') \qquad (12).$$

The first term is actually the back reaction in the B^+/B regenerative cell, equation (6), with the specific acceptor B^+ (O_2 in our example of Figure 4) replacing the general acceptor A. The second term arises from the possibility of conduction band electrons also reducing water itself (species C^+). The energy position of zero net electron current will be different for the two different redox couples C^+/C and B^+/B, so we must use a different concentration, n_{so}', in the second term of equation (12) than the surface electron concentration, n_{so}, used in the first term.

From equation (12), the net electron current can still be written in the form of equation (6), except that we will now use a combined electron transfer rate constant, k_n, to represent the sum of all the kinetic pathways for electrons to be transferred into acceptor species in the solution (Figure 5). k_n has a value of:

$$k_n = k_{et,\, B^+/B}\,[B^+] + k_{et,\, C^+/C}\,[C^+] \qquad (13).$$

k_n has units of cm/sec, *i.e.*, it combines the interfacial bimolecular charge transfer rate constant with the value of the acceptor concentration in the interphase region where charge transfer occurs.[15] The desired equation then has the form:

$$\text{"net" electron flux} = k_n\,(n_s - n_{so}'') \qquad (14).$$

Comparing equations (12-14) yields the value for the new constant, n_{so}", as:

$$n_{so}"=(1/k_n)\ \{n_{so}\ k_{et,\ B^+/B}\ [B^+] + n_{so}'\ k_{et,\ C^+/C}\ [C^+]\ \} \qquad (15).$$

n_{so}" represents the surface majority carrier concentration, in the presence of B^+/B and C^+/C, at which the net interfacial electron flux is zero, just as n_{so} in the simple B^+/B regenerative cell represents the surface majority carrier concentration that yields zero net electron current in the presence of only B and B^+.

Using a procedure analogous to that for the regenerative cell, the total current can now be obtained by subtracting the net electron flux from the net hole flux. This yields

$$i = q\ \{\phi\Gamma_o - \ k_n\ (n_s - n_{so}")\} \qquad (16).$$

This is the desired equation that will yield the explicit dependence of the current on incident light intensity. The key issue is to determine the value of n_s under the various scenarios, and then to use equation (16) to solve for the current produced by the semiconductor/liquid interface.

1. Dependence of Short Circuit Photocurrent on Incident Photon Flux

Unlike the regenerative B^+/B photoelectrochemical cell, for which short circuit conditions implied $n_s=n_{so}$, short circuiting the semiconductor and counterelectrode in the fuel-forming cell will produce a non-equilibrium bias voltage, $V_{cell}=(1/q)[\mathbf{E}(B^+/B)-\mathbf{E}(C^+/C)]$, across the semiconductor/liquid interface. This bias voltage will result in a change in the potential distribution at the semiconductor/liquid junction relative to the short circuit regenerative cell case, and will lead to a change in surface electron concentration relative to its equilibrium value. The most important point for our discussion is that the electron concentration in the semiconductor bulk will be maintained at a value that is in equilibrium with the Nernstian potential energy of the counterelectrode (Figure 5).[10]

Under these conditions, we can readily solve for n_s by writing $n_s=n_b\exp\{-q(V_{bi}-V_{cell})/kT\}$, or alternatively, $n_s=N_c\exp\{[(\mathbf{E}_{cb}-\mathbf{E}(C^+/C)]/kT\}$ (where N_c is the effective density of states in the semiconductor conduction band). Substituting into equation (14), we obtain

$$i = q\ \{\phi\Gamma_o - \ k_n\ n_b\exp[-q(V_{bi}-V_{cell})/kT] + k_n\ n_{so}"\}. \qquad (17a),$$

or

$$i = q\ \{\phi\Gamma_o - \ k_n\ N_c\exp\{[\mathbf{E}_{cb}-\mathbf{E}(C^+/C)]/kT\} + k_n\ n_{so}"\} \qquad (17b)$$

as the expressions for the short circuit current of the cell.

When $\Gamma_o=0$, equation (17) implies that $i<0$, because $n_s>>n_{so}"$ in this photoelectrosynthetic cell. This condition makes sense, because without light energy input into the system, the electrochemical cell will merely act as a fuel cell, and will yield a steady state current flow in a direction consistent with the thermodynamically favored reaction $C + B^+ \Rightarrow C^+ + B$. Increasing the light intensity striking the semiconductor will produce a current that opposes this spontaneous dark current, and will eventually result in the net production of fuels B^+ and C. Within the framework of equations (17), increasing the light intensity will produce an increase in the hole flux to the surface, $\phi\Gamma_o$. Equations (16) and (17) therefore yield a simple expression for the light intensity dependence of the total current. When the light intensity is sufficiently large that $i=0$, *i.e.*, when $\phi\Gamma_o=k_n(n_s-n_{so}")$, the threshold for fuel production will be reached, and the net current through the external circuit will be exactly zero. Higher light intensities will result in $i>0$, *i.e.*, $\phi\Gamma_o>k_n\ (n_s-n_{so}")$, and only under these conditions will the cell be capable of sustaining the net electrolysis of fuels B^+ and C.

2. Three Electrode Potentiostatic Behavior

The expressions describing the current flow under potentiostatic control of the semiconductor electrode are readily obtained from equation (17). The potentiostat controls the value of n_s through the relationship $n_s=N_c\exp[(\mathbf{E}_{cb}-qE_{pot})/kT]$, with E_{pot} the potential of the working (semiconductor) electrode. This relationship holds both in the dark and under steady state illumination conditions. The continuity condition for the interfacial minority carrier flux under illumination again implies that the hole flux to the interface has a value of $\phi\Gamma_o$. Combining these two relationships leads to the explicit dependence of i on E_{pot}:

$$i = q\ \{\phi\Gamma_o - k_n N_c\exp[(\mathbf{E}_{cb}-qE_{pot})/kT]+k_n n_{so}"\} \qquad (18)\ .$$

This expression closely resembles equation (17), except that in equation (18) the current is controlled explicitly by the value of qE_{pot}, instead of by the value of $\mathbf{E}(C^+/C)$. When $qE_{pot}=\mathbf{E}(C^+/C)$, the potentiostatic experiment and the two-electrode photoelectrosynthetic cell should produce identical dependences of the net current on the incident light intensity. Changing the applied potential in the three electrode potentiostatic cell configuration will merely alter the value of n_s, and will therefore correspond to the i *vs.* Γ_o characteristic of a two-electrode cell with a different value for $\mathbf{E}(C^+/C)$ but with all other parameters held constant. In these cases, when $n_s>n_{so}"$, a dark current opposite in sign to the light-induced current is present, and its value depends (in general, exponentially) on the value of qE_{pot}.

For certain values of the electrode potential E_{pot}, the photoelectrode current *vs* illumination intensity behavior will be identical to that of a regenerative photoelectrochemical cell. When E_{pot} is sufficiently positive that $n_s=n_{so}"$, the current flow through the semiconductor/liquid interface should be analogous to that predicted from equation (8) for a regenerative photoelectrochemical cell with $n_s=n_{so}$. Under this condition of applied bias, no threshold in current would be observed, and the observed current would

be linearly proportional to Γ_o, with i=0 in the absence of illumination. In the potentiostatic configuration, this linearity of net current with light intensity would apply whether the counterelectrode was actually sustaining the electrolysis of $B^+ \Rightarrow B$ or $C^+ \Rightarrow C$, because the potentiostat would provide the compliance voltage necessary to maintain the condition that $n_s=n_{so}$" at the semiconductor electrode. A similar dependence would hold when $qE_{pot}=E(B^+/B)$, *i.e.*, $n_s=n_{so}$ is established, except that a small dark current, of the same sign as the photocurrent, would be present due to the oxidation of species C at the semiconductor electrode. Variation in the value of qE_{pot} can thus lead to different dependences of i on Γ_o, depending on the value of n_s at the chosen potential of the semiconductor electrode. Below we describe experiments that investigate these predictions for the photoelectrolysis of H_2O at n-type $SrTiO_3$ surfaces.

III. EXPERIMENTAL

A. $SrTiO_3$ Photoelectrode

Single crystals of (100)-oriented $SrTiO_3$ (band gap = 3.2 eV) were obtained from Commercial Crystal Laboratories Inc., Naples, Florida. Samples were doped n-type by heating for 10 hours at 1100° C in a quartz tube furnace under a flowing atmosphere of forming gas (95% N_2, 5% H_2).[6a] The crystal was then allowed to cool for 8 hours under the flowing forming gas. During doping the color of the initially white, opaque, crystal changed to a dark blue/black color, which was consistent with the expected increase in conductivity accompanying the introduction of oxygen vacancies and/or titanium interstitials into the metal oxide lattice.[26]

Ohmic contact to the crystal was made by rubbing a Ga:In eutectic mixture onto the back of the sample. The back of the crystal was then contacted to Sn wire, and the electrode was insulated with epoxy to expose a square area approximately 2 mm on each

side. Before all experiments, the electrode was etched twice in concentrated nitric acid for 20 seconds, followed by rinsing in flowing water and drying in a stream of $N_2(g)$.

B. Electrochemical Cells and Instrumentation

All cells were made with high purity chemicals. NaOH was used as obtained from the supplier (EM Science Inc., New Jersey), and a Barnsted NANOpure water purifier provided 18 MΩ resistivity deionized water. The electrochemical cell was fabricated out of pyrex, but a Dynasil-type quartz window (California Quartz) was incorporated near the position of the working electrode to maximize optical transmission in the UV spectral region. The two electrode configurations consisted of the $SrTiO_3$ working electrode and a Pt black counter electrode. Three electrode configurations consisted of the $SrTiO_3$ working electrode, a standard calomel (SCE) reference electrode, and a Pt black counterelectrode of area > 2 cm^2. For the two electrode experiments the counter electrode was placed inside a separate compartment that was isolated from the remainder of the cell with a ceramic frit (Corning Glass, New York). Both compartments were purged with appropriate gases through thin polyethylene tubes that were immersed in the solutions.

For three electrode experiments, a PAR 362 Scanning Potentiostat (Princeton Applied Research, NJ) was used to control potentials, and data was recorded on a Houston Instruments (Houston, TX) Model 2000 Omnigraphics X-Y recorder. For two electrode experiments, the output from a Keithley Model 427 picoammeter, connected in series with the two electrodes, was read on a Keithley Model 177 Digital Multimeter. For all cells where the counterelectrode compartment was under $H_2(g)$, the potential of the counterelectrode was determined by measuring the voltage between the platinized Pt electrode under 1 Atm. of $H_2(g)$ and an SCE .

C. Light Source

The blue line (λ=325 nm, 3.8 eV) of a He:Cd laser (Liconix, Sunnyvale, CA) was used as the illumination source. To achieve a relatively uniform light intensity across the $SrTiO_3$ photoelectrode surface, the beam profile was diffused by transmission through a roughened quartz flat. The incident light intensity was controlled by using transmission filters fabricated from evaporation of thin (<100 Å) layers of metal onto glass. Light intensities were measured using a calibrated photodiode supplied from United Detector Technologies, Hawthorne, CA.

IV. RESULTS

A. Two Electrode non-Potentiostatic Experiments

$SrTiO_3$ was chosen for study because previous work has shown that illumination of n-type $SrTiO_3$/NaOH(aq)/Pt cells can yield the sustained, unassisted, electrolysis of water to produce H_2(g) and O_2(g).[6] In the first set of experiments to be described below, the $SrTiO_3$ compartment was purged with 1 atm O_2(g), and the Pt compartment was purged with 1 atm H_2(g). This established well-defined Nernst potentials in both portions of the cell, and also established kinetic conditions compatible with the theoretical analysis of photoelectrolysis reactions described in section IID.

Figure 6 depicts the dependence of the short circuit current on the light intensity incident onto the $SrTiO_3$ electrode. A dark current was observed in the external circuit, which is consistent with the expected, thermodynamically favored, reduction of O_2 at the $SrTiO_3$ electrode and oxidation of H_2 at the Pt electrode. Illumination of the n-$SrTiO_3$ surface produced a current that was opposite in sign to this dark current, and yielded an obvious threshold behavior as a function of the incident light intensity. This onset of measurable net photocurrent was observed for an illumination intensity between 0.023 and 0.03 mW/cm^2.

Data was also collected for n-type $SrTiO_3$ electrodes operated in a regenerative cell arrangement. This condition was established by purging both the $SrTiO_3$ and the Pt electrode compartments with 1 atm O_2(g). Under these conditions, O_2 was oxidized at the $SrTiO_3$ electrode and was reduced to H_2O at the Pt electrode. In this cell, no measurable dark current was observed at short circuit. For this cell, Figure 7 presents the data for the light intensity dependence of the net current through the external circuit. As expected for a regenerative cell, the current was linearly dependent on the incident light intensity, and no threshold in current was observed for light intensities as low as $5x10^{-3}$ mW/cm^2 of illumination onto the $SrTiO_3$ surface.

B. Three Electrode Potentiostatic Experiments

Three-electrode potentiostatic experiments were conducted with the $SrTiO_3$ compartment purged with 1 atm Ar(g). The thermodynamic potential for H_2 evolution in 5.0 **M** NaOH(aq) was measured at a Pt black electrode under 1 atm H_2(g) as -1.06 V *vs* SCE, and the O_2/H_2O potential was therefore +0.17 V *vs* SCE at this pH. Figure 8 displays typical I-V curves of the n-$SrTiO_3$/5.0 **M** NaOH(aq) interface at several different light intensities. At low incident light intensities, the onset of anodic current occurred at potentials more positive than the H^+/H_2 potential, whereas only higher light intensities yielded anodic current at potentials more negative than -1.06 V vs. SCE. Compared to previous I-V data on this system,[6] the fill factor of the junctions was quite high in the anodic potential region, with values of 0.58-0.64 typical for these conditions. In addition, for voltages V< -0.8 V vs. SCE, the cathodic current density was larger when the electrode was exposed to 1 atm O_2(g) than when it was exposed to 1 atm H_2(g).

For this three-electrode potentiostated experiment, at potentials positive of 0.0 V vs. SCE, the net current was linear with the incident light intensity, with no apparent threshold behavior. In contrast, at more negative potentials, a finite dark current with an apparent

threshold for photocurrent was observed. The value of the dark current depended on the electrode potential, but the slope of the photocurrent *vs.* light intensity was independent of the potential for E_{pot}>0.0 V vs. SCE.

A measure of the open circuit voltage of the semiconductor electrode can be obtained by considering the difference between the potential of zero net current and the Nernstian O_2/H_2O potential. This value represents the maximum free energy available from the photoelectrode at a particular light intensity, regardless of whether it is used in a regenerative cell configuration where the counterelectrode reduces $O_2(g)$ to H_2O or whether the counterelectrode is used to produce a fuel such as $H_2(g)$ from H_2O. Figure 9 displays this data, which indicates that the photovoltage increases logarithmically with increasing light intensity. The intercept of this plot will be the natural log of the sum of all of the back reaction rates at equilibrium.[9-11]

V. DISCUSSION

The data presented above are in accord with expectations based on the statistical approach to photoelectrolysis reactions.[3,9,10,14] In the two electrode experiment, a light intensity threshold was observed for the sustained production of 1 atm $H_2(g)$ at the Pt electrode and 1 atm $O_2(g)$ at the $SrTiO_3$ electrode. In the dark, or at very low light intensities, the overall electrochemical reaction comprised the oxidation of $H_2(g)$ to H_2O and the reduction of $O_2(g)$ to H_2O, and produced a current that was opposite in sign to the light-induced current. This is precisely the behavior expected when the free energy of the collection of photoexcited carriers in the semiconductor is a function of the incident light intensity (*vide supra*, section II). Such behavior is not consistent with the prediction of the stochastic treatment that each photoexcited electron-hole pair should be treated as an individual event with the full electron-hole pair free energy available over the entire range of illumination intensities.[8]

The light-intensity dependence of the semiconductor photovoltage was also indicated by the I-V behavior of the three-electrode potentiostatic experiments. At low light intensities, the onset of anodic current occurred at potentials positive of the H^+/H_2 Nernst potential, and only high light intensities yielded a net anodic current for $E_{pot}<E(H^+/H_2)$. This behavior is in accord with the properties of the two-electrode cells reported in Figure 6, and indicates that unassisted, sustained electrolysis of H_2O to produce H_2 and O_2, in the presence of 1 atm O_2 in the semiconductor compartment and 1 atm H_2 in the Pt compartment, can only proceed above a specific light intensity. This is equivalent to the statement that relative to the O_2/H_2O potential, the open circuit voltage of the illuminated n-$SrTiO_3$/NaOH junction is less than $E(O_2/H_2O)$-$E(H^+/H_2)$=1.23 V at low light intensities, and exceeds this critical thermodynamic value only above a certain light intensity threshold. The statistical theory and experimental data thus are in agreement with the conclusion that only when the available, light intensity dependent, photovoltage exceeds the initial cell electromotive force will the net current change sign relative to the dark current, and will the sustained production of fuels be possible.

The lack of a photocurrent threshold for n-type $SrTiO_3$ in a three electrode potentiostatic experiment for $E_{pot}>0.0$ V *vs* SCE can also be understood within the framework of section II. When the potentiostatically controlled voltage is sufficiently positive that $n_s \approx n_{so}$", equation (18) indicates that the net current is directly proportional to the incident light intensity. Under these potentiostatic conditions, the remaining (light-intensity dependent) voltage necessary to sustain current flow through the external circuit will be supplied by the compliance voltage of the potentiostat, and only variation in the electrode potential (*i.e.*, variation of n_s) will affect the dependence of the potentiostatically-controlled current on the value of the incident light intensity.

We can now understand the lack of observation of a photocurrent threshold that has been reported previously by Nozik for the TiO_2-induced water photoelectrolysis reaction.[8b] n-type rutile TiO_2 single crystals cannot sustain the electrolysis of H_2O without an external bias;[2,4,5a] thus, only the trivial case of no photocurrent at any light intensity would be observed under direct short circuit conditions to a Pt counterelectrode under 1 atm $H_2(g)$. In a potentiostatic experiment, a photocurrent would be observed for $E_{pot}>(E(H^+/H_2)+0.3$ V), but as for n-$SrTiO_3$, this current will be linear with the incident light intensity when E_{pot} is sufficiently positive that $n_s \approx n_{so}$". This linearity in light intensity when n_s is under potential control does not directly address the question of whether the free energy of the photoexcited semiconductor carriers is a function of light intensity; only experiments that probe the voltage developed by the photoexcited semiconductor can directly address this issue. Such experiments are provided by the two-electrode experiments with controlled Nernst potentials in each electrode compartment described in Figure 4, and/or by inspection of the position of zero net current in the three electrode potentiostatic experiment of Figure 8. Thus, the observation of no photocurrent threshold when $n_s \approx n_{so}$" is fully expected from the conventional statistical approach to semiconductor electrochemistry, and does not in itself distinguish between the stochastic and statistical treatment of photoelectrochemical events.

The prediction of a light-intensity threshold for water photoelectrolysis can also be obtained using the so-called quasi-Fermi level formalism.[10,14] Defining the hole quasi-Fermi level energy from the relationship $p(x)=N_v\exp[(\mathbf{E}_{fp}(x)-\mathbf{E}_{vb})/kT]$, and the electron quasi-Fermi level energy from the relationship $n(x)=N_c\exp[(\mathbf{E}_{cb}-\mathbf{E}_{fn}(x))/kT]$ (where the values of p, n, $\mathbf{E}_{fp}$, and $\mathbf{E}_{fn}$ can be dependent on the position, x, relative to the semiconductor/liquid interface) leads to a formalism in which hypothetical individual electrochemical potentials of minority and majority carriers can be calculated for specified conditions of applied bias, light intensity, *etc.* to the solid/liquid interface.[9-11] For a

regenerative cell in the dark at equilibrium, $\mathbf{E}_{fp}=\mathbf{E}_{fn}=\mathbf{E}_f=\mathbf{E}(A/A^-)$, as shown in Figure 10a. Illumination of the semiconductor electrode in this regenerative cell will lead to an increase in the surface electron and hole concentrations relative to their equilibrium values, with $n_s p_s >> n_{so} p_{so} = n_i^2$. The assumption of rapid hole transfer from equation (7), *i.e.*, that $p_s \approx p_{so}$, is equivalent to the statement that $\mathbf{E}_{fp} \approx \mathbf{E}(A/A^-)$ for the illuminated semiconductor/liquid junction. The lack of movement in $\mathbf{E}_{fp}$ due to this kinetic constraint therefore implies that, under illumination, the surface electron quasi Fermi level has moved closer to the conduction band energy, *i.e.*, $\mathbf{E}_{fn} << \mathbf{E}(A/A^-)$ (Figure 10b).

The extent of recombination will control the absolute value of the $p_s n_s$ product, and therefore the position of the electron quasi-Fermi level within this treatment. In a regenerative cell, the position of $\mathbf{E}_{fn}$ relative to $\mathbf{E}(A/A^-)$ is the open circuit voltage of the semiconductor/liquid interface. This leads to equation (10) as the quantitative expression of n_s, and therefore V_{oc}, under these conditions. For a photoelectrosynthetic cell, only when $\mathbf{E}_{fn}$ becomes more negative than $\mathbf{E}(C^+/C)$ will the illuminated semiconductor electrode develop sufficient photovoltage to sustain the light-induced electrolysis of fuels $B \Rightarrow B^+$ and $C^+ \Rightarrow C$. Because the position of $\mathbf{E}_{fn}$ is explicitly dependent on the light intensity (through equation (11) for the regenerative cell situation), a light intensity threshold for photoelectrolysis is also predicted from the quasi-Fermi level formalism of semiconductor/liquid contacts.[14] This prediction is in agreement with experimental data for the $SrTiO_3$/NaOH junction, as reported above. It is also a direct consequence of the values of the surface concentrations of majority carriers and minority carriers as expressed in the kinetic formalism of equations (1)-(18) in section II above.

It is also of interest to examine the conditions under which no photoelectrolysis threshold would be predicted from the kinetic model described above. The presence of a finite dark current, by any mechanism, will always lead to an apparent threshold behavior of the net current for the fuel-forming reaction in the external circuit of the cell. Therefore,

the only mechanism by which this threshold can be eliminated is to totally suppress all of the dark reactions, *i.e.*, to set $k_n=0$ in equation (14) and $k_{ht}^{-1}=0$ in equation (2). The $k_{ht}^{-1}=0$ assumption is not consistent with microscopic reversibility arguments for the interfacial hole transfer process.[27] These assumptions of $k_n=0$ and $k_{ht}^{-1}=0$ are not justified for real semiconductor systems, because there are always back reaction pathways by which the majority carriers can transfer into the solution; additionally, recombination reactions of the majority carriers with photogenerated minority carriers inside the semiconductor cannot be neglected and set to zero.[10,19] In the dark, the presence of a potential difference between the semiconductor electrode and the metal counterelectrode will insure that the carrier concentrations in the semiconductor deviate from their equilibrium values; any recombination mechanisms that tend to restore these concentrations to their equilibrium positions must be considered in determining the net current flowing through the external circuit. Even if no trapping sites are present, thermal generation/recombination processes such as radiative luminescence will act to restore the carrier concentrations towards their equilibrium values.[28] Thus, the above treatment always predicts a threshold in fuel-forming ability, regardless of the actual values of the interfacial minority or majority carrier charge transfer rate constants in the system.

Some of the evidence supporting the stochastic model for interfacial charge transfer has been obtained from the observation of high quantum yields for photocurrent collection at the n-TiO_2/liquid interface, and from experiments indicating the possibility of unthermalized, hot, hole transfer at TiO_2/H_2O junctions.[29] Within the kinetic framework developed above, the observation of a photoelectrolysis threshold is predicted regardless of the value of k_{ht}; in fact, the assumption of equation (7) that $p_s \approx p_{so}$ is more rigorous for larger values of k_{ht}. The hole continuity expression of equation (7) implies that as long as competing recombination pathways are sufficiently small, the condition $k_{ht}p_s[A^-]=\phi\Gamma_o$ will be met, and the quantum yield for collected minority carriers will approach unity regardless

of the actual value of k_{ht}. This condition is obviously expected to hold at large positive values of E_{pot}, because the strong interfacial electric field will reduce n_s and thereby suppress all bimolecular interfacial recombination rates at the semiconductor/liquid junction.

If k_{ht} is very small, then p_s must build up relative to p_{so} in order for current continuity to be satisfied; this will simply act as an overpotential for hole transfer and will act to increase the light intensity threshold value at which the photovoltage developed in the semiconductor is sufficient to sustain the water electrolysis reaction. Thus, the observation of a threshold for photoelectrolysis does not directly address the value of k_{ht}, nor the issue of whether thermalized or hot hole transfer has occurred at the n-$SrTiO_3$/NaOH(aq) interface.

In conclusion, the present experiments indicate that charge transfer at the n-$SrTiO_3$/5.0 **M** NaOH(aq) interface can be described using a conventional kinetic treatment of the collective behavior of photoexcited semiconductor carriers. The free energy of the illuminated $SrTiO_3$/NaOH(aq) interface is a function of the light intensity incident on the semiconductor surface, and only when the photovoltage exceeds the electromotive force for production of 1 atm H_2(g) and 1 atm O_2(g) from H_2O can a sustained photoelectrolysis of water be effected. The experimental data for $SrTiO_3$-based potentiostatic and non-potentiostatic cells are consistent with this conclusion. Straightforward expressions have been presented that offer an intuitive, chemical kinetic approach to this behavior, and this kinetic treatment appears to describe satisfactorily the behavior of typical regenerative photoelectrochemical cells and photoelectrosynthetic cells explored to date. The observation of a photoelectrolysis threshold does not directly address the question of whether interfacial charge transfer occurs from a thermalized carrier distribution, and such conclusions require independent experiments that probe the carrier dynamics and thermalization times in the system of interest.

ACKNOWLEDGEMENTS

We thank the National Science Foundation, grant CHE-8814263, for support of this work. A.K. also is grateful to the U.S. Department of Education for a graduate fellowship.

REFERENCES

1. Fujishima, A.; Honda, K. *Nature* **1972**, *238*,37.

2. Finklea, H.O. *Semiconductor Electrodes*; Elsevier: Amsterdam, 1988.

3. Morrison, S.R. *Electrochemistry at Semiconductor and Oxidized Metal Electrodes*; Plenum: New York, 1981.

4. Rajeshwar, K. *J. Appl. Electrochem.* **1985**, *15*, 1.

5. a) Wrighton, M.S.; Ginley, D.S.; Wolczanski, P.T.; Morse, D.L.; Linz, A. *Proc. Natl. Acad. Sci. USA*. **1975**, *72*, 1518. b) Carey, J.H.; Oliver, B.G. *Nature* **1976**, *259*, 554. c) Hardee, K.L.; Bard, A.J. *J. Electrochem. Soc.* **1975**, *122*, 739. d) Yoneyama, H.; Sakamoto, H.; Tamura, H. *Electrochimica Acta*, **1975**, *20*, 341.

6. a) Wrighton, M.S.; Ellis, A.B.; Wolczanski, P.T.; Morse, D.L.; Abrahamson, H.B.; Ginley, D.S. *J. Am. Chem. Soc.* **1976**, *98*, 2774. b) Mavroides, J.G.; Kafalas, J.A.; Kolesar, D.F. *Appl. Phys. Lett.* **1976**, *28*, 241. c) Wrighton, M.S.; Wolczanski, P.T.; Ellis, A.B. *J. Solid State Chem.* **1977**, *22*, 17.

7. a) Kung, H.H.; Jarrett, H.S.; Sleight, A.W.; Ferretti, A. *J. Appl. Phys.* **1977**, *48*, 2463. b) Wrighton, M.S.; Morse, D.L.; Ellis, A.B.; Ginley, D.S.; Abrahamson, H.B. *J. Am. Chem. Soc.* **1976**, **98**, 44. c) Dare-Edwards, M.P.; Goodenough, J.B.; Hamnett, A.; Trevellick, P.R. *J. Chem. Soc. Faraday Trans. I*, **1983**, *79*, 2027. d) Leygraf, C.; Hendewerk, M; Somorjai, G.A. *Proc. Natl. Acad. Sci. USA*. **1982**, *79*, 5737. e) Yamaguti, K.; Sato, S. *Nouv. J. Chimie,* **1986**, *10*, 217. f) Anpo, M.; Nakaya, H.; Kodama, S.; Kubokawa, Y.; Kazunari, D.; Onishi, T. *J. Phys. Chem.* **1986**, *90*, 1633. g) Justice, D.D.; Hurd, R.M. *J. Electrochem. Soc.* **1971**, *118*, 1417. h) Liska, P.; Vlachopoulos, N.; Nazeeruddin, M.K.; Comte, P.; Gratzel, M. *J. Am.*

Chem. Soc. **1988**, *110*, 3686. i) Lehn, J.M.; Sauvage, J.P.; Ziessel, R. *Nouv. J. Chimie.* **1980**, *4*, 623.

8. a) Williams, F.; Nozik, A.J. *Nature*, **1978**, *271*,137 b) Nozik, A.J. *Ann. Rev. Phys. Chem.***1978**, *29*, 189.

9. a) Gerischer, H. *J. Electroanal. Chem.* **1977**, *82*, 133. b) Gerischer, H. in *Semiconductor-Liquid Junction Solar Cells, Proceedings of the Conference on the Electrochemistry and Physics of Semiconductor-Liquid Interfaces Under Illumination, Airlie, VA*. Heller, A., Ed., Electrochem. Soc.:Princeton, NJ 1977, p. 1.

10. Fonash, S.J. *Solar Cell Device Physics*; Academic: New York, 1981.

11. a) Myamlin, V.A.; Pleskov, Y.V. *Electrochemistry of Semiconductors*, Plenum: New York, 1967. b)Pleskov, Y.V.; Gurevich, Y.Y. *Semiconductor Photoelectrochemistry*, Consultants Bureau: New York, 1986.

12. a) Eden, R.C.; Moll, J.C.; Spicer, W.E. *Phys Rev. Lett.* **1967**, *18*, 597. b) Williams, F.; Nozik, A.J. *Nature* **1984**, *312*, 21.

13. a) Wrighton, M.S. *Acc. Chem. Res.* **1979**, *12*, 303. b) Parkinson, B.A. *Acc. Chem. Res.* **1984**, *17*, 431. c) Heller, A. *Acc. Chem. Res.* **1981**, *14*, 5. d) Lewis, N.S. *Acc. Chem. Res.* **1990**, *23*, 176.

14. a) Gerischer, H. *Adv. Electrochem. and Electrochem. Eng.* **1966**, *4*, 249. b) Gerischer, H. in *Physical Chemistry: An Advanced Treatise, Vol IXA* , H. Eyring Ed. Academic: New York, 1970, p. 463. c) Memming, R. *Electroanalytical Chemistry*, Vol II. A.J. Bard, Ed. Dekker: New York, 1979. d) Memming, R. *Ber. Bunsenges. Phys. Chem.* **1987**, *91,* 353.

15. Lewis, N.S. *Ann. Rev. Phys. Chem.* in press.

16. Shockley, W.; Read, W.T. *Phys. Rev.* **1957**, *87*, 835.

17. Evenor, M.; Huppert, D.; Gottesfeld, S. *J. Electrochem. Soc.*, **1980**, *133*, 296.

18. Reiss, H. *J. Electrochem. Soc.* **1978**, *125*, 937.

19. Fahrenbruch, A.L.; Bube, R.H. *Fundamentals of Solar Cells*; Academic: New York, 1983.

20. Wilson, R.H. *CRC Crit. Rev. Mater. Sci.*, **1980**, *10*, 1.

21. Rosenbluth, M.L.; Lewis, N.S. *J. Phys. Chem.* **1989**, *93*, 3735.

22. This will occur even when the condition V_{oc}>>kT/q does not hold, although V_{oc} will not increase strictly logarithmically for such low light intensities.

23. Bard, A.J. *Science*, **1980**, *207*, 139.

24. Bard, A.J.; Faulkner, L.F. *Electrochemical Methods*; Wiley: New York, 1980.

25. Bockris, J. O'M.; Reddy, A.K.N. *Modern Electrochemistry*, Vol. II; Plenum: New York, 1970.

26. Perluzzo, G.; Destry, J. *Can. J. Phys.* **1978**, *56*, 453.

27. Note that k_{ht}' can be neglected in calculating the total "back reaction" rate when $k_{ht}'[A^-]$ is small compared to $k_{et}n_s[A]$. However, when using detailed balance to obtain the forward *vs* backward rate constants for the valence band process (equation (3)), the ratio k_{ht}/k_{ht}' must be considered, and k_{ht}' can therefore never be set to zero for a finite equilibrium constant for this charge transfer process. The value of k_{ht}' becomes important when considering the lower limit on the value of the total anodic back reaction rate when $k_{et}n_s[A]$ is small compared to the valence band anodic hole injection flux.

28. Blakemore, J.S. *Semiconductor Statistics*, Dover:New York, 1987.

29. Kasinski, J.J.; Gomez-Jahn, L.A.; Faran, K.J.; Gracewski, S.M.; Miller, R.J.D. *J. Chem. Phys.* **1989**, *90*, 1253.

Figure 1. Energy vs. distance diagram for an n-type semiconductor/liquid junction. At short circuit, the Fermi level energy in the semiconductor, $\mathbf{E}_f$, is equal to the redox energy of the electrolyte, $\mathbf{E}(A/A^-)$, and the voltage dropped across the semiconductor phase is equal to the so-called built-in voltage, V_{bi}. Under these short circuit conditions, no net charge flows through the interface unless the semiconductor is exposed to illumination. Light absorption by the semiconductor produces an electron-hole pair, which is separated by the interfacial electric potential gradient. The net interfacial current is the sum of the processes producing anodic current flow and those producing cathodic current flow. The separate processes are represented as follows: k_{ht} is the rate constant for capture of valence band holes by the electron donor, A^-, k_{et} is the rate constant for capture of conduction band electrons by the electron acceptor, A, k_{et}^{-1} is the rate constant for injection of electrons into the conduction band by the donor species A-, and k_{ht}^{-1} is the rate constant for injection of holes into the valence band by the acceptor species A. The solid arrows represent the forward reactions, i.e., anodic current for an n-type semiconductor, and the dashed arrows represent the back reactions that oppose this current flow.

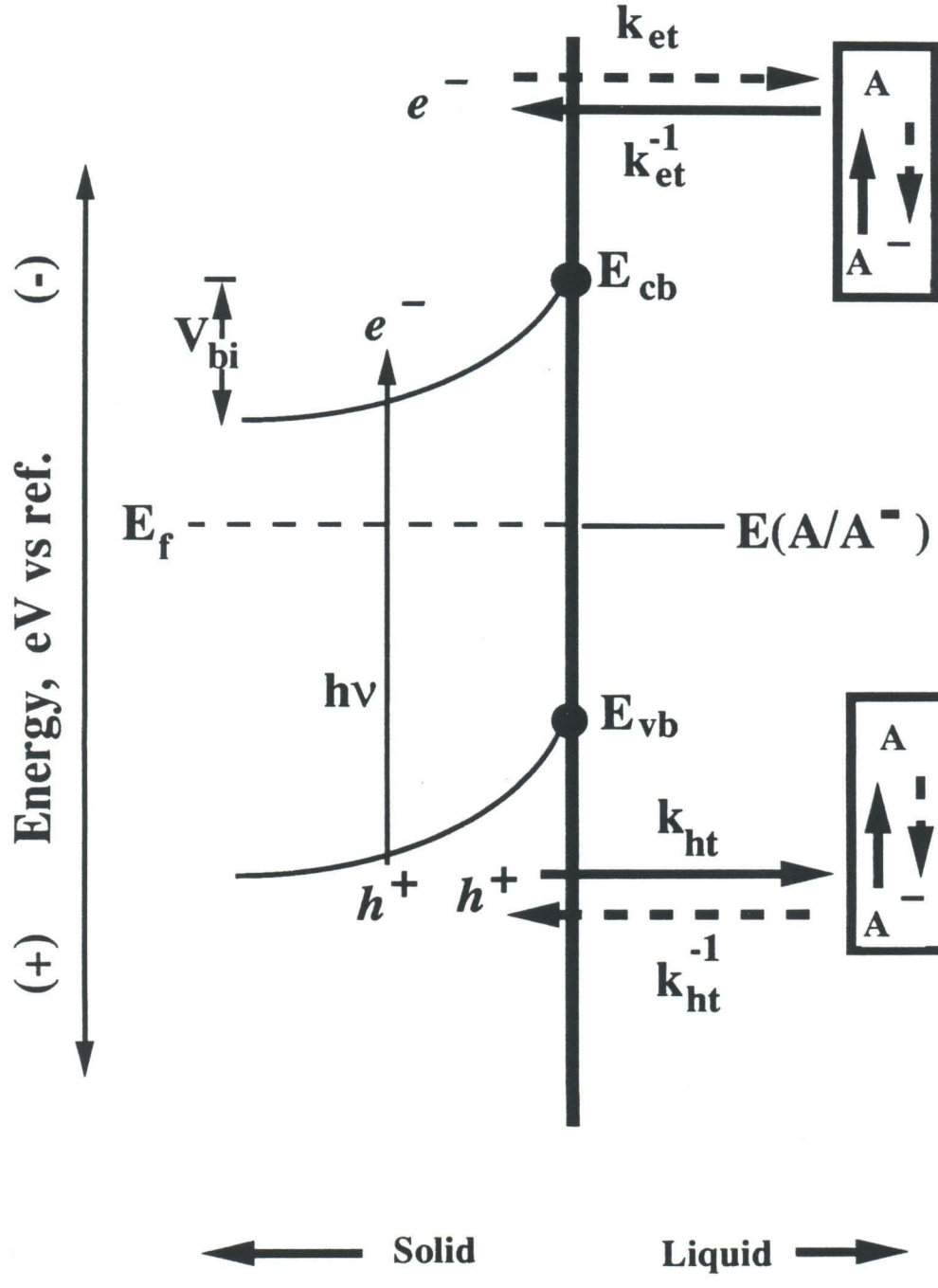
k et
e −
k -1 et
A
A −
E cb
V bi
e −
E f
E(A/A⁻)
hν
E vb
k ht
h+ h+
k -1 ht
A
A −
Energy, eV vs ref.
(-)
(+)
Solid
Liquid

Figure 2. Schematic of minority carrier flow at an illuminated semiconductor/liquid interface. Illumination of the semiconductor with a photon flux Γ_o will produce electron-hole pairs that will either recombine or survive to produce a net current through the interface. Combining all the possible recombination processes into one parameter, $1-\phi$, the minority carrier flux at the interface is equal to the number of carriers created, Γ_o, minus the fraction that is lost through recombination as the minority carriers move towards the interface, $(1-\phi)\Gamma_o$. The surviving flux of minority carriers available to participate in the charge transfer reaction is therefore $\phi\Gamma_o$. Continuity implies that the hole concentration at the interface will increase until the interfacial flux exactly balances the photogenerated minority carrier flux arriving to the semiconductor/liquid interface, yielding an interfacial hole flux of $\phi\Gamma_o$ under these illumination and bias conditions.

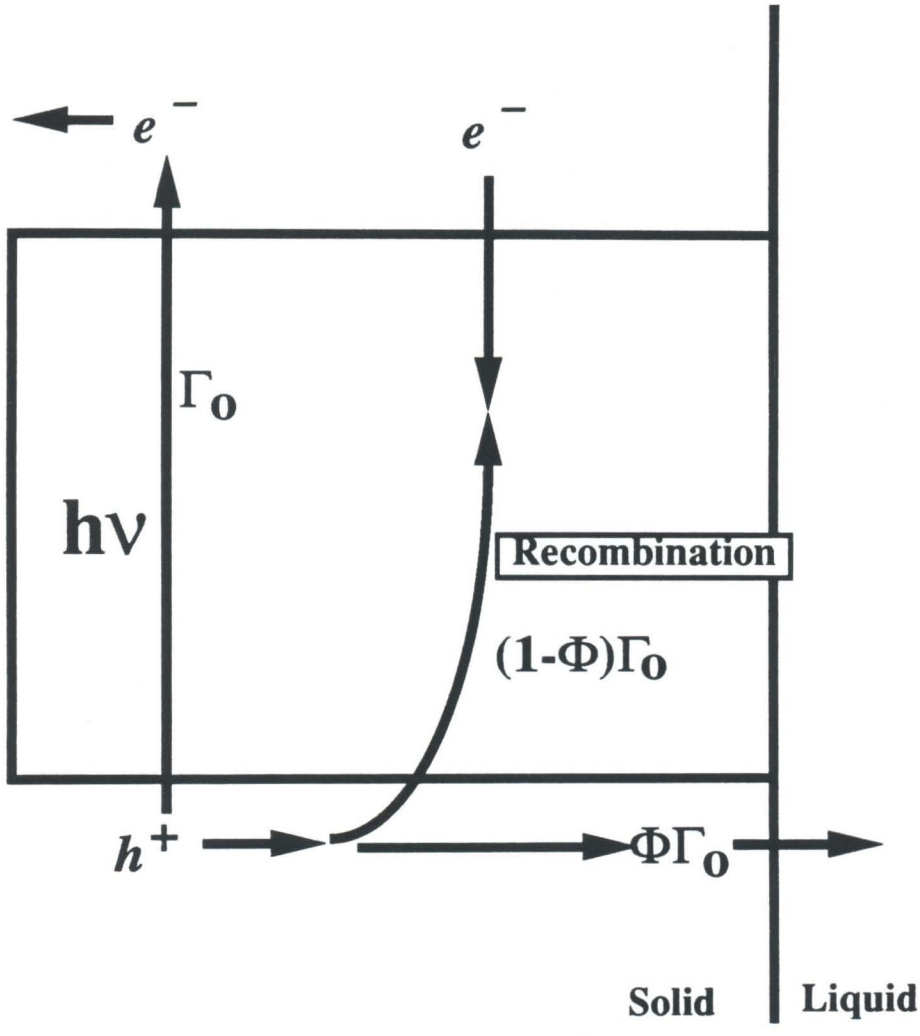
e⁻
e⁻
Γo
hν
Recombination
(1-Φ)Γo
h⁺
ΦΓo
Solid
Liquid

Figure 3. Kinetic processes for regenerative photoelectrochemical cells under various conditions of applied bias and light intensity. a) Under short circuit conditions in the dark, no net interfacial current is observed. Electron capture by the solution acceptor A is exactly offset by electron injection from the solution donor A^-, and a similar balance occurs between the two valence band hole currents (not shown). b) Under illumination at short circuit, the flux of photogenerated minority carriers is given by $\phi\Gamma_o$, as depicted in Figure 2. However, at short circuit, the net electron current arising from the conduction band processes is still zero, as depicted in Figure 3a under this short circuit bias condition. The non-zero interfacial valence band flux, but zero interfacial conduction band flux, results in a net anodic current through the illuminated semiconductor/liquid junction. c) Under open circuit conditions, in either the light or the dark, the value of the net interfacial current must be zero. In the dark, this occurs when the Fermi levels of the semiconductor and the electrolyte are equal, since equal and opposite exchange currents are flowing, as depicted in Figure 3a. d) Under illumination, as seen in Figure 3b, a net interfacial hole flux is present from the valence band. At open circuit, to maintain a net current equal to zero, the semiconductor/liquid junction counteracts this increased hole flux by increasing the surface electron concentration and increasing the conduction band electron flux. The surface electron concentration increases until zero net current is achieved. The resulting potential difference between the semiconductor and the redox level in the solution is defined as the open circuit voltage, V_{oc}, of the system.

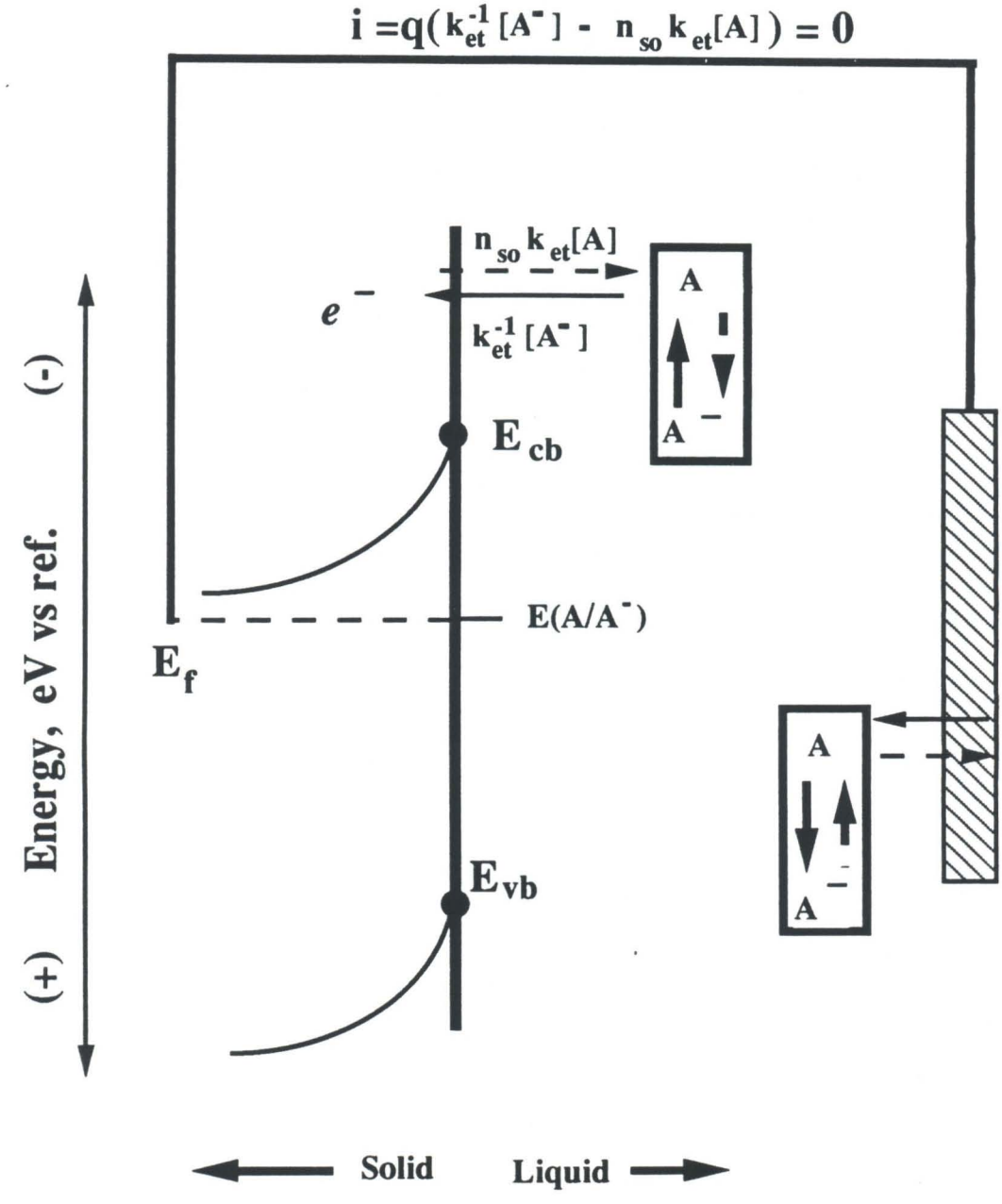
$i = q(k_{et}^{-1}[A^-] - n_{so} k_{et}[A]) = 0$
$n_{so} k_{et}[A]$
e^-
$k_{et}^{-1}[A^-]$
A
A
E_{cb}
$E(A/A^-)$
E_f
E_{vb}
(-)
Energy, eV vs ref.
(+)
Solid
Liquid

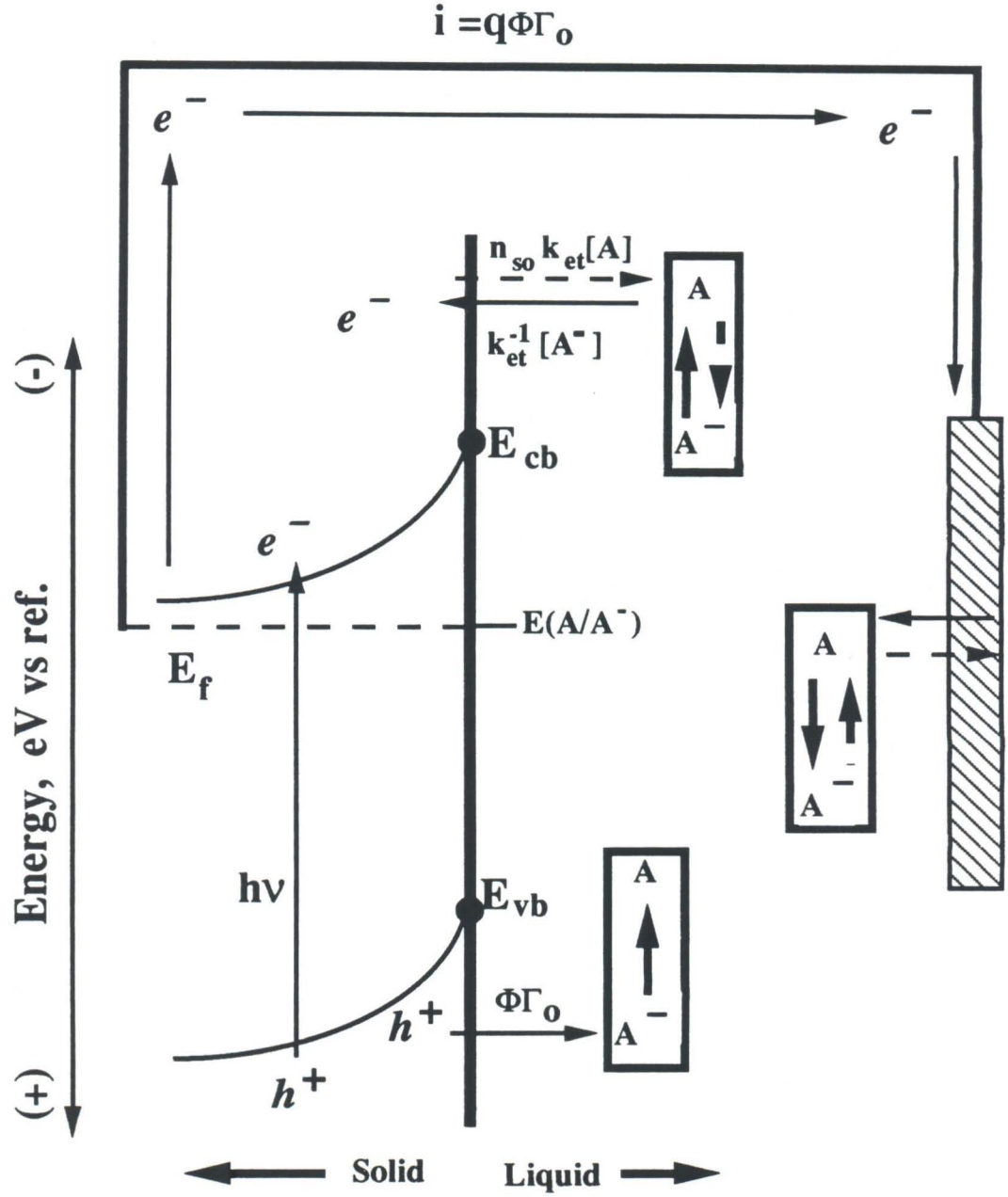
i =qΦΓo
e⁻
e⁻
nso ket[A]
e⁻
k-1et [A⁻]
A
A⁻
Ecb
e⁻
Ef
E(A/A⁻)
A
A⁻
hν
Evb
A
A⁻
Φ Γo
h+
h+
(-)
(+)
Energy, eV vs ref.
Solid
Liquid

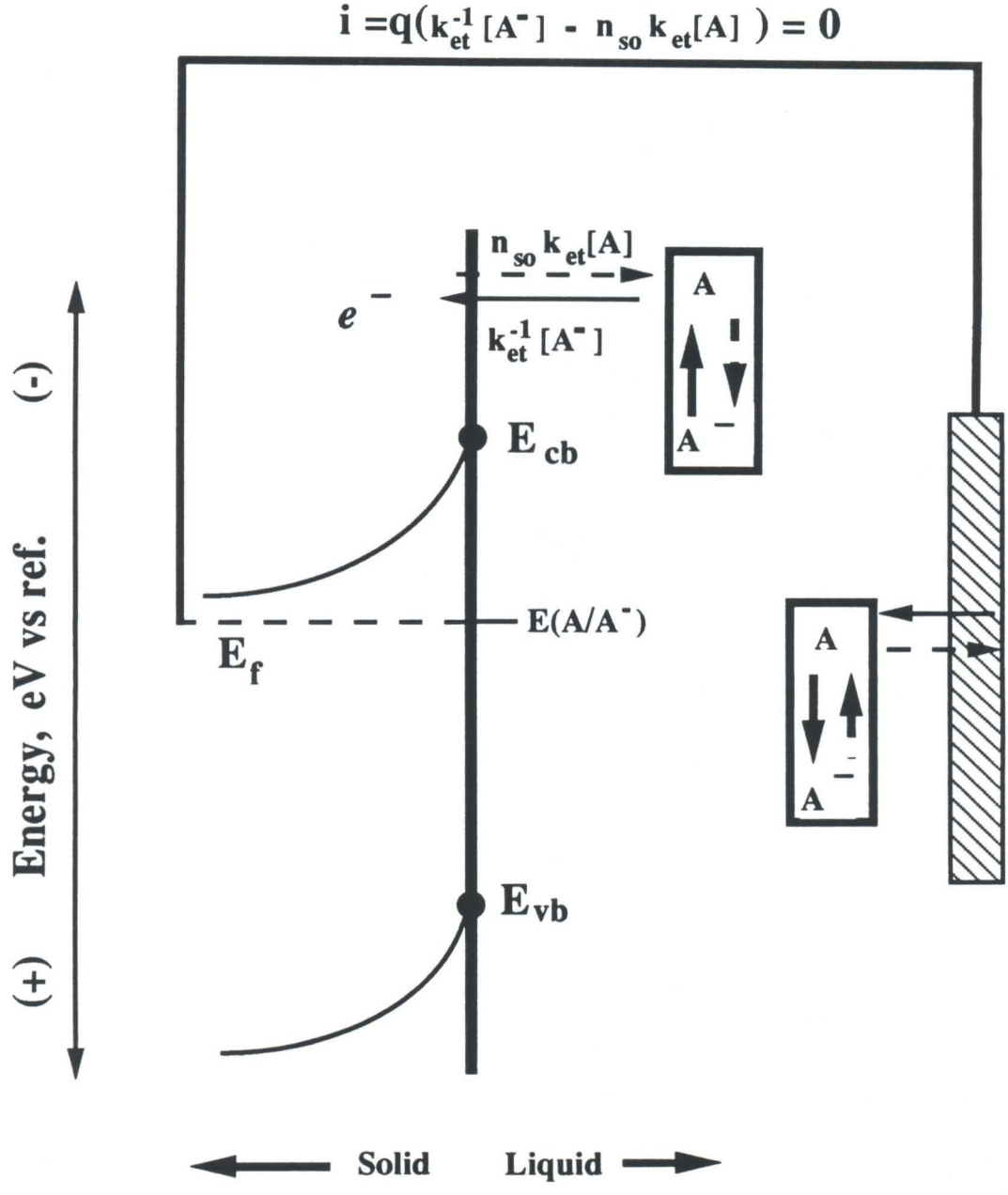
i =q(k_et^-1 [A^-] - n_so k_et[A]) = 0
n_so k_et[A]
e^-
k_et^-1 [A^-]
A
A^-
E_cb
E(A/A^-)
E_f
A
A^-
E_vb
(+) Energy, eV vs ref. (-)
Solid
Liquid

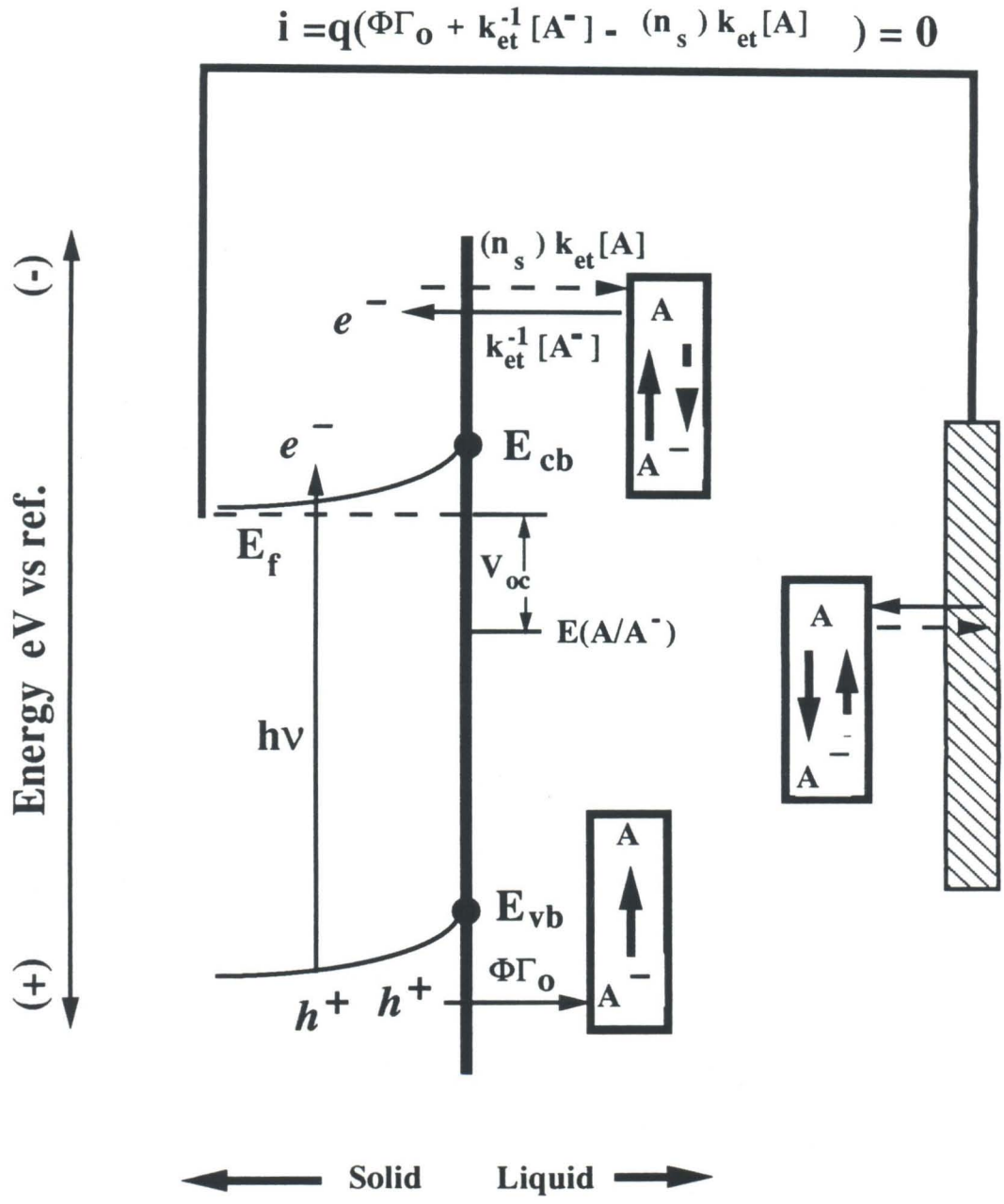
i =q(ΦΓo + k_et^-1 [A⁻] - (n_s) k_et[A]) = 0
(n_s) k_et[A]
e⁻
k_et^-1 [A⁻]
A
A⁻
e⁻
E_cb
E_f
V_oc
E(A/A⁻)
hν
A
A⁻
A
A⁻
E_vb
ΦΓo
h+ h+
(-)
Energy eV vs ref.
(+)
Solid
Liquid

Figure 4. Schematics of semiconductor/liquid junctions used in photoelectrosynthetic cell configurations. a) A schematic of the general system, in which the photoanode produces the net oxidation of species B to yield B^+, and the counterelectrode reduces species C^+ to yield C. The overall light-induced photoelectrosynthetic reaction is therefore $B + C^+ \Rightarrow B^+ + C$. For simplicity we will only consider minority carrier oxidation of B as the interfacial hole process, and majority carrier reduction of B^+ and C^+ as the "back reactions". This is appropriate for the oxidation of water at metal oxide photoanodes. b) Light-induced electrolysis of water using n-type semiconductor photoanodes. Water is oxidized to $O_2(g)$ at the photoanode, and water is reduced to $H_2(g)$ at the dark cathode. Only oxidation of water is considered by the photogenerated holes, because initially no H_2 (species C) will be available at the semiconductor interface. However, reduction of both $O_2(g)$ and H_2O can proceed at the semiconductor surface, and must be considered explicitly. The Fermi level at the back of the semiconductor is at the (C^+/C), *i.e.*, (H_2O/H_2), redox potential under these short circuit conditions, because 1 atmosphere of H_2 is maintained over the Pt counterelectrode, and the counterelectrode has been assumed to be ideally polarizable in this cell.

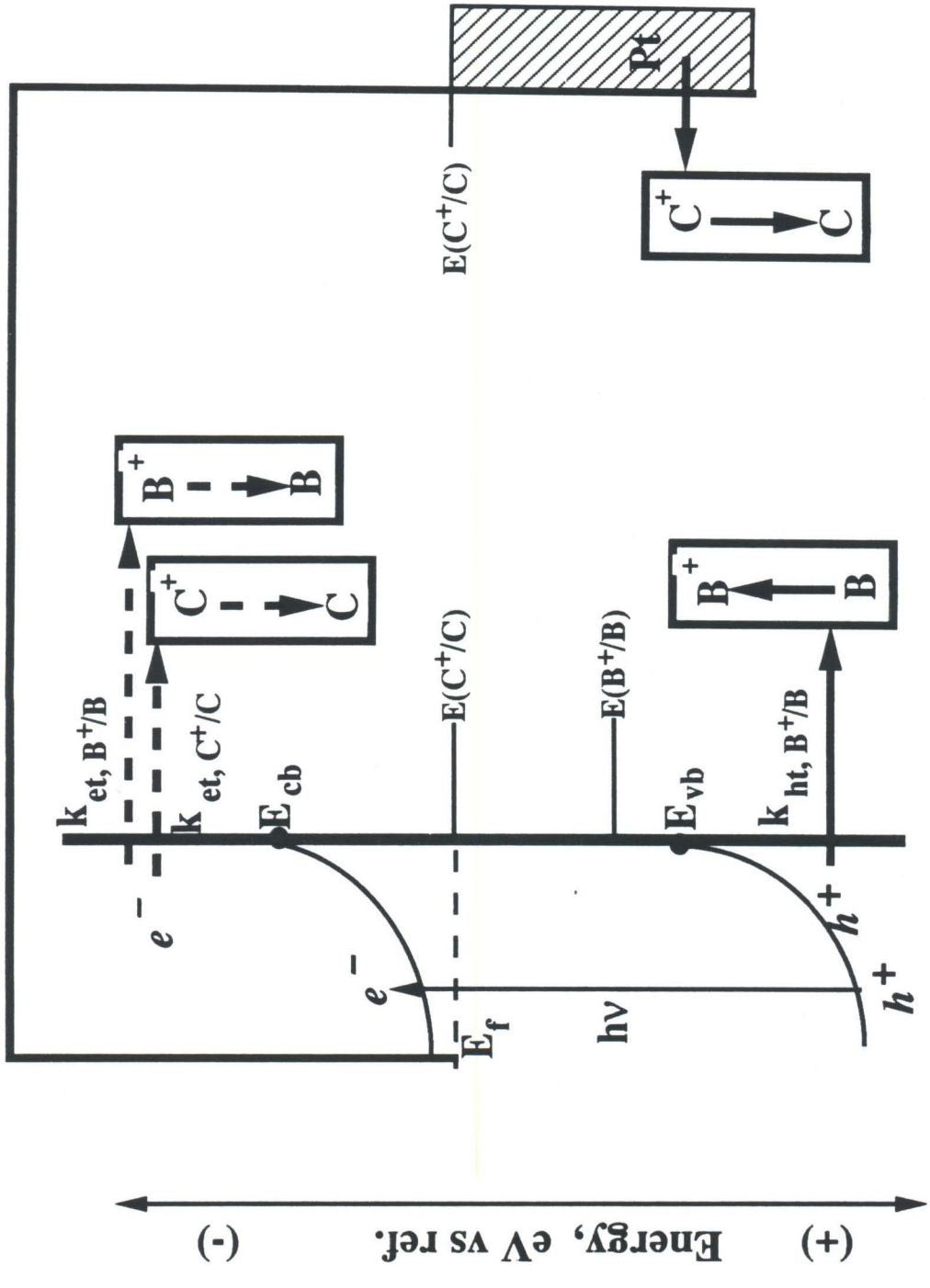
Energy, eV vs ref.
(+)
(-)
Solid
Liquid
Pt
$E(C^+/C)$
$C^+ \rightarrow C$
$B^+ \rightarrow B$
$C^+ - \rightarrow C$
$B^+ - \rightarrow B$
$k_{et,\,B^+/B}$
$k_{et,\,C^+/C}$
E_{cb}
$E(C^+/C)$
$E(B^+/B)$
E_{vb}
$k_{ht,\,B^+/B}$
e^-
e^-
E_f
$h\nu$
h^+
h^+

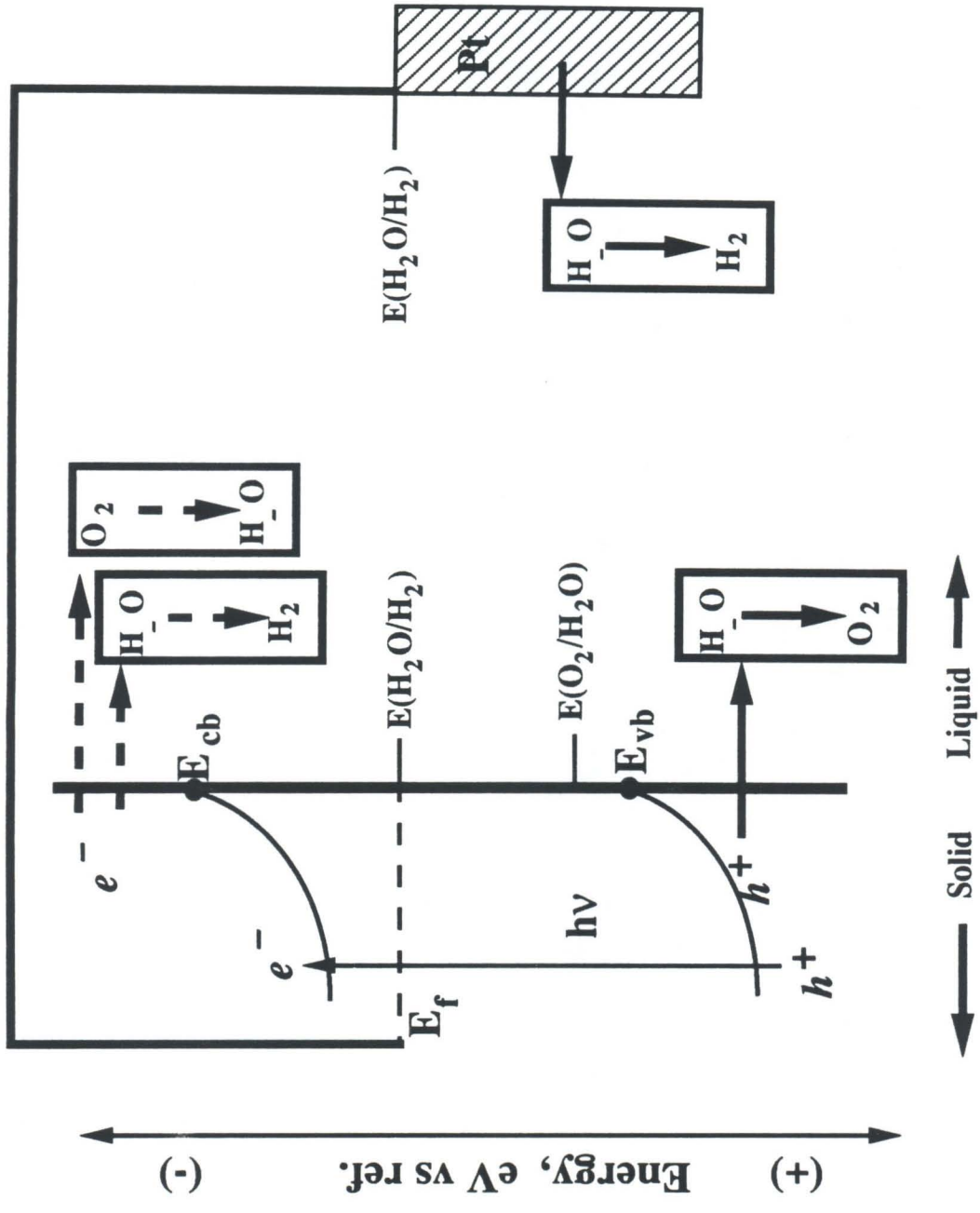
Pt
$E(H_2O/H_2)$
H_2O → H_2
O_2 ← H_2O
H_2O ← H_2
E_{cb}
$E(H_2O/H_2)$
$E(O_2/H_2O)$
E_{vb}
H_2O → O_2
e^-
e^-
E_f
hν
h^+
h^+
Solid
Liquid
(+) Energy, eV vs ref. (-)

Figure 5. Kinetic diagrams for semiconductor electrodes at short circuit in a water photoelectroysis experiment. a) In the dark, current will flow through the external circuit in response to the difference in Nernst potentials between the compartment containing the counterelectrode and the compartment containing the semiconductor electrode. This results in a net negative current, as shown, through the semiconductor/liquid interface, and yields the chemical reaction $C + B^+ \Rightarrow C^+ + B$. (b) Under illumination, the minority carrier current tends to oppose the dark current. When sufficient light intensity is obtained, no net current is present through the semiconductor/liquid interface, and the voltage produced by the illuminated semiconductor exactly offsets the Nernstian voltage difference between the two compartments of the complete cell. Above this threshold light intensity, the increased minority carrier flux provides a net positive current flow through the external circuit, and a sustained fuel electrolysis, in the direction $B + C^+ \Rightarrow B^+ + C$, can be achieved.

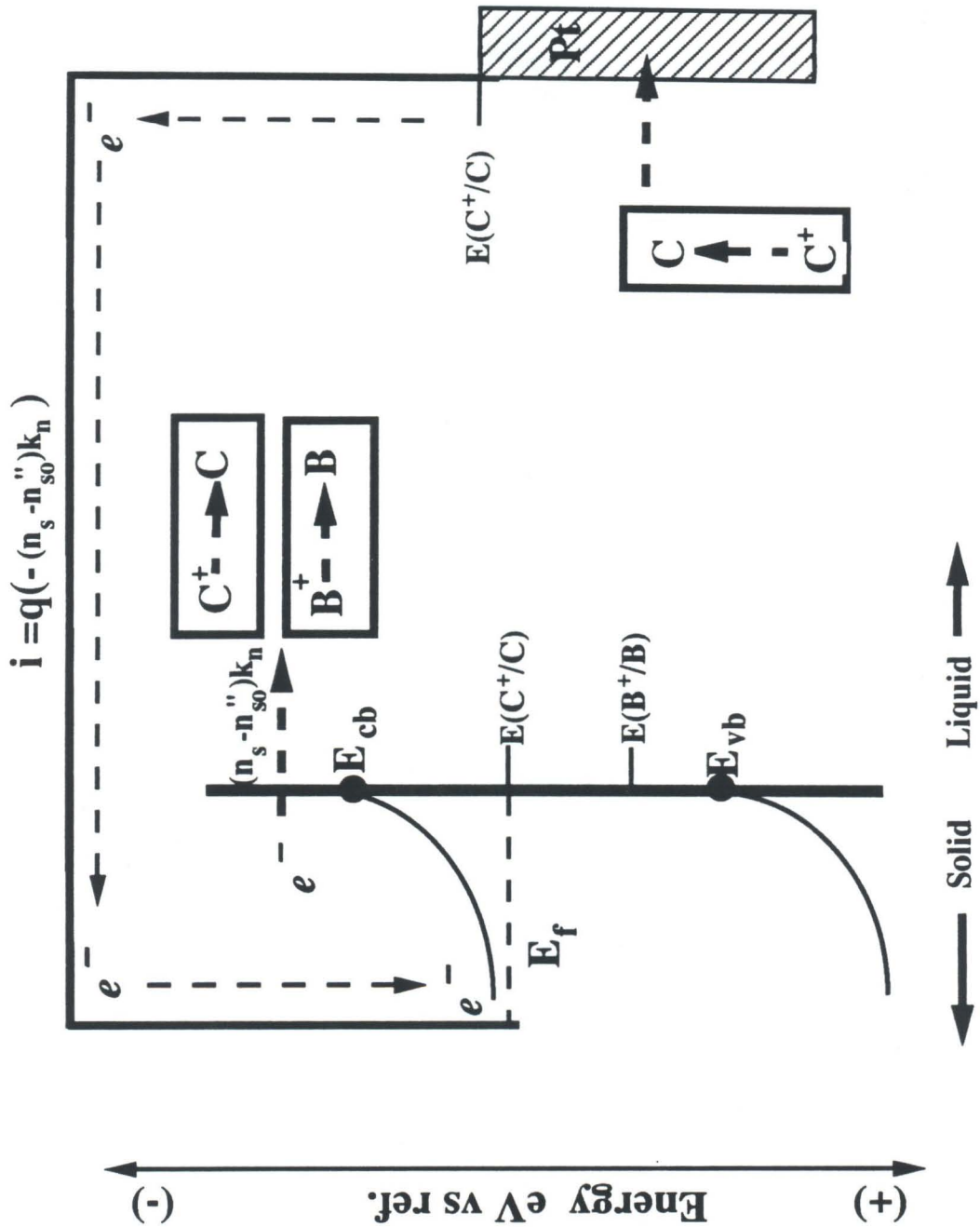
i =q(- (n_s -n''_so)k_n)
e⁻
e⁻
e⁻
e⁻
Pt
E(C⁺/C)
C
C⁺
C⁺ C
B⁺ B
(n_s -n''_so)k_n
E_cb
E(C⁺/C)
E(B⁺/B)
E_vb
E_f
Solid
Liquid
(-)
Energy eV vs ref.
(+)

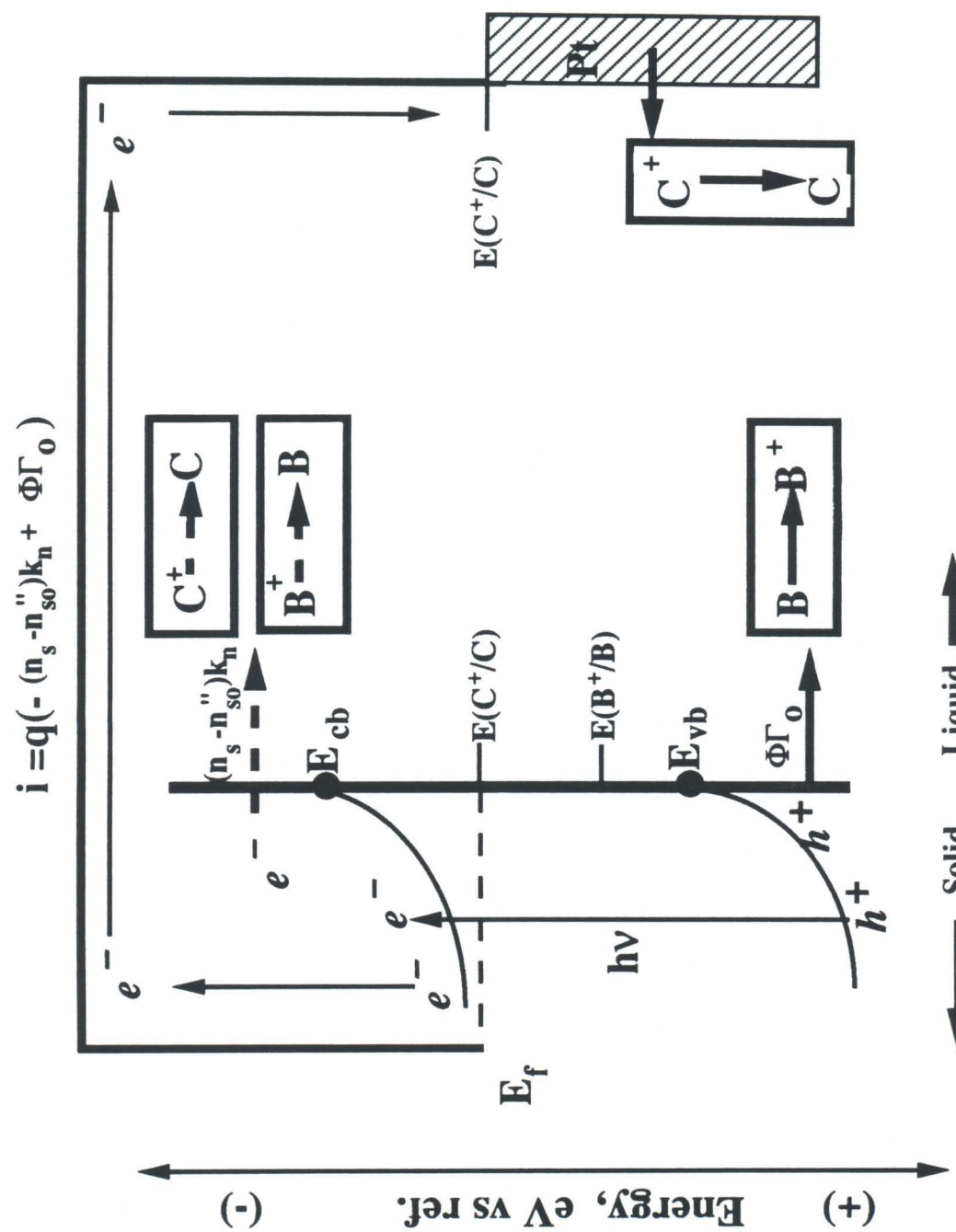
i =q(- (n_s -n''_so)k_n + ΦΓ_o)
e⁻
e⁻
Pt
E(C⁺/C)
C⁺ → C
C⁺ → C
B⁺ → B
B → B⁺
(n_s -n''_so)k_n
E_cb
E(C⁺/C)
E(B⁺/B)
E_vb
ΦΓ_o
e⁻
e⁻
e⁻
hν
h⁺
h⁺
E_f
Solid
Liquid
(+) Energy, eV vs ref. (-)

Figure 6. a) Plot of short circuit current density as a function of the illumination intensity for a two-electrode photoelectrolysis cell. The $SrTiO_3$ electrode and the Pt electrode were kept in different compartments that were separated by a ceramic frit. An O_2 pressure of 1 atm was maintained over the semiconductor electrode, and a H_2 pressure of 1 atm was maintained over the Pt electrode. The threshold in net photoelectroysis current was observed between 2.3×10^{-5} and 3.0×10^{-5} W/cm^2. b) Linear plot of the positive current values reported in Figure 6a. At high enough current densities, where the magnitude of the short circuit majority carrier dark current was negligible, the total current density was proportional to the illumination intensity.

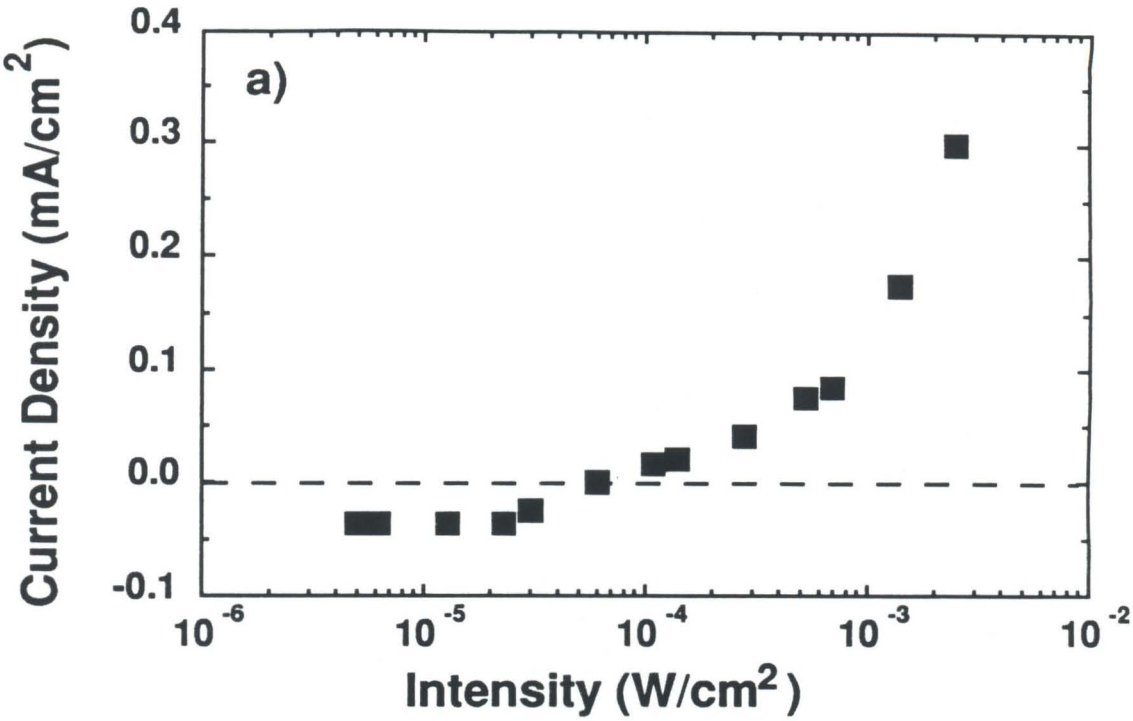
a)
Current Density (mA/cm^2)
0.4
0.3
0.2
0.1
0.0
-0.1
10^{-6}
10^{-5}
10^{-4}
10^{-3}
10^{-2}
Intensity (W/cm^2)

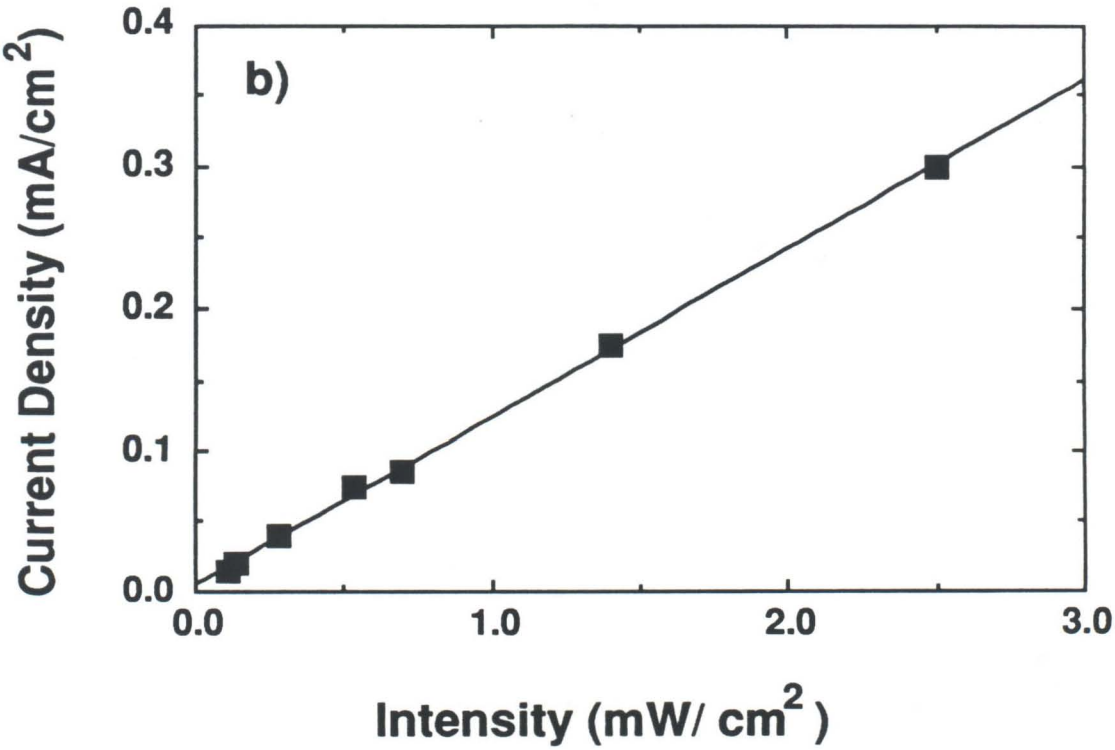
b)
Current Density (mA/cm^2)
0.4
0.3
0.2
0.1
0.0
0.0
1.0
2.0
3.0
Intensity (mW/ cm^2)

Figure 7. a) Plot of short circuit current density as a function of the illumination intensity for a two-electrode regenerative cell. In this system, 1 atm of O_2 was maintained over both the $SrTiO_3$ and the Pt electrodes. For this cell, no net free energy change occurs in the electrolyte, and no threshold was observed in the current *vs* illumination intensity relationship. b) A linear plot, at higher light intensities, of the current density *vs* light intensity, showing the proportionality between the current density and illumination intensity.

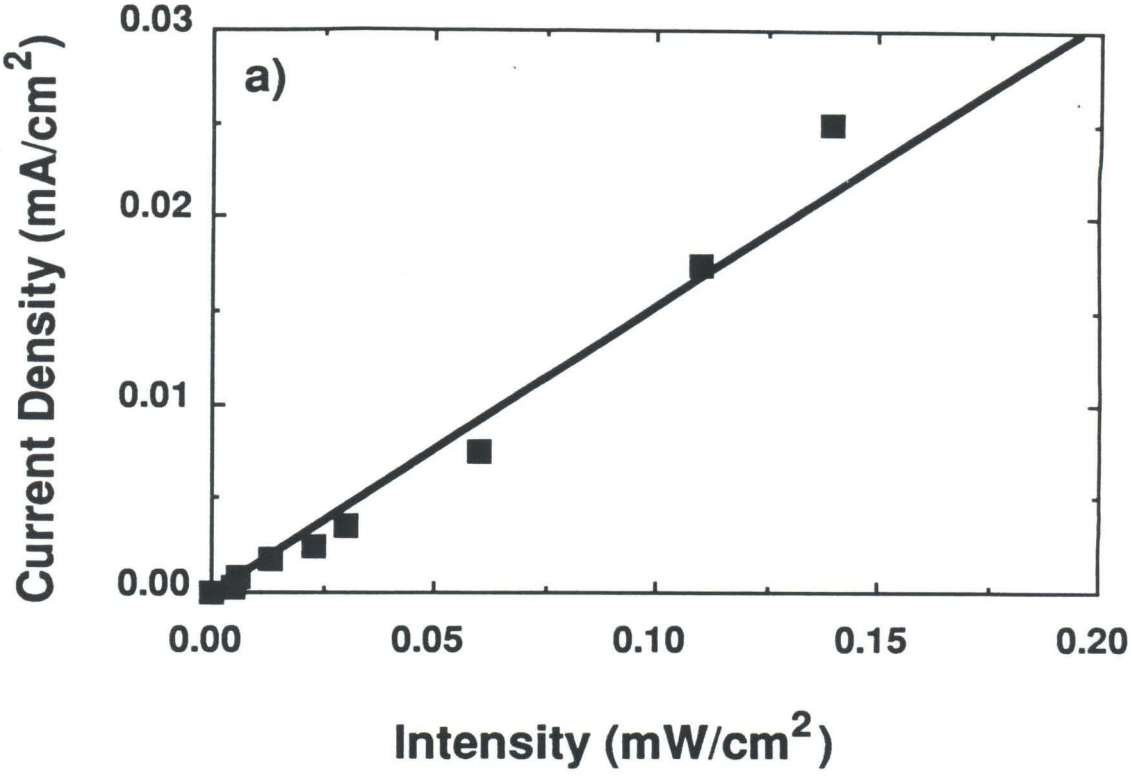
a)
Current Density (mA/cm^2)
0.03
0.02
0.01
0.00
0.00
0.05
0.10
0.15
0.20
Intensity (mW/cm^2)

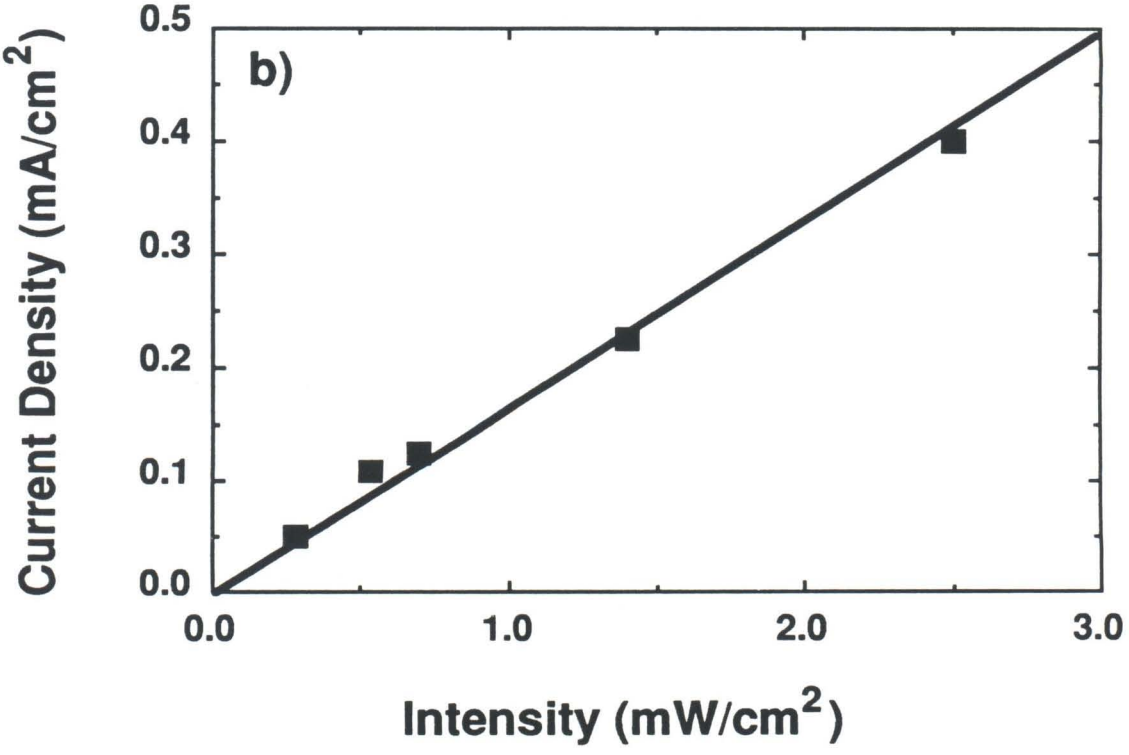
b)
Current Density (mA/cm^2)
0.5
0.4
0.3
0.2
0.1
0.0
0.0
1.0
2.0
3.0
Intensity (mW/cm^2)

Figure 8. Current-voltage behavior for the n-$SrTiO_3$/5.0 **M** NaOH/Pt system under various illumination intensities. The scan rate was 50 mV/sec, and the cell was purged with 1 atm of Ar. a) I-V behavior at high light intensities. b) I-V behavor at low light intensities. Note that at sufficiently low light intensity, the net current is not anodic until potentials more positive than the hydrogen evolution potential at this pH.

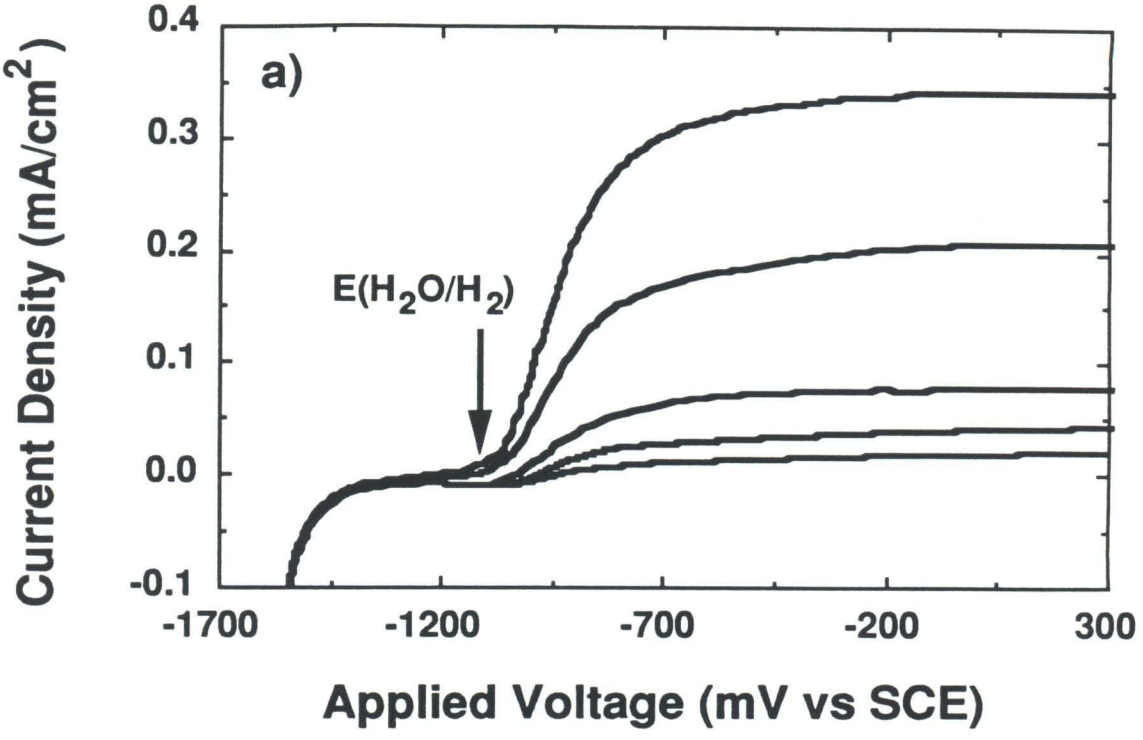
a)
0.4
0.3
0.2
0.1
0.0
-0.1
E(H2O/H2)
Current Density (mA/cm2)
-1700
-1200
-700
-200
300
Applied Voltage (mV vs SCE)

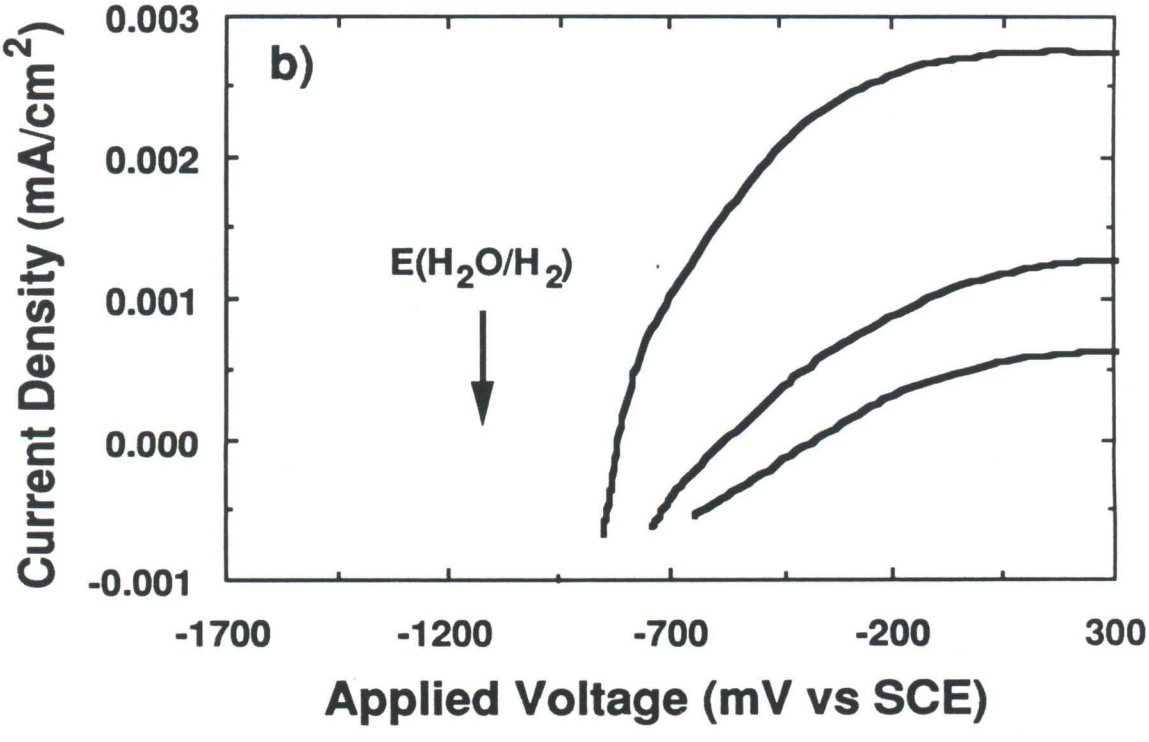
b)
0.003
0.002
0.001
0.000
-0.001
E(H2O/H2)
Current Density (mA/cm2)
-1700
-1200
-700
-200
300
Applied Voltage (mV vs SCE)

Figure 9. Plot of V_{oc} as a function of the light intensity. The V_{oc} was equated to the difference between the potential for O_2 evolution and the potential at which zero net current was observed in a three-electrode potentiostatic experiment.

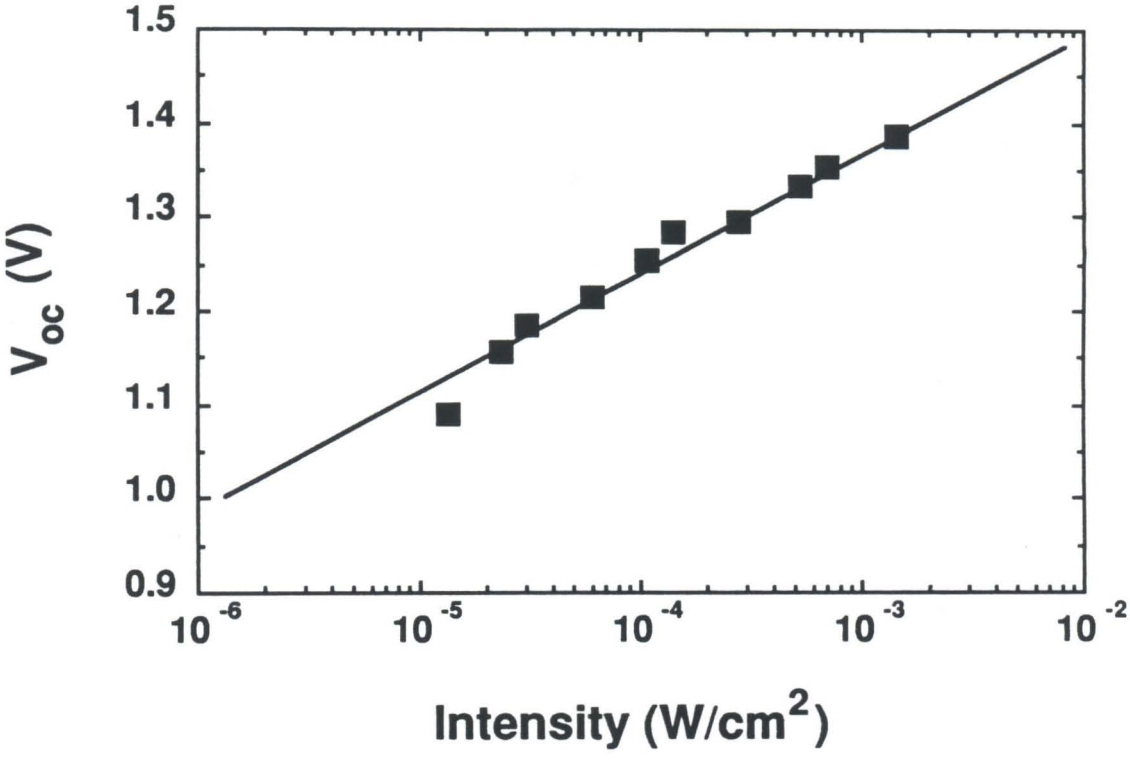
1.5
1.4
1.3
1.2
1.1
1.0
0.9
V_{oc} (V)
10^{-6}
10^{-5}
10^{-4}
10^{-3}
10^{-2}
Intensity (W/cm^2)

Figure 10. Position of electron and hole quasi-Fermi levels for different illumination conditions. a) For a regenerative cell at equilibrium in the dark, only one Fermi level is required to depict the occupancy of electrons and holes, and to equilibrate with the electrochemical potential of the liquid phase. b) Under illumination, at open-circuit, non-equilibrium concentrations of carriers exist, and separate quasi-Fermi levels are required to describe the electron and hole concentrations. For rapid charge transfer between the redox couple and minority carriers, the hole quasi-Fermi level at the surface will coincide in energy with the redox potential of the electrolyte. In general, the open circuit voltage, V_{oc}, is the potential difference between the redox couple and the position of the majority carrier quasi-Fermi level at the back of the electrode. For the rapid minority carrier charge transfer kinetics depicted in this figure, V_{oc} is simply given by the potential difference between the values of the electron and hole quasi-Fermi levels at the semiconductor/liquid interface.

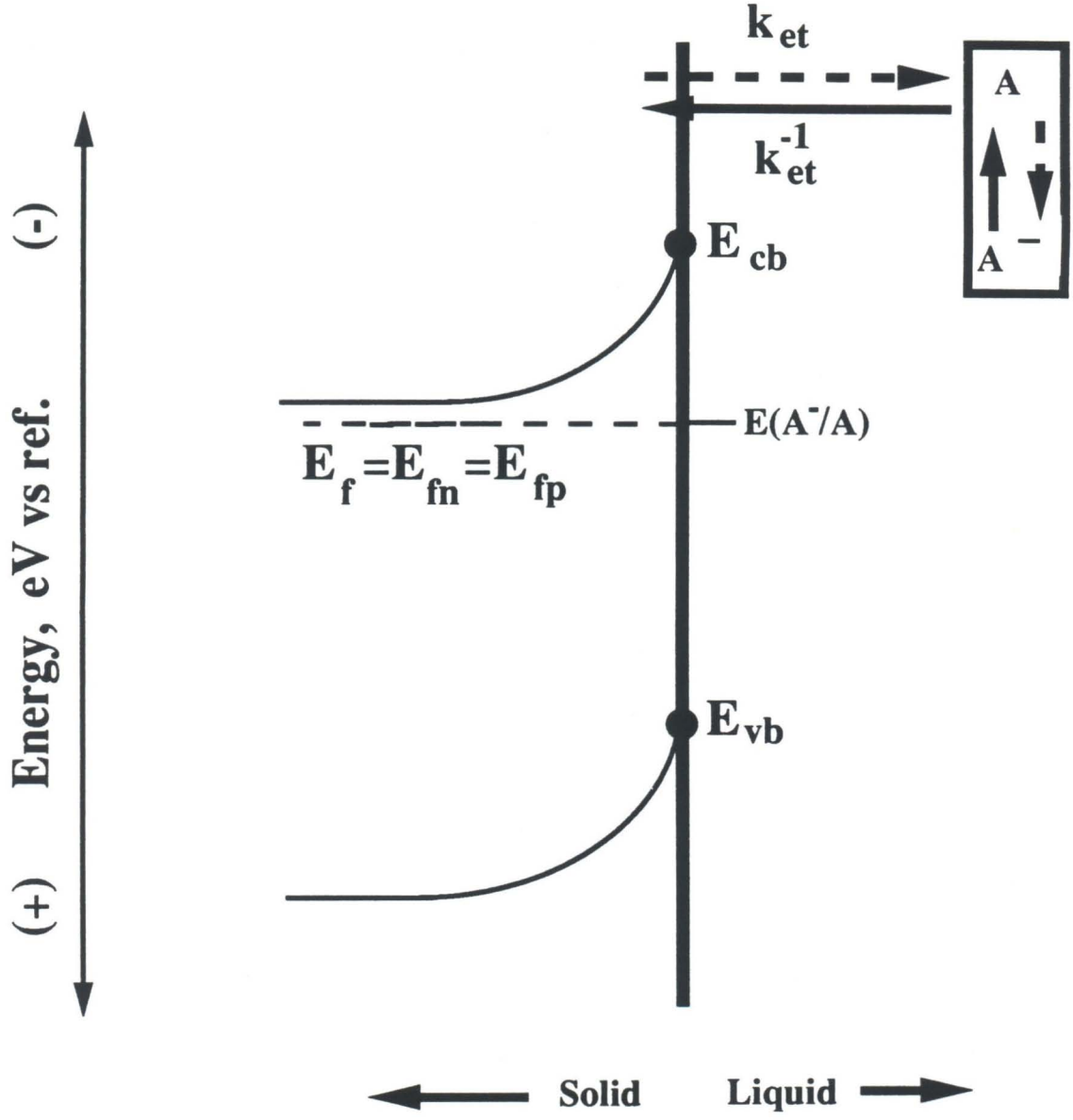
k et
k -1 et
A
A –
E cb
E(A-/A)
E f =E fn =E fp
E vb
Energy, eV vs ref.
(-)
(+)
Solid
Liquid

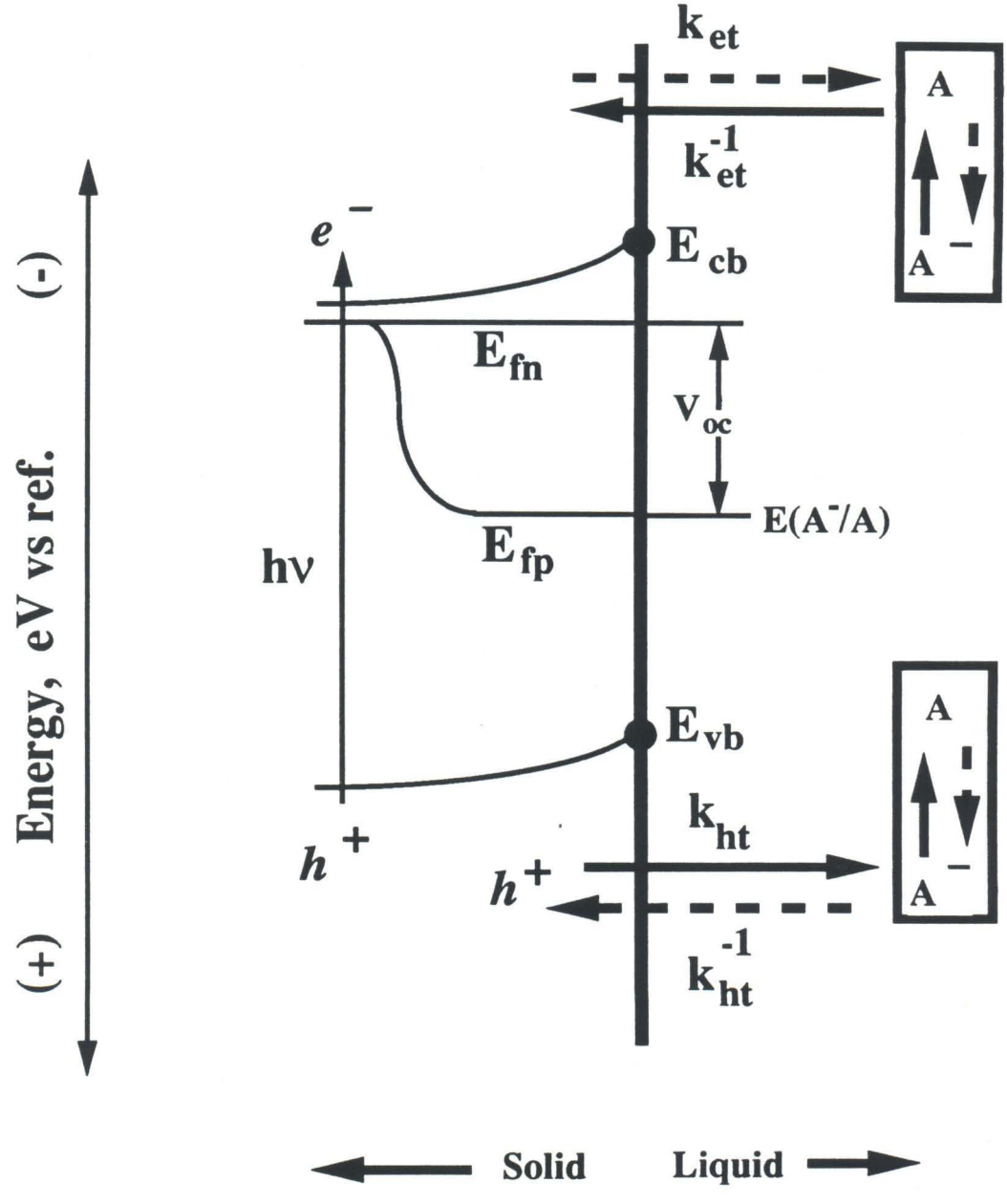
k et
k -1 et
A
A −
e −
E cb
E fn
V oc
E(A-/A)
E fp
hν
E vb
k ht
h +
h +
k -1 ht
A
A −
(+) Energy, eV vs ref. (-)
Solid
Liquid

Charge Transfer Studies of Semiconductor Interfaces

Chapter 7: Studies of Silicon Photoelectrochemical Cells Under High Injection Conditions

Studies of silicon photoelectrochemical cells under high injection conditions

Amit Kumar and Nathan S. Lewis[a)]
Division of Chemistry and Chemical Engineering, California Institute of Technology, Pasadena, California 91125

(Received 2 July 1990; accepted for publication 21 September 1990)

The behavior of Si/CH_3OH-dimethylferrocene $^{+/0}$ junctions has been investigated under high injection conditions. Open circuit voltages of (626 ± 5) mV were obtained at short circuit photocurrent densities of 20 mA/cm^2 for samples with an n^+-diffused back region, point contacts on the back surface, and with a base of thickness 390 μm and a 1 ms hole lifetime. The diode quality factor and recombination current density were 1.8 ± 0.1 and $(2.6 \pm 1.5) \times 10^{-8}$ A/cm^2, respectively. These data are consistent with recombination dominated by the base and back contact regions, and not at the Si/CH_3OH interface.

We have previously shown that n-Si/CH_3OH interfaces are of remarkable electronic quality, and exhibit open circuit voltages that are superior to those obtained from Si/metal junctions and from conventional Si p-n homojunctions.[1-3] Over a range of Si dopant densities and diffusion lengths, the open circuit voltage (V_{oc}) for n-Si/CH_3OH-dimethylferrocene (Me_2Fc) $^{+/0}$ junctions follows the Shockley diode equation,[2,3] as expected for a junction in which interfacial recombination losses are negligible compared to the minority-carrier bulk diffusion/recombination process.[4] Since these previous systems were operated under low-level injection conditions, the trade-off between high donor densities (N_d) and maximum minority-carrier diffusion lengths (L_p) resulted in maximum n-Si/CH_3OH V_{oc} values of 635 mV (light-limited photocurrent density, $J_{ph} = 20$ mA/cm^2, 298 K) for $N_d = 3.2 \times 10^{16}$ cm^{-3} n-Si with $L_p = 195$ μm, while higher V_{oc} values of 670 mV ($J_{ph} = 20$ mA/cm^2, 298 K) for $N_d = 1.8 \times 10^{17}$ cm^{-3} n-Si were only achieved with a concurrent degradation of base lifetime ($L_p = 20$ μm).[3] An alternative design exploited recently in solid-state Si photovoltaics to preserve high base lifetimes is to operate the base region under field-free, high injection conditions.[5] This approach has allowed fabrication of high efficiency (> 22%) photovoltaic cells displaying air mass 1.0 V_{oc} values as high as 705 mV.[6] We now report studies of n-Si/liquid junctions operated under high injection conditions. These cells take advantage of the electronic quality of the Si/CH_3OH interface, and have resulted in 630 mV V_{oc} values (on unoptimized base/back contact combinations) with no processing steps performed on the liquid side of the Si base region. In addition to advancing our basic knowledge of the electronic properties of semiconductor/liquid junctions, these Si/liquid systems might be useful for simple, nondestructive, spatially resolved diagnostics of Si base quality.

Figure 1 depicts the liquid junction cell. The semiconductor photoelectrode (typically squares of edge dimension 6–8 mm) consisted of an intrinsic Si layer (390 μm thick, $N_d = 1.3 \times 10^{13}$ cm^{-3}; low-level hole lifetime = 1 ms), with an n^+-type diffused layer (sheet resistivity = 40 Ω/□) on the back side of the wafer. Contact to the n^+ layer was achieved by an array of metal points (5 μm × 5 μm squares) covering 2% of the active device area. The remaining back surface area of the wafer was covered by a high quality thermally grown SiO_2 layer. This structure is similar to the processing used in high efficiency p-i-n solid-state concentrator cells,[5,6] and reduces parasitic recombination losses in the diffused region and at the back surface. For use in the liquid junction arrangement, no processing or diffusion steps were performed on the front surface; the Si samples were merely etched in 49% HF(aq) and were rinsed with H_2O and CH_3OH before use in a conventional photoelectrochemical cell arrangement.[3,7] For comparison purposes, a complete p-i-n cell was evaluated in parallel with the Si/liquid junctions. This p-i-n cell was not fabricated in the identical batch process as the structures examined in the liquid junction, but it nominally had the same back contact and base characteristics, with a front emitter consisting of an 80 Ω/□ p^+ region with point contacts, oxide passivation, and a textured front surface for light trapping purposes. The p-i-n test cell behavior was typical of such devices, although optimized cells with higher hole lifetimes and thinner bases have been reported to display slightly larger V_{oc} values.[6]

Figure 2 displays the current-voltage (I-V) behavior at

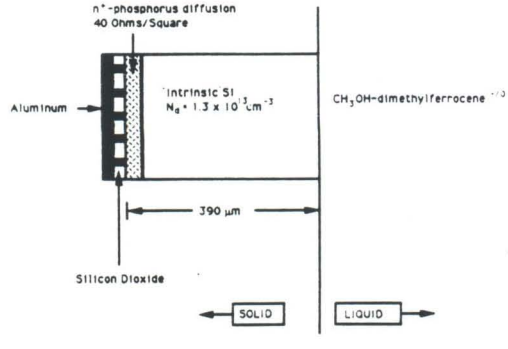

FIG. 1. Schematic diagram of photoelectrode used in this study. Contact to the electrode was made through the Al back, and the electrode edges and back surface were encapsulated in epoxy to expose 0.4–0.6 cm^2 of active area to the electrolyte.

a)Address correspondence to this author.

 0003-6951/90/512730-03$02.00

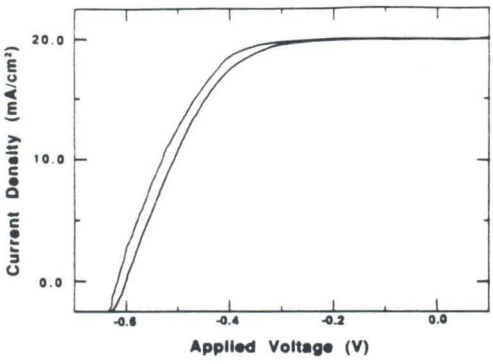

FIG. 2. Potentiostatic three-electrode current-voltage (I-V) property of high injection Si/CH_3OH-$Me_2Fc^{+/0}$ photoelectrochemical cell. The reference electrode was a Pt wire in a Luggin capillary placed 0.2 mm from the photoelectrode surface. The counter electrode was a large area (>3 cm^2) Pt foil. The poor fill factor is due to the concentration overpotential and to the large residual uncompensated resistance of the solution in this unoptimized semiconductor/liquid cell configuration.

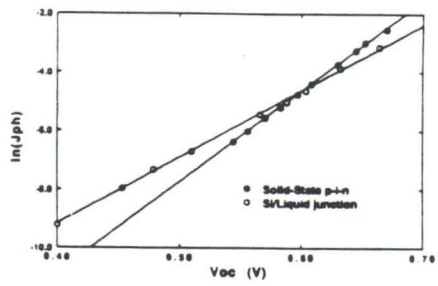

FIG. 3. $\ln(J_{ph})$ vs V_{oc} for the solid-state p-i-n cell (dark circles) and for the photoelectrochemical cell (light circles). In this figure the ordinate is the natural logarithm of J_{ph} measured in A/cm^2. The V_{oc} for the liquid junction cell becomes greater than that for the p-i-n cell at high current densities.

298 K of the Si photoelectrode in contact with the CH_3OH-1.0 M $LiClO_4$-0.20 M dimethylferrocene (Me_2Fc)-0.010 M Me_2Fc^+ electrolyte. The $Me_2Fc^{+/0}$ redox system established the Fermi level of the liquid phase, and insured a high degree of equilibrium band bending in the Si base while maintaining electrode stability to photocorrosion.[7,8] The Si surface in the liquid junction was not optimized for light trapping or for minimization of optical reflection losses; thus, to facilitate comparison of electrical properties with the solid-state p-i-n test cell, the light intensity was adjusted to provide short circuit photocurrent densities (J_{ph}) of 20.0 mA/cm^2. Under these conditions, the V_{oc} of 626 ± 5 mV obtained from the liquid junctions compares closely to the V_{oc} of 625 mV measured for the p-i-n device at $J_{ph} = 20$ mA/cm^2. This indicates that the ratio of minority-carrier collection to majority-carrier recombination is similar in the two systems, and underscores the high electronic quality of the HF-etched Si/CH_3OH junction. The V_{oc} values reported for the liquid junctions are statistically averaged results from 3 different Si samples used in a total of 11 separate Si/CH_3OH cells. The Si/CH_3OH junction in Fig. 2 is clearly operating in high-level injection, because the low-level injection bulk recombination/diffusion V_{oc} value for $N_d = 1.3 \times 10^{13}$ cm^{-3} Si with an effective minority-carrier diffusion length of 400 μm is only 473 mV at $J_{ph} = 20$ mA/cm^2.[4] Under these conditions, a V_{oc} higher than this 473 mV value can only be achieved if the injected majority-carrier density exceeds the equilibrium majority-carrier density, implying that the high injection condition has indeed been obtained. The poor fill factor in Fig. 2 results from the uncompensated resistance losses and concentration overpotentials that are inherent to an unoptimized liquid junction cell design. The V_{oc} values for such systems are still useful, because use of a thin layer cell configuration has been shown to minimize these cell-based losses while still preserving the V_{oc} determined in the unoptimized cell arrangement used in Fig. 2.[9]

Plots of the dependence of V_{oc} on the light-limited photocurrent density for $J_{ph} = 0.10$–50 mA/cm^2 are presented in Fig. 3 for both the n-Si/CH_3OH junction and the p-i-n test cell. Analysis of the data using the standard diode relationship[4]

$$V_{oc} = (AkT/q)\ln(J_{ph}/J_0), \tag{1}$$

(where A is the diode quality factor, kT/q is the thermal voltage, J_{ph} is the light-limited photocurrent density, and J_0 is the magnitude of the recombination current density) yielded values of $J_0 = 7.9 \times 10^{-11}$ A/cm^2 and $A = 1.2$ for the p-i-n cell, and $J_0 = (2.8 \pm 1.6) \times 10^{-8}$ A/cm^2 and $A = 1.8 \pm 0.1$ for the liquid junction. The dominant recombination mechanism for the p-i-n test cell has been assigned previously to recombination in the diffused regions of the device, leading to the observed A and J_0 values for the solid-state system.[5] In contrast, the liquid junction has no front diffused region, but consists of a high quality Si/liquid interface. The higher A value in the Si/liquid cell reflects this lack of front emitter recombination loss. For the relatively thick Si base (390 μm) with a 1 ms minority-carrier lifetime, recombination in the base region is expected to determine the device properties provided that the front emitter recombination can be suppressed. This is in accord with the observed A and J_0 values of the Si/CH_3OH junction. At high light intensities, use of the liquid contact to eliminate front emitter recombination results in higher V_{oc} values for the n-Si/CH_3OH junction than for the test p-i-n cell. Variation in processing to achieve further reductions in base recombination, such as using longer lifetime Si samples with thinner base regions, might allow air mass 1.0 V_{oc} values of Si/CH_3OH junctions to be competitive with the 705 mV values obtained from optimized p-i-n structures.

Considering the high concentration of both electron donors (Me_2Fc) and acceptors (Me_2Fc^+) in the liquid phase, it is remarkable that the n-Si/CH_3OH cell displays such large V_{oc} values under high injection conditions. The spectral response behavior, displayed in Fig. 4, underscores

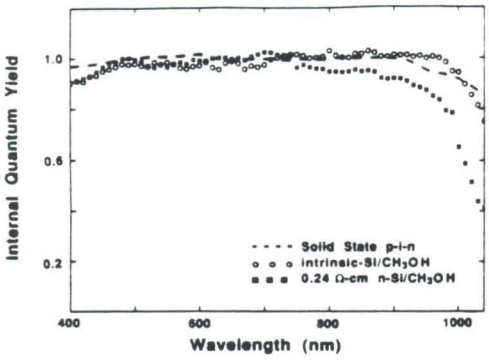

FIG. 4. Internal short circuit quantum yield vs wavelength for the *p-i-n* cell (dashed line, last part of Ref. 5), the intrinsic Si liquid junction (light circles), and for a $N_d = 3.2\times10^{16}$ cm^{-3}, float zone grown, *n*-Si sample ($L_p = 195\ \mu$m). The concentrations of redox ions for the liquid junctions were 0.001 M Me_2Fc and 0.0001 M Me_2Fc^+.

the excellent hole collection properties of this junction. Figure 4 compares the internal quantum yield of the *n*-Si/CH_3OH interface using $N_d = 1.3\times10^{13}$ cm^{-3} and $N_d = 3.2\times10^{16}$ cm^{-3} Si samples to that for a typical $N_d = 1.3\times10^{13}$ cm^{-3} base *p-i-n* cell. In the long-wavelength region, the internal quantum efficiency of the $N_d = 1.3\times10^{13}$ cm^{-3} *n*-Si/CH_3OH junction is substantially higher than that of the $N_d = 3.2\times10^{16}$ cm^{-3} sample[3] and is comparable to the response of the *p-i-n* Si test cell. This behavior correlates with the larger effective minority-carrier diffusion length in the low-doped Si samples. For the mirror-finished Si surfaces used in contact with liquids, the maximum absolute external quantum yield of the *n*-Si/CH_3OH interface was 0.75–0.80; however, it has been shown that surface texturizing etches can yield improvements in maximum external quantum yield to greater than 0.95 for $N_d = 3.2\times10^{16}$ cm^{-3} *n*-Si/CH_3OH junctions.[1,7,10] Thus, despite the potential for interfacial recombination at the Si/liquid interface, the achievable quantum yields are comparable to maximum external quantum yields achievable in optimized *p-i-n* devices.[5,6]

We have also investigated the dependence of V_{oc} on the concentration of donors and acceptors in the liquid phase. The concentration of Me_2Fc was varied from 0.005 to 0.20 M, the concentration of Me_2Fc^+ was varied from 0.0001 to 0.10 M, and the $[Me_2Fc^+]/[Me_2Fc]$ ratio was varied from 20 to 5.0×10^{-4}. For all combinations studied, and over a range of J_{ph} from 2.0 to 20 mA/cm^2, V_{oc} did not change ($\pm$10 mV) when the redox concentrations were varied. This is somewhat surprising, because under high injection conditions, carrier transport in the intrinsic layer should be purely diffusional. With no electric field to repel majority carriers, conventional electron transfer theories[11,12] predict that the highly exoergic electron capture by Me_2Fc^+ should be more kinetically facile than the less exoergic hole capture by Me_2Fc. The independence of V_{oc} with changes in redox concentrations, and the excellent majority-carrier rejection indicated by the spectral response data, both indicate that the rate-limiting recombination step for majority carriers does not involve bimolecular interfacial recombination with the dissolved redox ions. The present data cannot address whether the underlying cause of the high (minority/majority) carrier collection ratio is due to a failure of the conventional Marcus–Gerischer electron transfer theory[11,12] in this system or is due to strong surface inversion induced by the CH_3OH-$Me_2Fc^{+/0}$ contact. The latter situation would result in *in situ* formation of a p^+-doped layer at the Si/CH_3OH interface, making the *p-i-n* cell and the Si/liquid cell very similar in device properties. Experiments designed to distinguish between these alternatives are currently in progress; however, the present data clearly show that the collection properties of the *n*-Si/CH_3OH interface can approach those of the best known solid-state Si photovoltaic systems.

Although the *n*-Si/CH_3OH interface yielded V_{oc} values that were higher than those in the *p-i-n* test cell used in this work, this requires operation under high light concentration, where the efficiency performance of a liquid junction suffers relative to solid-state systems. Even in thin (10 μm) electrolyte layers, mass transport limitations on the supply of redox couple to the Si interface lead to declines in power conversion efficiency at current densities higher than 50 mA/cm^2,[2,9] which is the range in which the high injection *p-i-n* devices exhibit superior efficiency performance.[6] The liquid junction behavior under high injection conditions is valuable, however, in advancing our understanding of carrier transport and recombination at solid/liquid boundaries. It is encouraging to note that the performance of such single-crystal Si/CH_3OH interfaces can approach that of the most technologically advanced photovoltaic systems, and that these semiconductor/liquid systems can afford relatively stable junction performance from simple, available chemicals and liquids.

We thank the National Science Foundation for support of this work. This is contribution No. 8167 from the Caltech Division of Chemistry and Chemical Engineering. We also thank Ronald A. Sinton and Richard M. Swanson of the Stanford Electronics Laboratory (Stanford, CA) for invaluable discussions and for supplying the samples used in this study. A. K. acknowledges the Department of Education for a Research Fellowship.

[1] M. L. Rosenbluth, C. M. Lieber, and N. S. Lewis, Appl. Phys. Lett. **45**, 423 (1984).
[2] N. S. Lewis, Ann. Rev. Mater. Sci. **14**, 95 (1984).
[3] M. L. Rosenbluth and N. S. Lewis, J. Am. Chem. Soc. **108**, 4689 (1986).
[4] W. Shockley, Bell Syst. Tech. J. **28**, 435 (1949); A. L. Fahrenbruch and R. H. Bube, *Fundamentals of Solar Cells* (Academic, New York, 1983).
[5] R. M. Swanson, Solar Cells **17**, 85 (1986); R. A. Sinton and R. M. Swanson, IEEE Trans. Electron. Devices **ED-34**, 2116 (1987).
[6] R. R. King, R. A. Sinton, and R. M. Swanson, Appl. Phys. Lett. **54**, 1460 (1989).
[7] C. M. Gronet, N. S. Lewis, G. W. Cogan, and J. F. Gibbons, Proc. Nat. Acad. Sci. USA **80**, 1152 (1983).
[8] K. D. Legg, A. B. Ellis, J. M. Bolts, and M. S. Wrighton, Proc. Natl. Acad. Sci. USA **74**, 4116 (1977).
[9] J. F. Gibbons, G. W. Cogan, C. M. Gronet, and N. S. Lewis, Appl. Phys. Lett. **45**, 1095 (1984).
[10] J. A. Bruce and M. S. Wrighton, J. Electroanal. Chem. **122**, 93 (1981).
[11] H. Gerischer, in *Physical Chemistry, An Advanced Treatise*, edited by H. Y. Eyring, D. Henderson, and W. Yost, 9A, pp. 463–542, 1970.
[12] S. R. Morrison, *Electrochemistry at Semiconductor and Oxidized Metal Electrodes* (Plenum, New York, 1981).